The Pennsylvania State University

The Graduate School

College of Engineering

SPACE DIVERSITY TECHNIQUES IN INDOOR BROADBAND OPTICAL WIRELESS COMMUNICATIONS

A Thesis in

Electrical Engineering

by

Yazan A. Alqudah

Submitted in Partial Fulfillment
of the Requirements
for the Degree of

Doctor of Philosophy

August 2003

The thesis of Yazan Al Qudah has been reviewed and approved* by the following:

Mohsen Kavehrad
W.L. Weiss Professor of Electrical Engineering
Thesis Advisor
Chair of Committee

John J. Metzner
Professor of Electrical Engineering

Shizhuo Yin
Associate Professor of Electrical Engineering

Natarajan Gautam
Associate Professor of Industrial and
Manufacturing Engineering

Kenneth Jenkins
Professor of Electrical Engineering
Head of the Department of Electrical Engineering

*Signatures are on file in the Graduate School.

ABSTRACT

Wireless optical (infrared) link provides a secure and a promising alternative to radio for wireless indoor connectivity, be it for terminals or sensors. The large spectrum of unregulated band enables a link to provide broadband access needed for multimedia and other bandwidth demanding applications. The spatial confinement of infrared light provides interference-free bandwidth-reuse in adjacent rooms. The ability to create spatially independent channels in a small physical space holds the promise of large link capacity.

The main challenges in the design of an infrared link include: susceptibility to shadowing, multipath dispersion, and limited range resulting from noise generated by ambient light. Shadowing caused by benign objects blocking signal path results in service degradation, if not complete interruption. Configurations employing wide beam transmitter to service many receiver locations suffer multipath. Noise at receiver is generated by ambient light. Even in a uniformly lit environment, noise generated by natural and artificial light varies depending on receiver location and orientation.

To combat the adverse effects of temporal dispersion in high-speed applications, an accurate channel impulse response is needed. The impulse response is used to analyze and to compensate for the effects of multipath dispersion. In this work, a new approach for obtaining the channel impulse response is presented resulting in tremendous savings in calculation time and bringing insight into the channel behavior.

The ability to create spatially independent channels has motivated a new configuration called Multi-Spot Diffusing (MSD) configuration. In which, a transmitter acts as an array antenna, with each element transmitting data over an independent channel. A multibranch receiver is employed to receive independent copies of transmitted data through each of its branches. In our research, we analyze MSD link with the objective of determining the optimal number of branches that results in maximum signal-to-noise ratio, minimum probability of error and minimum outage probability.

The MSD configuration increases link capacity and reliability by providing a multi-input multi-output channel between transceivers. The availability of N spatial channels implies the possibility of increasing data rate by N folds compared to a single channel. In order to improve link reliability, our research considers novel spatial diversity coding techniques. In orthogonal spatial coding, each channel is responsible for carrying one of N symbols. The receiver decides on a transmitted symbol by comparing received signals on its branches and selects the branch corresponding to maximum signal. In another proposed scheme, a symbol is represented by N bit code word. Each bit is transmitted through a separate channel. The diversity receiver decides on a symbol that corresponds to the highest correlation with a received code word. Thus, information is transmitted not only through signal shapes, but also through branches that receive them.

Traditionally, a non-directed non-line-of sight link configuration uses a ceiling as crossover between a transmitter and a receiver. In many practical environments, the ceiling is not available, either due to environment structure or poor reflectivity of ceiling surface. In this work, we propose and assess the feasibility of using a new configuration

that relies on a wall's upper region as crossover. Both configuration are characterized and compared based on path loss and delay spread.

TABLE OF CONTENTS

List of Figures……...…...ix

List of Tables……...….xi

Acknowledgment……..xii

Chapter 1 INTRODUCTION.....1

1.1 Motivation.....1
1.2 Objective.....3
1.3 Thesis Overview.....4

Chapter 2 WIRELESS OPTICAL LINK MODELING.....7

2.1 Introduction.....7
2.2 Link Configuration.....10
2.2.1 Single-Element Diffusing.....10
2.2.2 Non-directed non-LOS (diffuse).....11
2.3 Channel Model.....12
2.4 Multi-Input Multi-Output (MIMO) System.....16
2.4.1 Source Profile (F).....17
2.4.2 Environment Matrix (Φ).....18
2.4.3 Receiver Profile (G).....19
2.4.4 Direct Response Vector (D).....19
2.4.5 Total Response (H).....21
2.5 Computer Simulation.....23
2.5.1 Received Power per Reflection.....24
2.5.2 Impulse Response.....26
2.5.3 Delay Spread.....28
2.5.4 Received Power.....30
2.6 Conclusions.....31

Chapter 3 RECEIVER NOISE CALCULATION.....33

3.1 Introduction.....33
3.2 Receiver Design.....34
3.2.1 Photodetector Statistics.....36
3.2.2 Linear Filter.....39
3.2.3 Data Recovery Circuit.....40
3.3 Ambient incident light.....41
3.3.1 Window Light.....42
3.3.2 Light Fixtures.....43
3.3.3 Total Noise.....44

Chapter 4 ON OPTIMUM ORDER OF ANGLE DIVERSITY WITH EQUAL-GAIN COMBINING RECEIVERS 46

4.1 Introduction 46
4.2 Available Diversity Channels 48
4.3 Channel and Noise Models 50
4.3.1 Noise Model 50
4.3.2 Channel Model 52
4.3.3 Channel Constraints 55
4.3.4 Receiver Output 57
4.3.5 Link Performance 59
4.4 A More Accurate Channel Model 60
4.5 Performance Measures 64
4.5.1 Receiver with Sub Optimal Timing Circuit 65
4.5.2 Receiver with Optimal Timing Circuit 68
4.6 Simulation Results 70
4.7 Conclusions 76

Chapter 5 ON OPTIMUM ORDER OF ANGLE DIVERSITY WITH MAXIMAL RATIO COMBINING RECEIVERS 78

5.1 Introduction 78
5.2 Maximal Ratio Combining 79
5.2.1 Receiver Output 81
5.2.2 Performance Measures 83
5.3 A More Accurate Channel Model 84
5.3.1 Performance Measures 85
5.4 Simulation Results 87
5.5 Conclusions 91

Chapter 6 SPATIAL CODING IN INDOOR OPTICAL WIRELESS LINK Reducing Power and Bandwidth Requirements 93

6.1 Introduction 93
6.2 Channel Response 95
6.3 Receiver Front-End Design 97
6.4 Link Design 98
6.5 Space Diversity Coding Techniques 101
6.5.1 Equal Gain Combining 101
6.5.2 Orthogonal Spatial Signaling 102
6.6 Simulation Results 103
6.6.1 Fixed Power Per User 103
6.6.2 Fixed Power Per Channel 104
6.7 Conclusions 106

Chapter 7 ON MERITS OF SPATIAL CODING IN MULTILEVEL OPTICAL WIRELESS LINKS 108

7.1 Introduction 108
7.2 Available Spatial Channels 109
7.3 Spatial Coding Technique 111
7.3.1 Multi-Level Signaling with Equal Gain Combining 112
7.3.2 Spatial Coding 113
7.3.3 Simulation Results 114
7.3.3.1 Fixed Power Per Channel 114
7.3.3.2 Fixed Power Per User 116
7.4 Impact of Shadowing 117
7.4.1 Multi-Amplitude Signaling with Combining 117
7.4.2 Spatial Coding 118
7.4.3 Computer Simulation 120
7.5 Conclusions 124

Chapter 8 ASSESSING THE FEASIBILITY OF NEW DIFFUSED CONFIGURATION FOR OPTICAL WIRELESS LINK DESIGN 125

8.1 Introduction 125
8.2 Channel Model 126
8.3 Link Profile 129
8.3.1 Path Loss 129
8.3.2 Delay Spread 132
8.4 Conclusions 136

Chapter 9 CONCLUSIONS AND FUTURE WORK 137

9.1 Summary of Results 137
9.2 Recommendations for Future Work 140
9.2.1 Environment Characterization 141
9.2.2 Spatial Coding 142
9.2.3 Spatial Channel Hopping (SCH) Multiple Access 143
9.3 Publications 144

Bibliography 146

LIST OF FIGURES

Figure 3-1: Simplified block diagram of optical receiver. 34

Figure 3-2: Photodetector Model. 35

Figure 3-3: Illustration of photocarrier generation. (a) Incident optical signal, (b) Times at which photocarriers are produced, (c) Photocarrier displacement current response waveform, (d) Current response resulting from photocarriers. 38

Figure 3-4: Linear filter in optical receiver 40

Figure 3-5: Ceiling view showing the location of 9 Tungsten lamps. 43

Figure 3-6: Incident Power distribution for single branch receiver with FOV=40^{o}. Each pixel represents a location and its intensity represents a power level (a) Incident power resulting from light through window, (b) Incident power resulting from 9 Tungsten lamps. 45

Figure 4-5: Multibranch angle diversity receiver, using equal-gain combining. 59

Figure 5-1: The *j*th channel with an angle diversity receiver. 80

It can be seen from Eq. (5.19) that the receiver output suffers from ISI caused by the residual temporal dispersion. This ISI degrades the receiver performance and results in a higher probability of bit error. 85

Figure 5-2: Average probability of error for 1156 receiver locations. 89

Figure 5-3: Outage probability versus number of branches for different FOV_{branch} used. 90

Figure 5-4: Average SNR versus the total number of branches (for all 1156 locations) 91

Figure 6-1: Cross section of MSDC indoor link. By properly selecting receiver parameters, uncorrelated spatial channels are created. 94

Figure 6-2: The channel impulse responses as seen by 8-branch receiver. 97

Figure 6-3: Ceiling view showing diffusing spots and receiver coverage area. 98

Figure 6-4: (a) Equivalent link model using combining. (b) Link model using spatial coding. 99

Figure 6-5: Probability of bit error when power allocated per user is fixed..... 104

Figure 6-6: Comparing coding gain and bandwidth saving for different coding techniques. 105

Figure 7-1: Available spatial channels for different receiver locations. A '+' symbol represents a diffusing spot. 110

Figure 7-2: Percentage of locations vs. the number of available channels for an 11-branch receiver. 111

Figure 7-3: Probability of bit error when power allocated per channel is fixed. 115

Figure 7-4: Probability of bit error when power allocated per user is fixed. 116

Figure 7-5: Comparing BER for combining and spatial coding links under normal operation (a) and shadowing (b) when the power per channel is fixed. 122

Figure 7-6: Comparing BER for combining and spatial coding links under normal operation and the power per user is fixed. 123

Figure 8-1: (a) Traditional diffused configuration. A transmitter placed at the room center is used to illuminate the ceiling. (b) Proposed configuration. A transmitter placed at the ceiling is used to illuminate the upper regions of the walls 126

Figure 8-2: Comparing the impulse response of a receiver located at (1,2,0.9). 129

Figure 8-3: (a) Histogram plot of path loss for a ceiling diffused configuration. (b) Histogram of path loss for wall diffused configuration. 131

Figure 8-4: (a) Contour plot of path loss (dBo) for a ceiling diffused configuration. (b) Contour plot of path loss (dBo) for a wall diffused configuration. 132

Figure 8-5: (a) Histogram plot of delay spread for a ceiling diffused configuration. (b) Histogram of delay spread for wall diffused configuration. 134

Figure 8-6: (a) Contour plot of delay spread (sec) for a ceiling diffused configuration. (b) Contour plot of delay spread (sec) for wall diffused configuration. 135

LIST OF TABLES

Table 2-1: Link parameters used in computer simulations. 24

Table 4-1: Available FOV_{total} for different number of branches. 50

Table 4-2: Parameter values used in the computer simulations. 72

Table 5-1: Parameters used in computer simulation. 87

Table 6-1: Comparing coding gain and bandwidth saving for different coding techniques. 106

Table 8-1: Room parameters used in study 128

ACKNOWLEDGEMENTS

I wish to express my deepest appreciation to my professor and thesis advisor, Professor Mohsen Kavehrad. His guidance, encouragement, enthusiasm, sense of humor and creative ideas have made this program especially educational and rewarding experience.

Much gratitude and thanks are also extended to my committee members: Professors J. Metzner, S. Yin and N. Gautam, for their time, encouragement and help. I had the pleasure of knowing the faculty, students and staff of the Center for Information and Communication Technology Research at Penn State University over the past few years, many of whom have helped me immeasurably. Thank you very much. In particular, I wish to acknowledge my colleague Dr. Samer Taha for his help and friendship.

I would like to thank my wife, Michelle, for her patience, support and understanding. Without her encouragement, the completion of this work would not have been possible.

Finally, I would like to dedicate this thesis work to my parents, Ahmad and Hajer. They were my first teachers, and the ones who gave me endless love and support throughout my life. I shall forever be grateful to them.

Chapter 1

INTRODUCTION

1.1 **Motivation**

Indoor wireless communication is driven by the ever-growing demand for portable and mobile devices capable of processing and displaying high quality images, videos, and other broadband applications. The popularity of indoor wireless connectivity will lead to even higher demand on limited resources. This created many challenges that frame our optical wireless communications research.

Two technologies, characterized by the electromagnetic spectrum band used by their carriers, enable indoor wireless communications: radio frequency (RF) and infrared (IR) [1]-[5]. Using IR in optical wireless links provides a secure and a promising alternative to radio for indoor wireless connectivity. The large spectrum of unregulated band enables a link to provide broadband access needed for multimedia and other bandwidth-demanding applications. The inability of the infrared light to pass through opaque obstacles provides interference-free bandwidth-reuse in adjacent rooms. Optical links do not suffer from multipath fading due to spatial diversity reception provided by a large detector area compared to signal wavelength. The ability to create spatially independent channels in a small physical space, such as a room, not only holds the promise of large link capacity, it also facilities the application of novel techniques to enhance performance that can only be used at large cost in radio frequency links. The creation of spatial channels is made

possible by the narrow beam widths afforded by optical frequencies. A low cost laser transmitter is able to generate a narrow beam that suffers little diffraction while traveling to a receiver. Most of the energy in the beam can be captured by a photodetector of surface area that does not exceed 1 cm^2.

The main challenges in the design of an IR link include: susceptibility to shadowing, multipath dispersion, and limited range resulting from the noise generated by ambient light. Shadowing caused by benign objects blocking signal path results in service degradation, if not complete interruption. Multipath results in configurations that employ wide beam transmitter to service many receiver locations. This multipath results from signal reflections off of walls, furniture and other objects. Multipath can potentially result in dispersion that would limit the achievable data rate without countering effects of intersymbol interference. Noise at the receiver is generated by ambient light. Even in a uniformly lit environment, noise generated by sunlight through windows and other light fixtures, varies depending on the receiver location and orientation with respect to light sources.

Several configurations are proposed and studied for link design [6-10]. These configurations are classified according to their directivity and Line-of-Sight (LOS). A link is referred to as directed if the receiver and the transmitter have a narrow radiation pattern and Field-of-View (FOV), respectively. In a non-directed link, the transmitter has a broad radiation pattern and the receiver uses a large FOV. A LOS/non-LOS classification depends on whether an unobstructed path between a transmitter and a receiver exists.

Directed LOS link reduces path loss at the expense of disabling receiver mobility. The link can easily be lost if obstructed by an object. To solve this problem, non-directed non-LOS link (also known as diffuse) is used, where the optical power is projected onto a reflecting surface, chosen to be accessible to most receiver locations. The link does not require transmitter/receiver alignment, and thus provides robustness against link loss due to blockage. This configuration, however, suffers from a high path-loss due to the absence of a direct path and data rate limitation caused by reflections. This latter limitation results from multipath temporal dispersion caused by different paths (including reflections off of walls and ceiling) the signal takes to travel to a receiver.

1.2 **Objective**

To combat the adverse effects of temporal dispersion in high-speed applications, an accurate channel impulse response is needed. The impulse response is used to analyze and compensate for the effects of multipath dispersion. In this work, a new approach of obtaining the channel impulse response is presented. This results in tremendous savings in calculation time and brings insight into the link behavior.

The ability to create spatially independent channels has motivated a new configuration, namely multi-spot diffusing (MSD) configuration [11]. The transmitter generates multi-spots on a reflective surface that can be accessed by a receiver. Thus, the transmitter acts an array antenna, with each element transmitting data over an independent channel. A multibranch receiver with branches matched to diffusing spots is employed to receive an independent copy of transmitted data through each of its branches

[12]. In this thesis, we analyze the link with the objective of determining the optimal number of branches at receiver that results in the maximum signal-to-noise ratio, minimum probability of error, and minimum outage probability. Links that utilize equal gain combining and maximal ratio combining are studied.

The availability of N spatial channels implies the possibility of increasing the data rate by at least N-fold compared to a single channel. This can be accomplished simply through a serial to parallel conversion of transmitted data using available channels for simultaneous transmission of data. This, however, does not take advantage of the added dimensionality made available through spatial information from the channel carrying the data. This information enables the receiver to make a decision based not only on the received data, but also through comparing and contrasting data from different channels. If the received signals are plotted on a signal space diagram, information is exchanged not only through the location of the individual signal in the space, but also from its location relative to other signals. It is this relative location that can be used to carry information over the link. This thesis considers different coding techniques that make use of the spatial information and investigates their performance. These coding techniques are based on the signal parameters, as well as spatial channels information.

1.3 **Thesis Overview**

The thesis is divided into 9 chapters, including the introduction. In Chapter 2, indoor channel impulse response is discussed. A novel approach is introduced to efficiently calculate the impulse response. The approach is based on decomposing the correlated

impulse response paths into independent components. Therefore, when a single component is changed, the other calculated components can still be used to obtain the new impulse response. The efficiency in the new approach is demonstrated in this chapter by considering a diffuse link configuration. The new technique can be used with any link configuration and is used throughout the thesis to obtain the impulse response for different link configurations.

In Chapter 3, a receiver design is introduced with a focus on calculating the noise at receiver output. Unlike optical fiber communication, the noise in an optical wireless link is caused by ambient light, which varies according to receiver location and orientation. This creates an added degree of complexity when evaluating link performance. A link design has to ensure performance measures are met at a large percentage of receiver locations. This gives rise to using outage statistics to evaluate a link performance. A small area outage indicates that performance can be satisfied at a large percentage of locations throughout a room.

Chapter 4 considers the design and analysis of link space diversity employing multi diffusing spot configuration. Diffusing spots act as sources and thus create independent spatial channels between transceivers to attain diversity. A multibranch receiver is employed to align transmitted signals through channels to remove time dispersion caused by different path lengths of channels. An equal gain combining is assumed. The chapter gives the optimal number of branches that can be used at the receiver to minimize outage probability. In Chapter 5 we look at the impact the choice of receiver branch FOV has on optimal number of branches when maximal ratio combining is employed. Different values of branch FOV are considered.

Chapter 6 proposes orthogonal spatial coding technique to improve power and bandwidth efficiency. In this technique, each channel is dedicated to carry one of M symbols. The M-branch receiver decides on a transmitted symbol by comparing signals at its input and selecting the symbol that corresponds to a maximum signal.

Chapter 7 looks at another scheme of spatial coding. In this scheme, a symbol is represented by M bits, each transmitted over an independent channel. The performance is compared to multilevel signaling with combining. The chapter also considers the impact of channel shadowing on performance of both schemes.

Chapter 8 uses the approach presented in chapter 2 to assess the feasibility of a diffuse configuration that illuminates upper walls regions, instead of ceiling. This is needed when the ceiling in an environment cannot be used either due to its structure and poor reflection or when it is occupied. For both configurations, delay spread and path loss are compared for large number of receiver locations.

Finally, Chapter 9 summarizes the contributions of the thesis and proposes plans for future work.

Chapter 2

WIRELESS OPTICAL LINK MODELING

2.1 **Introduction**

Several configurations are proposed for the design of an optical wireless link. These configurations are classified according to their directivity and Line-of-Sight (LOS). A link is referred to as directed if the receiver and the transmitter have a narrow radiation pattern and Field-of-View (FOV), respectively. In a non-directed link, the transmitter has a broad radiation pattern and the receiver uses a large FOV. A LOS/non-LOS classification depends on whether or not an unobstructed path between a transmitter and a receiver exists.

Directed LOS link reduces path loss at the expense of disabling receiver mobility. The link can easily be lost if obstructed by an object. To solve this problem, non-directed non-LOS link (also known as diffuse) is used, where the optical power is projected onto a reflecting surface, chosen to be accessible to most receiver locations. The link does not require transmitter/receiver alignment, and thus provides robustness against link loss due to blockage. This configuration, however, suffers from a high path-loss due to the absence of a direct path and data rate limitation caused by reflections. This latter

limitation results from multipath temporal dispersion caused by different paths (including reflections off of walls and ceiling) the signal takes to travel to a receiver.

To combat the adverse effects of temporal dispersion in high-speed applications, an accurate channel impulse response is needed. The impulse response is used to analyze and compensate for the effects of multipath dispersion. Researchers have proposed different approaches to obtain channel impulse response [13]-[25]. Barry et al. [13] introduced a recursive method to compute the impulse response accounting for any number of reflections. A fast method to calculate multipath dispersion using Monte Carlo simulation that enables evaluation of Lambertian and other specular reflections is presented in [14]. In [15], a statistical approach to estimate channel impulse response of a diffuse source is studied to solve the computational complexity using an iterative approach. By slicing into time steps rather than into number of reflections, [16] proposed a fast algorithm for developing comparisons of pulse broadening for several sources and receivers, simultaneously. Using ceiling bounce functional model, a method is developed in [17] to predict path loss for diffuse link based on transmitter and receiver locations within a room. A model based on integration sphere for estimating path loss and bandwidth of diffuse links in rectangular room is provided in [19]. Characterization of indoor environment was also provided through measurements in different room structures and link configurations [21]-[25]. Measurements show good agreement between simulation results and actual measured impulse responses.

All of the above mentioned techniques provide a trade off between impulse response accuracy and simulation time with the technique presented in [13] having very high accuracy at the cost of inefficient and long simulation time. Advancements in processing

and storage of personal computers facilitate extending this technique to enable an efficient computation of impulse response between any number of transmitters and receivers. The method described here consolidates the parameters that determine the impulse response into 4 components: (1) source component contains dependence of impulse response on the source parameters; (2) environment component contains dependence on environment geometry, dimensions, and reflection coefficients; (3) receiver component contains dependence on receiver parameters; and finally, (4) direct component which accounts for direct response. Once calculated, these components are stored for future calculations. Changing parameters of one of the components (e.g. receiver/transmitter location) only affects the value of a single component. When the new value of the affected component is calculated, stored values of other components are used to evaluate a new impulse response. Impulse response dependence on transmitter and receiver components is linear; therefore, impulse response of a transmitter producing L diffusing elements can be calculated by evaluating a component equivalent to L elements. This is helpful when a link uses a large number of diffusing elements, as in diffuse configuration.

When designing a link, it is often the case that only one of the components changes. For instance, the objective might be to calculate the impulse response for a given transmitter configuration at different locations within a room. In this case, an equivalent source-environment component is calculated and used, with the varying receiver component, to obtain an impulse response. This results in tremendous saving in computation time.

This chapter is organized as follows: in section 2, we introduce two configurations that are considered in the chapter. Section 3 discusses the channel model, and the complexity involved in calculating impulse response. In section 4, a new approach to channel modeling is presented. The results of simulation of the impulse response using the proposed approach are provided in section 5. Section 6 uses the new model to obtain profiles for a room using delay spread and received power. Concluding remarks are presented in section 7.

2.2 **Link Configuration**

The two link configurations considered in this chapter are single-element diffusing and non-directed non-LOS. Although, a single-element diffusing is a hypothetical configuration, its consideration serves as a benchmark in deriving the model of non-directed non-LOS. Therefore, we present it as a separate configuration.

2.2.1 **Single-Element Diffusing**

In a single-element diffusing configuration, a transmitter generates a diffusing spot on a reflecting surface, which acts as a Lambertian reflector. Thus, the diffusing spot behaves as a wide-beam transmitter. A receiver with large FOV is used to ensure a LOS component in the impulse response as illustrated in Figure 2-1. The configuration differs in functionality from directed non-LOS in that a receiver is assumed to have a wide FOV.

It also differs from non-directed LOS in not requiring a path between a transmitter and a receiver.

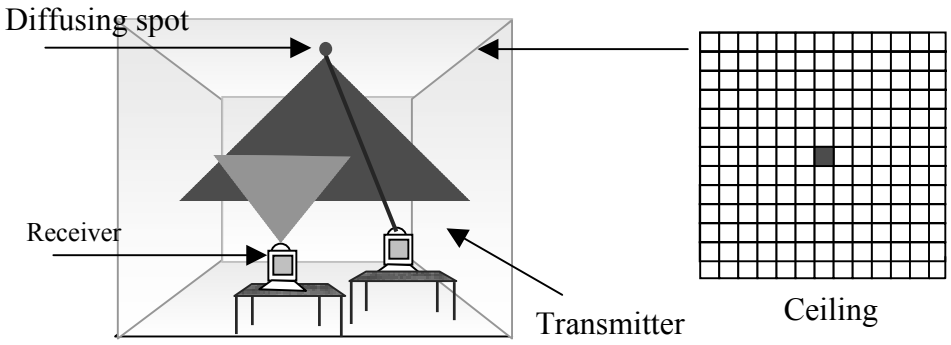

Figure 2-1: Single-element diffusing configuration.

2.2.2 **Non-directed non-LOS (diffuse)**

The non-directed non-LOS is a generalization of single-element diffusing. The transmitter produces diffusing elements on the entire ceiling, as illustrated in Figure-Figure 2-2. A large FOV receiver is used to reduce path loss. The diffuse link enables one-to-many communication without the need for receiver alignment.

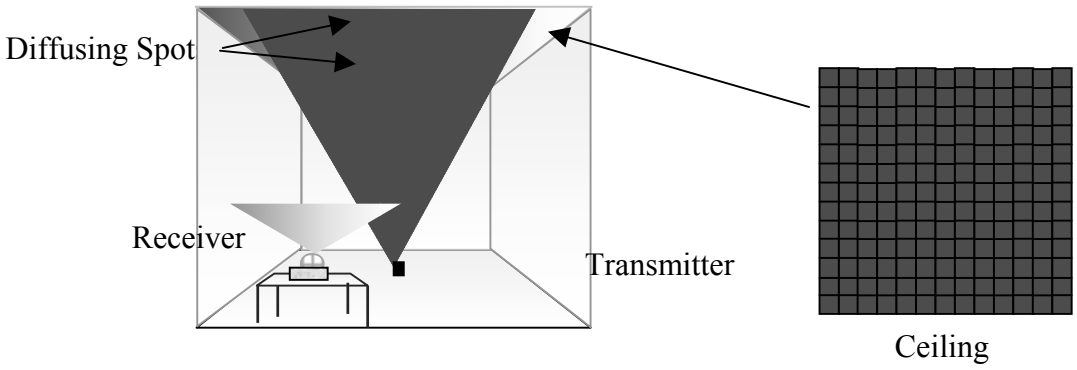

Figure 2-2: Diffuse Link. A transmitter placed at room center is used to illuminate the ceiling.

2.3 **Channel Model**

The complexity in obtaining channel impulse response is brought about by the multiple paths signals take, in traveling from a transmitter to a receiver. This multipath results from reflection off of walls, ceiling, furniture, etc. Room surfaces act as Lambertian reflectors that reflect an incident signal in all directions. Assuming room surface exposed to a transmitter is made of N surface elements, each reflection produces N-1 new reflections, as illustrated in Figure 2-3. When determining channel impulse response, contribution of each element on a surface within receiver FOV should be considered. Since surfaces do not offer perfect reflection and signal strength is inversely proportional to the distance traveled, a finite number of reflections is considered in obtaining an impulse response.

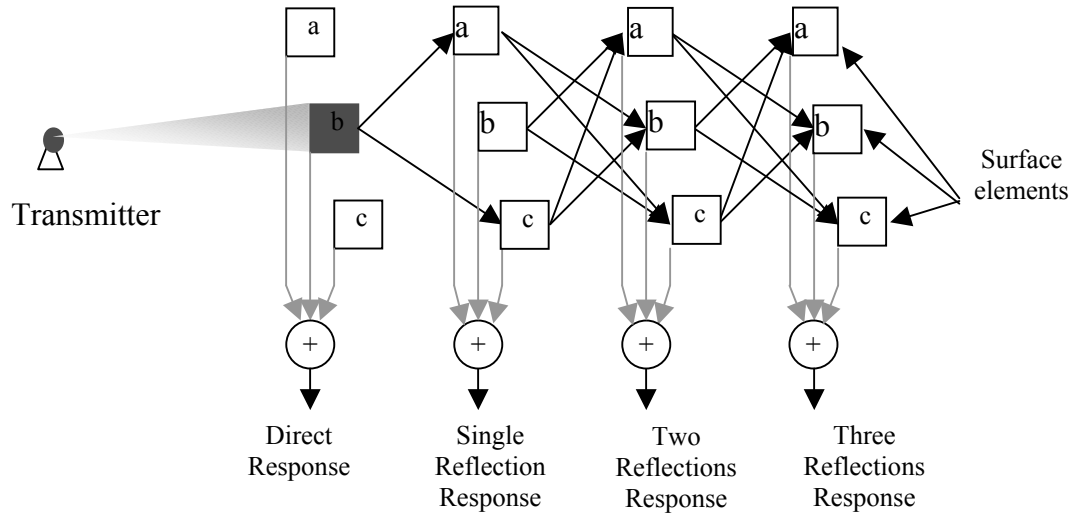

Figure 2-3: Illustration of signal propagation. The room surface is composed of 3 elements: **a**, **b**, and **c**. A transmitter illuminates element **b**. The impulse response of any reflection is found by considering all the elements within the receiver FOV. In this example, all the elements are within the receiver FOV. Complexity in calculating impulse response is caused by reflections. Each reflection results in N-1 new reflections.

Impulse responses are obtained by dividing the reflecting surface into a finite number of reflecting elements N [13]. If N is large, accurate samples of continuous impulse response are obtained. The number of elements N for a rectangular room, of dimensions equal to (W, L, H), is given by:

$$N = 2 \times (n_x \times n_z + n_x \times n_y + n_y \times n_z), \tag{2.1}$$

where

$$\frac{W}{n_x} = \frac{L}{n_y} = \frac{H}{n_z} = \mathrm{d}.$$

Constant d represents the distance between centers of neighboring elements, which is taken to be the same for all surfaces. Every surface element contributes directly to received signal if that element is within receiver FOV, or indirectly through reflections

off of other surfaces, as illustrated in Figure 2-4. The radiation pattern of surface elements is assumed to be first order Lambertian [26]-[28]. They reflect incident light with equal intensity in all directions as shown in Figure 2-5. Therefore, the intensity at an angle θ from the surface norm is proportional to $\cos(\theta)$.

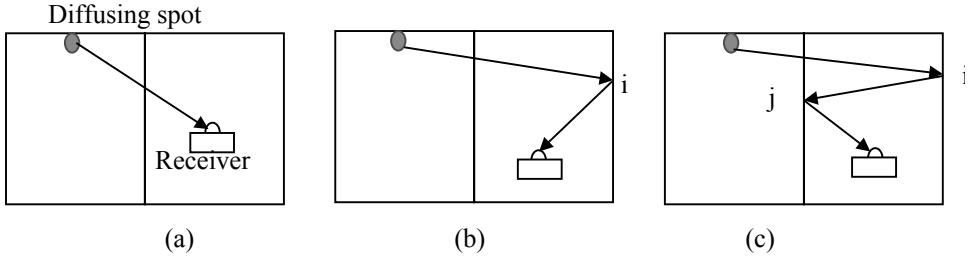

Figure 2-4: Illustration of (a) direct path, (b) single reflection, and (c) two reflections. Reflections are counted from diffusing spots to a receiver.

Figure 2-5: Lambertian Reflector.

The line-of-sight response $h^0(t)$, when the source T is within the FOV of the receiving element R can be expressed as [13]:

$$h_{TR}^{0}(t) = \frac{\cos(\varphi_{TR}) \cdot \cos(\theta_{TR}) \cdot A_R}{\pi \cdot R_{TR}^{\,2}} \delta\left(t - \frac{R_{TR}}{c}\right), \qquad (2.2)$$

where $\cos(\varphi_{TR})$ is equal to dot product of two unit vectors. The first is perpendicular to T and the second originates from R and extends toward T. The angle θ_{TR} is the angle

between a vector perpendicular to R and a vector that lays on the straight line that connects T and R. A_R is the receiving element area, R_{TR} is the distance between T and R, and c is the speed of light. The response after a single reflection off an element i is obtained by treating i as a receiver, and then as a source. The impulse response is given by:

$$h_{TR}^{1}(t) = \frac{\cos(\varphi_{Ti})\cos(\theta_{Ti})A_i}{\pi R^2_{Ti}} \frac{\rho_i \cos(\varphi_{iR})\cos(\theta_{iR})A_R}{\pi R_{iR}^{\ 2}} \delta(t - \frac{R_{Ti} + R_{iR}}{c}), \qquad (2.3)$$

where A_i is the area of the reflecting element i, and ρ_i is its reflectivity. The response resulting from two reflections off element i first and then off element j is found by extending Eq. (2.3) to include impulse response between j and receiver, and is expressed as:

$$h_{i,j,R}^{2}(t) = \frac{\cos(\varphi_{Ti})\cos(\theta_{Ti})A_i}{\pi R^2_{Ti}} \frac{\rho_i \cos(\varphi_{ij})\cos(\theta_{ij})A_j}{\pi R_{ij}^{\ 2}} \frac{\rho_j \cos(\varphi_{jR})\cos(\theta_{jR})A_R}{\pi R^2_{jR}} \delta(t - \frac{R_{Ti} + R_{ij} + R_{jR}}{c}) . \qquad (2.4)$$

Higher reflections impulse response is obtained by adding impulse response of new reflections similar to Eq.(2.4). It is apparent, however, that as more reflections are considered, received power becomes smaller. This is the case since n-th order impulse response is equal to n-1-th order multiplied by a quantity that is much smaller than 1.

Total impulse response is obtained by summing direct and reflection responses. In doing so, all surface elements must be considered. In calculating the 2nd reflection response for instance, N values are used for both i and j in Eq. (2.4) and the resultant second reflection response is the sum of NxN responses. Therefore, calculation complexity is directly proportional to the number of surface elements raised to number of

reflections considered. The impulse response obtained is only valid for a specific transmitter/receiver configuration. Changing any of transmitter/receiver parameters requires the calculations to be performed again. When studying a communication link, we are interested in obtaining impulse responses for a large set of receiver/transmitter parameters. Obtaining the delay spread profile, for instance, requires the calculation of impulse response for hundreds of receiver locations. Performing the above calculations can become prohibitively intensive. It can easily be recognized that many calculations involved in obtaining the impulse response do not change. In the next section, we propose a new representation of transmitter-channel-receiver that makes efficient use of calculations performed. The new representation also provides more insight into the channel characteristics.

2.4 **Multi-Input Multi-Output (MIMO) System**

In the new model, the transfer function between a transmitter and a receiver is divided into 4 components. The first represents the transfer function between a source and surface elements. The second block contains the transfer function between surface elements. The third has the transfer function from surface elements to a receiver. The last component accounts for direct response between a source and a receiver. In our discussion, we assume geometry as well as reflection coefficients are fixed, and the room internal surface is made up of N neighboring elements of equal area. Elements are numbered sequentially, and each element is identified by an index. We refer to diffusing spots as

sources and the device generating them as transmitter. The number of reflections is counted from a source to a receiver.

2.4.1 **Source Profile (F)**

The first component in the new model represents transfer function between source (diffusing spot) and surface elements. It is referred to as Source Profile and is modeled by a single-input multiple-output system with N outputs. The transfer function between a source and each of surface elements is expressed by an entry in a vector F_s. Since surface elements 1 through N receive the signal directly, the transfer function f_{sk} between a source s and element k, is obtained using Eq. (2.2), and is given by:

$$f_{sk} = \rho_k \delta(t - \frac{R_{Ts}}{c}) \frac{\cos(\theta_{sk}) \cos(\varphi_{sk}) A_R}{\pi \cdot R_{sk}^2} \delta(t - \frac{R_{sk}}{c}) u(\frac{\pi}{2} - \theta_{sk}), \quad (2.5)$$

where the first two terms are added to account for the transfer function between a transmitter and a source. For a single source s, the vector F_s is expressed as:

$$F_s = [f_{s1} \quad \cdots \quad f_{sN}]. \quad (2.6)$$

The expression can be extended to include more than a single source. In the case of a diffuse link, where transmitter illuminates ceiling, the equivalent vector F_{eq} is defined as the equivalent of $n_x \times n_y$ sources and is given by:

$$F_{eq} = \sum_{i=1}^{n_x \times n_y} F_i = [f_{eq1} \quad \cdots \quad f_{eqN}], \quad (2.7)$$

where $f_{eqj} = \sum_{i=1}^{n_x \times n_y} f_{ij}$. The source vector is shown as block F_s in Figure 2-4 (a).

2.4.2 **Environment Matrix (Φ)**

The second component consolidates dependence on indoor geometry, dimensions, and reflection coefficients. This component contains the transfer functions between any two reflecting elements. In matrix format, and considering up to n reflections, it is expressed as:

$$\Phi_n = \begin{cases} I_{NxN} + \phi + \phi^2 + \phi^3 + \cdots \phi^{n-1} & , n \geq 2 \\ I_{NXN} & , n = 1 \end{cases} , \tag{2.8}$$

where I_{NxN} is the NxN identity matrix, and ϕ is given by

$$\phi = \begin{bmatrix} \phi_{11} & \cdots & \phi_{1N} \\ \vdots & \ddots & \vdots \\ \phi_{N1} & \cdots & \phi_{NN} \end{bmatrix}. \tag{2.9}$$

The entry ϕ_{ik} represents transfer function between two elements i and k and is given by

$$\phi_{ik} = \begin{cases} 0 & , i = k \\ \dfrac{\rho_i \cos\theta_{ik} \cos\varphi_{ik} A_k}{\pi R_{ik}^2} \delta(t - \dfrac{R_{ik}}{c}) u(\pi/2 - \theta_{ik}) & , i \neq k \end{cases}. \tag{2.10}$$

The environment matrix is independent of transmitter and receiver. Once it is calculated, it can be used with any transmitter/receiver configuration.

2.4.3 **Receiver Profile (G)**

This component contains impulse response dependence on receiver parameters such as location and FOV. It is represented by block G_r in Figure 2-4. The block contains transfer functions between a receiver and N surface elements. In vector form, it is expressed as:

$$G_r = \begin{bmatrix} g_{1r} \\ \vdots \\ g_{Nr} \end{bmatrix}, \tag{2.11}$$

where the entry g_{ir} is given by:

$$g_{ir} = \frac{\rho_i \cos\theta_{ir} \cos\varphi_{ir} A_r}{\pi R_{ir}^2} \delta(t - \frac{R_{ir}}{c}) u(FOV_r - \theta_{ir}) . \tag{2.12}$$

Figure 2-7 shows the amplitude of G entries for different locations and FOV values. It is clear from the figure that the number of non-zero elements is directly proportional to the receiver FOV. The symmetry of the G vector is lost when the receiver is located close to more than one surface, each in a different plane.

2.4.4 **Direct Response Vector (D)**

When a source is within a receiver FOV, a direct response results. This response is expressed as:

$$H^{(0)} = D \cdot G_r , \tag{2.13}$$

where D is a 1xN vector given by

$$D = [d_1 \quad \cdots \quad d_N]. \tag{2.14}$$

The entry d_i is equal to $\delta(t - \frac{R_{Ti}}{c})$ if an element i corresponds to a diffusing spot and 0, otherwise. R_{Ti} accounts for the delay between transmitter and source i. In diffuse configuration, there are $n_x \times n_y$ nonzero elements in D. The direct response is represented by block d_s in Figure 2-6 (a).

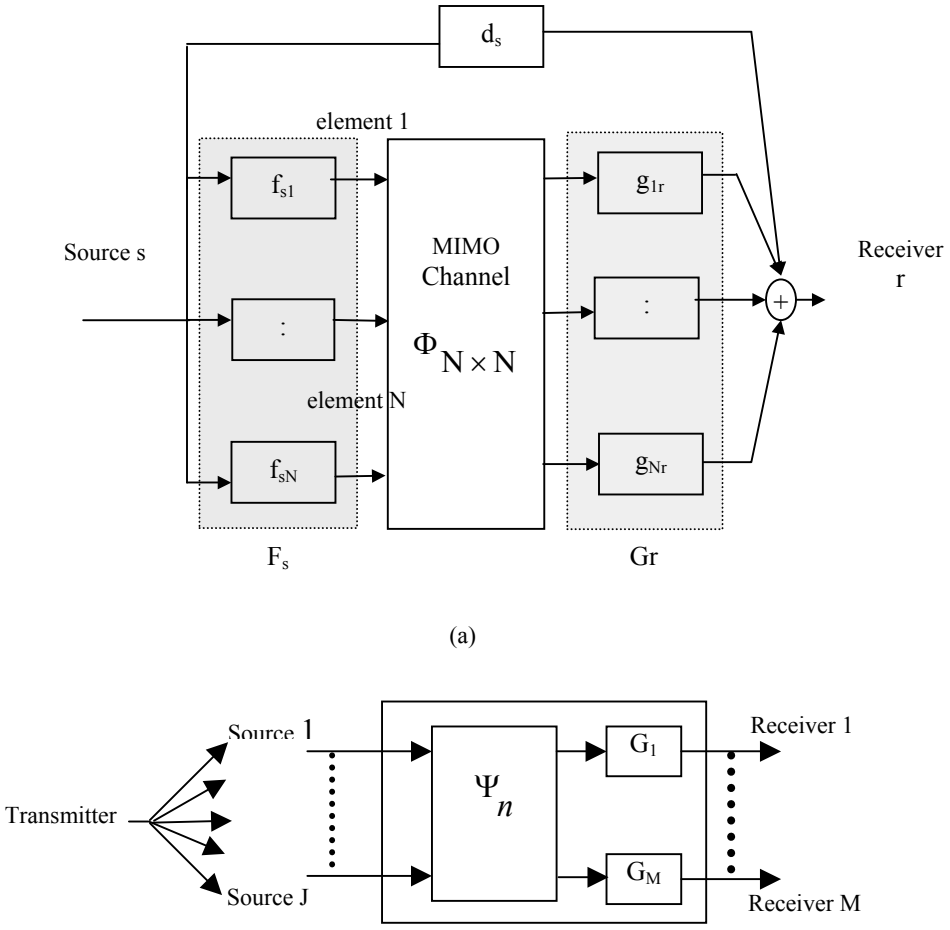

Figure 2-6: (a) New representation of impulse response for a single source and a single receiver. (b) Representation of J sources and M receivers.

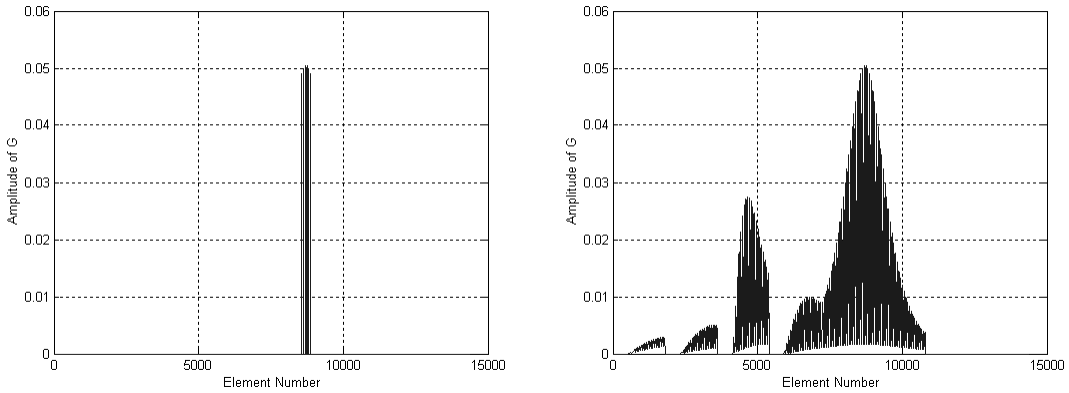

Figure 2-7: (a) Amplitude of the G vector for a small FOV (7^o), the receiver is located at (2.5,4.5,0.9). (b) Amplitude of G at the same location with a larger FOV (90^o). Room dimensions are 6mx6mx3m.

2.4.5 **Total Response (H)**

The total impulse response H between a source s and a receiver when n reflections are considered can be expressed as:

$$\begin{aligned} H &= \sum_{i=0}^{n} H^{(i)} \\ &= D \cdot G_r + F_s \cdot \Phi_n \cdot G_r . \end{aligned} \tag{2.15}$$

If a vector Ψ_n that contains N entries is defined as:

$$\Psi_n = D + F_s \cdot \Phi_n . \tag{2.16}$$

H can be written as:

$$H = \Psi_n G_r . \tag{2.17}$$

The matrix Ψ_n contains the signals seen by each element of a room surface. By multiplying by G_r, the signal is shifted to account for the delay between elements and receiver and multiplied by a factor that depends on the path between each element and receiver. The expression for H in Eq. (2.17) readily applies to a diffuse link by substituting for F the F_{eq}.

One of the advantages attained by the new model is highlighted in Eq. (2.17). In analyzing an IR link, we are often interested in the impulse response for many receiver locations within a room. The room and transmitter parameters do not change, only the parameters of the receiver change. Using Eq. (2.17) to calculate a new impulse response requires calculating the new value of G_r and multiplying by Ψ_n, which is already calculated. This is illustrated for M receiver locations in Figure 2-4(b). The time required for calculating Ψ_n is comparable to that required to calculate a single impulse response. Once Ψ_n is calculated and stored, however, the time required to calculate a new impulse response is reduced to calculating the multiplication of two matrices, which takes a very short time.

The new model can result in timesaving even when a single impulse response is calculated. By calculating receiver vector G_r first, the elimination of any unnecessary calculation is possible. This is especially true when the receiver FOV is small, since the nonzero entries in G_r are a small fraction of total entries. When the k^{th} entry in G_r is zero, the corresponding k^{th} column in Ψ_n does not affect the calculation since it is multiplied by

zero. Therefore, for n nonzero entries in G_r, only corresponding n columns in Ψ_n have to be calculated.

2.5 **Computer Simulation**

In carrying out simulation on a personal computer, entries in the F,Φ, and G are represented as complex numbers with phase equal to time delay. Since the delay takes on a very small value, it is expressed as an integer multiple of sampling time T_s. The value of T_s is chosen to be equal to the time it takes light to travel between two neighboring elements [13], i.e.

$$T_s = \frac{d}{c}. \tag{2.18}$$

When performing addition, only terms that have equal delay are added together. Thus,

$$ax^{-n_i} + bx^{-n_j} = \begin{cases} (a+b)x^{-n_i} & ; i = j, \\ ax^{-n_i} + bx^{-n_j} & ; i \neq j. \end{cases} \tag{2.19}$$

The impulse response H_c is defined as the received optical power when a transmitted optical power is equal to a delta function with a unit-area, i.e., 1 W [1]. In order for area under the impulse response to be equal to received power, Eq. (2.15) is divided by T_s. The impulse response H_c resulting from matrix multiplication and simplification is in the form:

$$\begin{aligned} H_c &= (\frac{1}{T_s}) \times [D \cdot G_r + F_s \cdot \Phi_n \cdot G_r] \\ &= h_0 x^{-n_0} + \cdots + h_{K-1} x^{-n_{K-1}}, \end{aligned} \tag{2.20}$$

where h_i is the amplitude of the impulse response at time equal to $n_i \times T_s$. Environmental parameters used in computer simulation are summarized in Table 2-1.

Table **2-1**: Link parameters used in computer simulations.

Room Parameters	Diffuse
Width(W)	6 m
Length(L)	6 m
Height(H)	3 m
$\rho_{wall1}=\rho_{wall2}=\rho_{wall3}=\rho_{ceiling}$	0.7
$\rho_{wall4\ (Window)}$	0.04
ρ_{floor}	0.2
Source Parameters	
Location (x,y,z)	Covering the ceiling
Number of spots	3600
Transmitter	
Location	(3.0,3.0,0.9)
Receiver Parameters	
FOV	90^o
Other Parameters	
d	0.2
N	3600

2.5.1 **Received Power per Reflection**

The new model makes it possible to obtain received power for any order of reflection. Received power for a reflection order is defined as the area under impulse response of that reflection when 1W power is transmitted. In terms of the new model, this can be expressed as:

$$P_i = \begin{cases} |F| \cdot |\Phi_i| \cdot |G| & ,i \geq 1, \\ |D| \cdot |G| & ,i = 0, \end{cases} \tag{2.21}$$

where |x| denotes amplitude of x, and i is the reflection order. For the same receiver parameters, the amount of received power in each reflection depends on the receiver's location. When the receiver is close to a reflecting surface, the reflected power contributes more to the total receiver power. The average percentage of total power, as more reflections are added for the environment considered in the simulation, is shown in Figure 2-8. The figure shows that, on the average, more than 95% of total power is contained in the direct, 1^{st}, 2^{nd} and 3^{rd} reflections. In addition, the contribution of a reflection decreases as reflection order increases. As the complexity in calculating Eq.(2.8) grows as more reflections are considered. A trade off that guarantees 95% of total power is achieved by considering 3 reflections. Therefore, all results below are calculated by considering direct response along with 3 reflections in the impulse response.

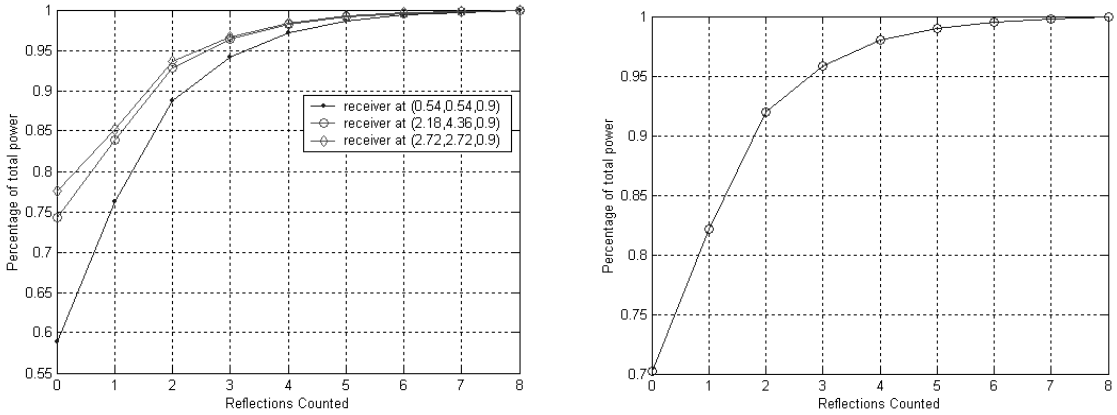

(a) (b)

Figure 2-8**:** (a) Percentage of received power in each reflection for different locations. (b) Average percentage of total received power versus number of reflections considered, 100 receiver locations are used to calculate the average.

2.5.2 **Impulse Response**

The impulse responses resulting from direct, single reflection, 2 reflections, 3 reflections, and total response are plotted in Figure 2-9(a)-(e), respectively, for a single diffuse source. It is apparent from the figure that the total power contributed by a reflection decreases as the reflection order increases. The impulse responses of receivers, located at the room center and close to room corner, are shown in Figure 2-10, for a diffuse configuration. The figure illustrates temporal dispersion, when a diffuse configuration is used.

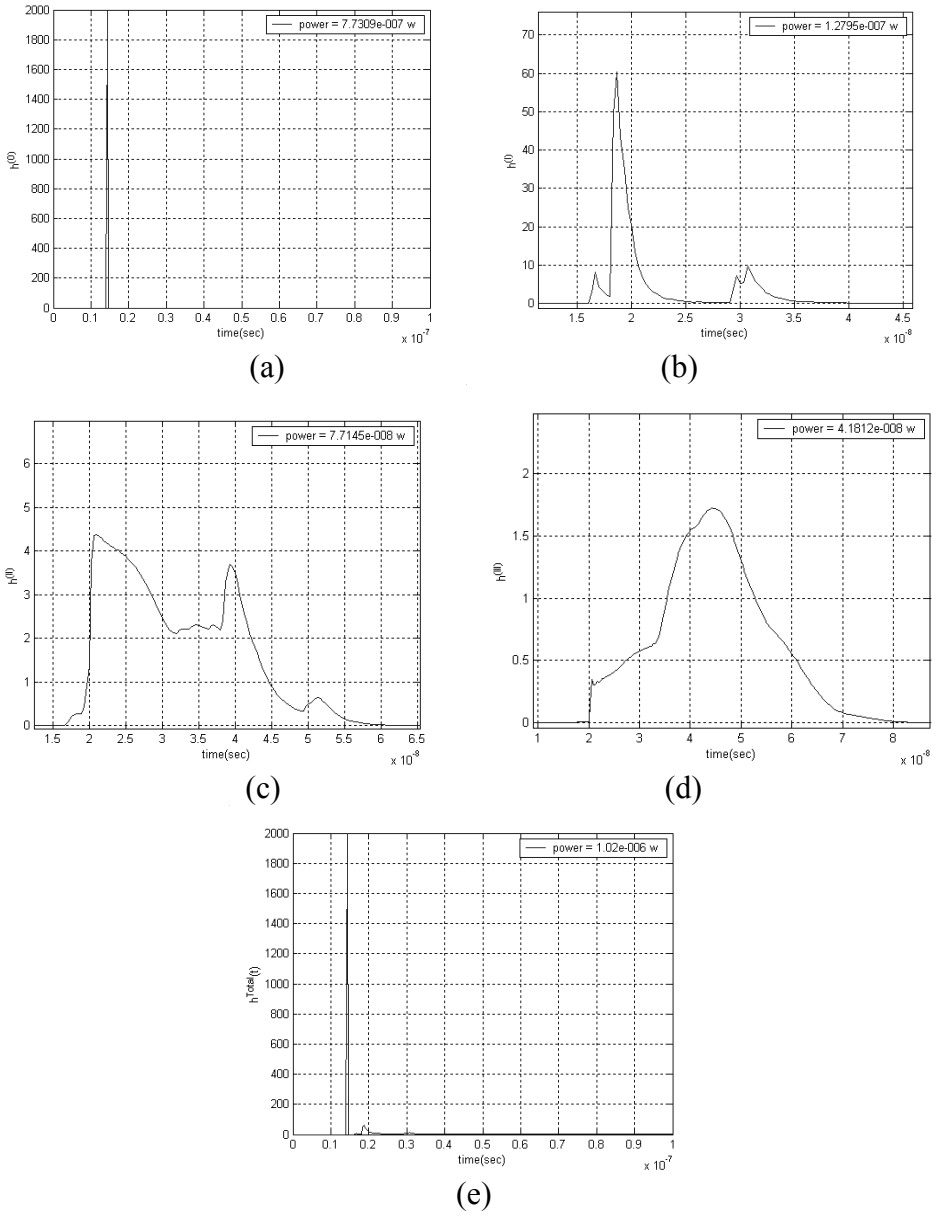

Figure 2-9: (a) Direct response. (b) The response resulting from single reflection. (c) The response resulting from two reflections. (d) The response resulting from three reflections. (e) Total response given by the sum of the direct, first and second responses. The link uses a single diffusing source.

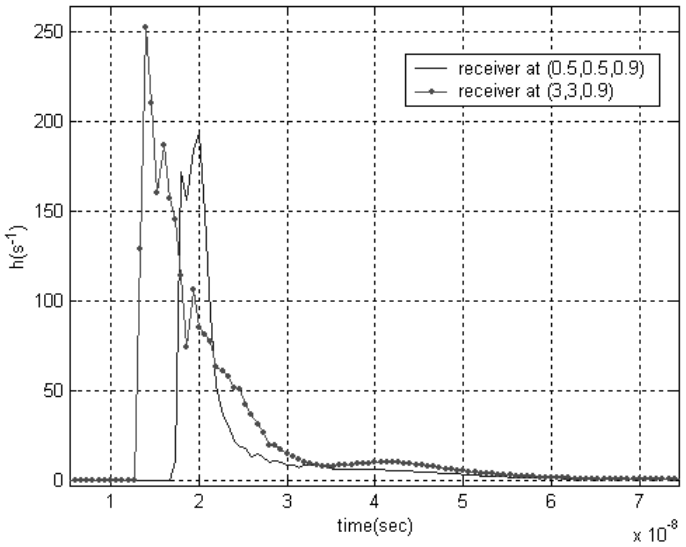

Figure 2-10: Impulse responses of a diffuse link for receivers located at (0.5,0.5,0.9) and (3,3,0.9).

2.5.3 **Delay Spread**

Intersymbol interference resulting from propagation in a dispersive channel is a major problem in the design of a broadband wireless link. The dispersion in the channel sets the limit on the symbol length that can be used. As dispersion increases, symbols have to be placed at farther time intervals in order to reduce the adverse effect of dispersion [21]. This, in turns, reduces achievable bit rate. A measure of dispersion is provided by root mean square delay spread $T_{delayspread}$ defined as the second moment of the impulse response, and is given by [25]:

$$T_{delayspread} = \sqrt{E(\tau^2) - (E(\tau))^2} \ . \qquad (2.22)$$

In terms of H

$$E(\tau^n) = \frac{\sum_i \tau_i^n h_i^2}{\sum_i h_i^2} = \frac{\sum_{i=0}^{K-1} (i \times T_s)^n \times h_i^2}{\sum_{i=0}^{K-1} h_i^2}. \quad (2.23)$$

The profile of delay spread is shown in Figure 2-11. The highest delay spread is shifted from the room center away from the wall covered by a window; the spread decreases as receiver locations move away from the room center. Equal delay spread Locations belong to rings surrounding the maximum spread location. A total of 5776 receiver locations are considered in the computer simulations.

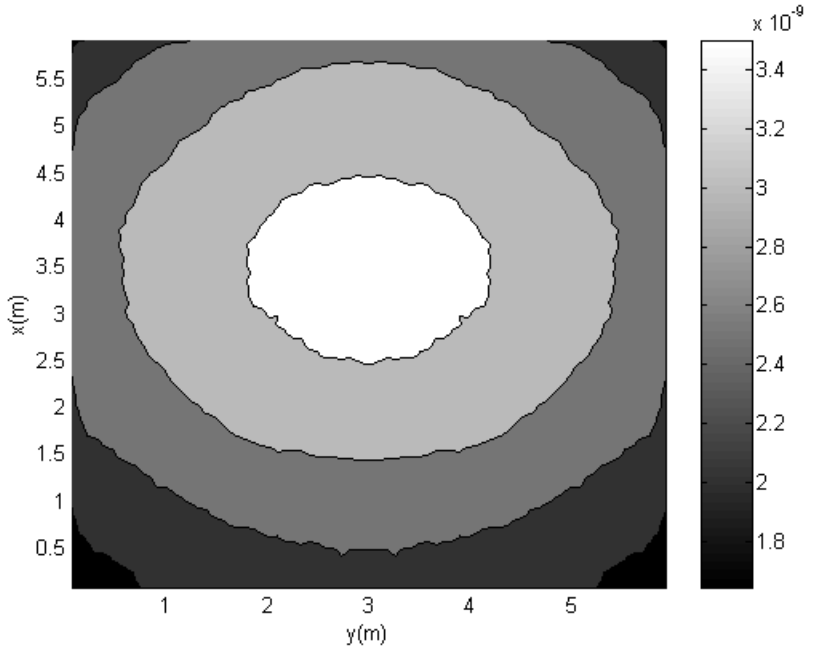

Figure 2-11**:** Delay spread contour plot. The window wall is located at x=0.

2.5.4 **Received Power**

Another measure of an optical link quality is provided by the total received power defined as the area underneath the impulse response curve:

$$P_{received} = T_s \times \sum_{i=0}^{K-1} h_i \quad . \tag{2.24}$$

Received power provides a measure of attenuation for a transmitted signal due to propagation and reflections. The received power is related to path loss PL by [46]:

$$PL = -10\log_{10}[P_{received}]. \tag{2.25}$$

Figure 2-12 shows the received power profile. Received power takes the highest value at a receiver location shifted from the room center away from the window. The power level falls as the receiver moves away from the maximum power location. The figure shows a small received power in the regions close to room corners. The regions of constant power are defined by rings surrounding the maximum power location.

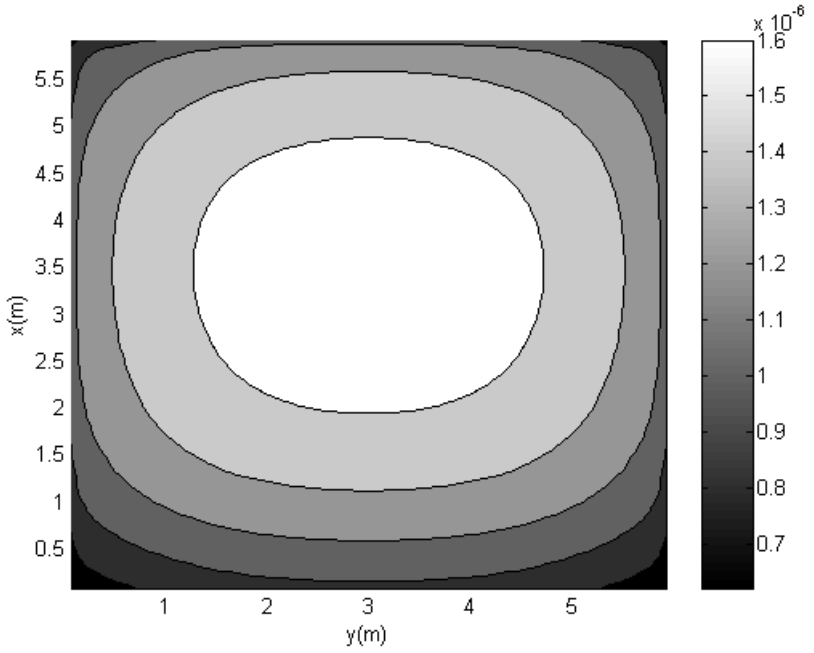

Figure 2-12: Received power contour plot. The window wall is located at x=0.

2.6 **Conclusions**

In this chapter, a new representation of indoor optical link is introduced. The representation divides the physical path between a transmitter and a receiver into stages. Each stage consolidates a set of parameters upon which an impulse response depends.

This results in a tremendous savings in calculation, especially when only one of the parameters is changed, such as location of a transmitter or a receiver.

The new representation enables us to calculate received power per reflection for a very high order of reflections. It is shown that the received power falls sharply with every new reflection. This justifies the consideration of the first few reflections when calculating an impulse response.

Temporal dispersion caused by multipath is one of the factors that limits achievable bit rate over a diffuse link. Through the efficient calculation of impulse response, delay spread and received power profiles were generated. Both are obtained from channel impulse response. The matrix Ψ is calculated and stored in a file and is used to calculate impulse response at each new location. The time required to calculate Ψ is comparable to that required to calculate a single impulse response. Once Ψ is obtained, the calculation of a new impulse response requires less than 30 seconds.

Chapter 3

RECEIVER NOISE CALCULATION

3.1 Introduction

One of the impairments in a wireless optical communication system results from ambient light produced by sun radiation through windows, and other artificial light sources [29]-[34]. In optical links, a receiver converts impinging optical signal into an electrical signal that can later be processed. This conversion adds shot noise resulting from ambient light that determines among other parameters the link achievable bit rate.

To combat the effects of ambient light, both electrical [33] and optical filtering [34] are employed. Electrical filtering is used to reduce low frequencies components caused by ambient light, thus reducing power penalty on transmission system. Optical filtering reduces undesired optical power reaching the photodetector. Both long-pass and band-pass (interference filters) can be used [30].

In its simplest form, an optical receiver contains a photodetector, a filter, and a data recovery circuit. In the first part of this chapter, receiver components are discussed to model noise at receiver output. The noise is found to depend on the incident optical power, which varies according to receiver location and orientation. The second part of the

chapter presents the technique used to calculate incident power from ambient light sources.

3.2 Receiver Design

The design of an optical receiver depends on the modulation scheme used. In a link using intensity modulation/direct detection scheme (assumed in this chapter), the receiver is composed of a front-end photodetector, a linear filter, and a data recovery circuit, as illustrated in Figure 3-1 [35].

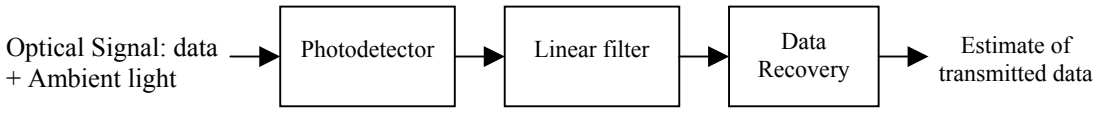

Figure 3-1: Simplified block diagram of optical receiver.

In photon effects, the photodetector absorbs photons from incident lightwave through atomic interactions in the photodetector material. These interactions produce photocarriers, which corresponds to the formation of an electron-hole pair. The photocarriers transport a charge that results in an electrical photocurrent.

The incident optical signal at the photodetector can be modeled as a stream of photons. For a monochromatic lightwave, photons have the same energy, which is independent of the incident signal [36]. This is true since the energy depends only on the frequency i.e. E=hv, where h is the Plank's constant and v is the frequency of the light.

The rate of photon arrivals is proportional to incident power. Therefore, it is possible to measure power levels of incident signal by counting the photons during a time interval. This is referred to as photon counting. Figure 3-2 illustrates the model of a photodetector that uses photon effects [36]. The model consists of a photon to photocarrier converter and a low pass filter to account for the finite response time of a photodetector. The photocarriers i'(t) are a series of impulses, each carries a charge of q (coulombs), corresponding to the charge of a single electron. The process that describes the times at which the photocarriers are generated is random.

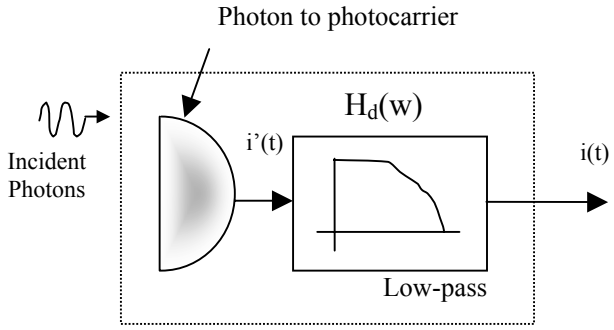

Figure 3-2: Photodetector Model.

The number of carriers generated depends on the power in the incident optical signal during an observation time. Since there are more photons per watt at long wavelengths than there are at short wavelengths, and the number of photons determines the current, longer wavelengths produce more current per watt than do shorter wavelengths.

3.2.1 Photodetector Statistics

In order to understand the performance of a receiver, the statistics of detection process must be considered. Unlike microwave systems, an optical system is not limited by thermal background noise. This can be understood by considering the corrected expression for noise spectral density [37]:

$$N(f) = \frac{hf}{\exp(\frac{hf}{kT}) - 1}, \tag{3.1}$$

where f is the frequency, h is Planck's constant, k is Boltzman's constant, and T is the temperature (k). The noise spectral density falls to a very small value in the optical frequency range compared to microwave frequency. For example, the spectral density is equal to 3.99×10^{-21}(watt/Hz) at f=10 GHz, and it drops to 1.66×10^{-33}(watt/Hz) when the frequency is increased to 200THz ($1.5\ \mu m$). Therefore the thermal noise is negligible whenever the frequency is larger than 150THz.

The limit on detectable optical power level is set by a phenomenon known as shot (quantum) noise. When an ideal photodetector is illuminated by a pulse with optical energy equals to E (joules), the number of photocarrier generated is given by a Poisson distribution [37], i.e., the probability that m photocarriers are generated is:

$$P(m) = \frac{(\Lambda)^m e^{-\Lambda}}{m!}, \tag{3.2}$$

where $\Lambda = \mathrm{E}/\mathrm{hv}$ is the average number of photons in the pulse. Thus, even when E is known, any number of photocarriers can be generated. On average, however, the number

is equal to E/hv. A realization of this event is depicted in Figure 3-3 [37]. The current generated in response to a constant optical signal can be expressed as:

$$i(t) = I_{DC} + i_s(t), \tag{3.3}$$

where $I_{DC}=RP_{rcvd}$ is the average current, $i_s(t)$ is the shot noise current, and $R = \frac{\eta q}{hv}$ is detector responsivity. The parameter η accounts for the inherent inefficiency in the conversion from photons to photocarriers known as quantum efficiency and is given by [36]:

$$\eta = \frac{\text{number of photo carriers produced}}{\text{number of incident photons}}. \tag{3.4}$$

Statistically, $i_s(t)$ is a random process with Poisson statistics. When the mean photocarrier counting rate is high exceeding one hundred photocarriers per observation time, it is possible for photo detection statistics to be well approximated by a Gaussian distribution [35][36]. This simplifies the analysis since Poisson distribution does not lend itself to a convenient analytical manipulation. The detection statistics can be expressed as:

$$P(i) = \frac{1}{\sqrt{2\pi}\sigma_s} \exp\left\{-\frac{(i - I_{DC})^2}{2\sigma_s^2}\right\}. \tag{3.5}$$

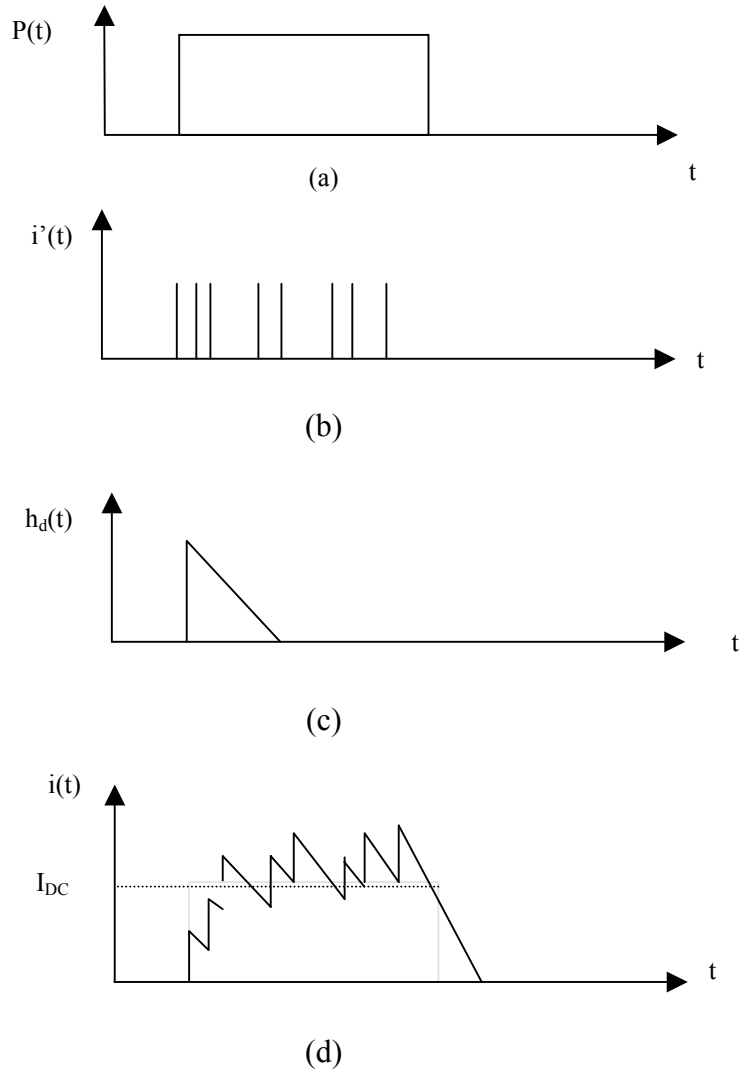

Figure 3-3: Illustration of photocarrier generation. (a) Incident optical signal, (b) Times at which photocarriers are produced, (c) Photocarrier displacement current response waveform, (d) Current response resulting from photocarriers.

The spectral density of shot noise at the input to the filter is constant and is given by $S_s(f)=qI_{DC}$ [35]. The noise variance at the output of the filter represents the amount of power in the noise and is given by:

$$\sigma_s^2 = R_{ss}(0) = E[i_s(t)i_s(t)] = \int_{-\infty}^{\infty} S_{ss}(f)df = qI_{DC}\int_{-\infty}^{\infty} \left|H_d(f)\right|^2 df \ . \qquad (3.6)$$

If the filter is an ideal low pass filter with amplitude spectrum equals to one and bandwidth equals to B, the expression simplifies to:

$$\sigma_s^2 = 2qI_{DC}B \ . \qquad (3.7)$$

Two observations are made with regard to shot noise. First, the variance of shot noise increases as I_{DC} increases; this is fundamentally different from a microwave receiver where an increase in received power only increases the recovered signal component. The microwave receiver's noise, being set by thermal noise, stays constant [35]. Second, unlike fiber optic system, the incident power is determined by ambient light and not the information signal. This is the case, since ambient light power level far exceeds the information modulated transmitted power in a wireless optical system.

In order to obtain the noise at a receiver, the ambient light falling on the surface of the receiver must be calculated. In the next part of the chapter, we present the technique used to evaluate the incident optical power at the receiver.

3.2.2 Linear Filter

The linear filter in the optical receiver provides three functionalities. First, it equalizes the limited bandwidth of front-end photodetector. Second, combined with transmitter filter, it is designed to reduce intersymbol interference ISI resulting from the spreading of a pulse beyond its allocated bit slot. Finally, the filter amplifies the signal by incorporating a high-gain amplifier.

If the channel is ideal, ISI is prevented by employing a transmitter/receiver filter with a raised cosine response. When the receiver is responsible for half of the pulse shaping, a square root cosine filter $G_r(f) = \sqrt{A} \times X_{src}(f)$ is employed, as shown Figure 3-4, where $\sqrt{A}$ is the amplifier gain and $X_{src}(f)$ is a unit energy square raise cosine pulse. The noise variance at the output of the linear filter can be obtained using Eq.(3.6), and is given by:

$$\sigma^2 = qI_{DC}\int_{-\infty}^{\infty}(\sqrt{A})^2\left|X_{src}(f)\right|^2 df = qI_{DC}A \tag{3.8}$$

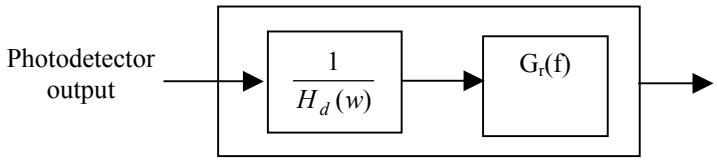

Figure 3-4: Linear filter in optical receiver.

3.2.3 Data Recovery Circuit

The data recovery circuit consists of a decision circuit and a timing circuit. The latter provides the sampling time of the filter output and it is responsible for the alignment of strong signal components in a multibranch receiver. The decision circuit uses the sampled value of timing circuit output to decide on the transmitted data. Since the noise is

stationary, the variance at the sampler output is equal to that at its input. Therefore, the noise variance at the input to decision circuit is:

$$\sigma^2 = E\{n^2(t)\} = E\{n^2(t)\} = qI_{DC}A\,. \tag{3.9}$$

3.3 Ambient incident light

The expression for the noise variance (Eq.(3.9)) shows the dependence on ambient light, i.e., I_{DC} in the expression is directly proportional to incident light. Unlike a fiber optic system, a wireless optical link has to contend with ambient light coming from the sun through a window, light fixtures, and other light sources. It is ambient light that gives rise to shot noise at the receiver. The incident light varies depending on the receiver parameter and its location relative to the light sources.

The approach used to calculate the incident optical power is similar to that used to calculate the channel impulse response with one difference. Since the ambient light is assumed time invariant, only the channel dc gain is needed and not the exact shape of the channel impulse response. If the impulse response between a light source s and a receiver r is expressed as:

$$h = \sum_{i=0}^{K-1} h_i \delta(t - T_i)\,. \tag{3.10}$$

It suffices to know $\sum_{i=0}^{K-1} T_s h_i$ in order to be able to calculate the incident power. The channel dc gain can be expressed as:

$$\sum_{i=0}^{K-1} T_s h_i = F \times \Phi \times G_r + D \times G_r , \tag{3.11}$$

where the multiplication is performed without regard to entries time components. Two ambient light sources are assumed. The first is light coming from solar radiation through a window and the second is caused by light fixture on the room ceiling.

3.3.1 Window Light

The light passing through a window makes up a significant component of ambient light. This especially true when the receiver is placed close to a window, with the window being in the receiver FOV. The radiance through an element depends on the direction of the window, time of the day, location of the room, etc. For a west-facing window (assumed in this chapter) the average incident solar radiation is 57 w/m^2 [38]. In order to reduce the ambient light, the receiver employs an optical filter that blocks signals with wavelengths outside 750-950 nm band. This band makes up approximately 14.8% of the total solar energy [39]. Therefore, the total radiation D_r, considering the filter, is equal to 14.8%*57 = 8.32 w/m^2. The ambient light from a window is calculated by dividing the window surface into elements, and modeling each element as diffused source with first order Lambertian radiation. The incident power $P_{i,window}$ from the *i*th element of area equals to $A_{element}$ can be expressed as:

$$P_{i,window} = D_r \times A_{element} \times \sum_{k=0}^{K-1} T_s h_k \ . \tag{3.12}$$

3.3.2 Light Fixtures

The room is lit by 9 Tungsten lamps placed at equal distances as illustrated in Figure 3-5. The lamps are modeled as second order Lambertian sources [42] i.e. the intensity at an angle θ from the norm is equal to the intensity at the norm multiplied by $\cos^2\theta$. This change affects the D and F vectors in Eq. (3.11). The expression for the incident power from the *i*th lamp is:

$$P_{i,lamp} = U \times \Delta\lambda \times \sum_{i=0}^{K-1} T_s h_k \ . \tag{3.13}$$

where U is the optical spectral density (W/m) and is equal to 0.037W/nm [42], and $\Delta\lambda$ is the band pass width of the optical filter.

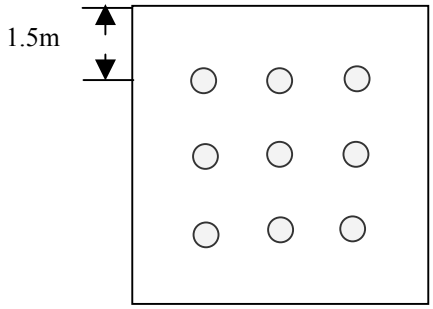

Figure 3-5: Ceiling view showing the location of 9 Tungsten lamps.

Figure 3-6 shows the variation of incident power for different receiver locations throughout the room. The plots show the dependence of incident light on the receiver location relative to the window and the lamps. The variations of ambient light, demonstrated in the figure, propose a challenge in the wireless optical link design. Any link design has to be examined against all possible receiver locations. This motivates

measuring a link performance by the percentage of locations meeting a quality of service. This percentage is referred to as outage; a low outage indicates the quality of service can be met at high receiver locations.

3.3.3 Total Noise

The total noise at the receiver output can be calculated by summing the noise contribution from the window elements and light fixtures. This can be expressed as:

$$\sigma^2 = E\{n^2(t)\} = E\{n^2(t)\} = qI_{DC}A, \tag{3.14}$$

where I_{DC} is given by:

$$I_{DC} = R \times \sum_{i=1}^{M} P_{i,window} + R \times \sum_{i=1}^{N} P_{i,lamp}, \tag{3.15}$$

where M is the number of elements making up the window and N is the number of lamps.

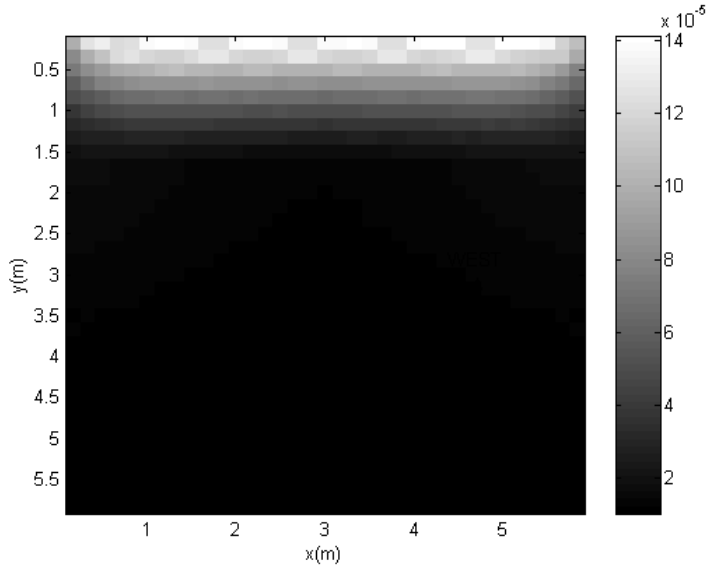

(a)

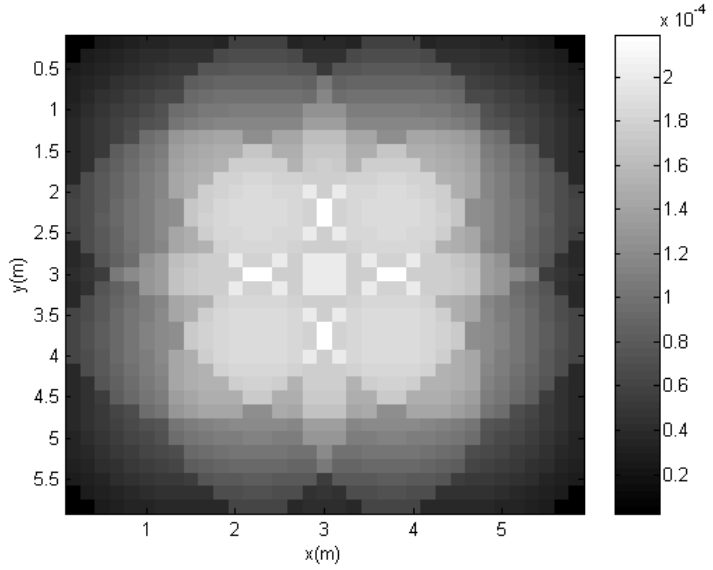

(b)

Figure 3-6: Incident Power distribution for single branch receiver with FOV=40^{o}. Each pixel represents a location and its intensity represents a power level (a) Incident power resulting from light through window, (b) Incident power resulting from 9 Tungsten lamps.

Chapter 4

ON OPTIMUM ORDER OF ANGLE DIVERSITY WITH EQUAL-GAIN COMBINING RECEIVERS

4.1 Introduction

Optical (infrared) wireless local access links provide an attractive alternative to radio frequency (RF) links. A large unregulated bandwidth along with a spatial confinement of infrared propagation provides an abundance of bandwidth and bandwidth reuse for broadband wireless local access applications.

Optical wireless links can be classified according to the directivity of a transmitter and a receiver and whether a line-of-sight exists between the transmitter and receiver [2]. Unlike radio frequency transmission, both narrow- and wide-angle infrared communications can support high data rates, but at a substantial cost. Narrow-angle transmission requires precise alignment of transmitter and receiver, while wide-angle transmission demands high power. In [11], a novel configuration was proposed called Multi-Spot Diffusing Configuration (MSDC). This model combines elements of both narrow- and wide-angle systems to deliver high data rates with low power. In this configuration, a multi-beam transmitter is used to distribute the optical power uniformly within a room. Angle diversity is used at the receiver to combat the induced multipath temporal dispersion and background noise.

Several researchers studied different implementations of MSD configuration [40]-[54]. Using a composite receiver [42], a prototype with 8 beams generated using laser diodes and 9 receiving elements relying on reflections from the ceiling and other surfaces is found to achieve 70 Mb/s within a range of 4.2m. Implementing angle diversity through an imaging diversity receiver that employs a photodetector segmented into pixels [43], imaging receivers reduce required transmitted power by 20 dB compared to single-element receivers. A computer-generated hologram (CGH) can be used as beam splitter to enable multibeam creation [47]-[50], thus creating a grid of small illuminated spots on a room ceiling. A holographic element is also proposed in receiver front-end design, using a holographic curved mirror, signal-to-noise ratio can be improved by as much as 18.5 dB when at most one diffusing spot is covered by a branch FOV [50]-[52].

This chapter investigates angle diversity at the receiver, with the objective of determining the optimal number of branches[1] needed under MSD configurations to reduce receiver cost and complexity. Reducing the number of branches also reduces the shadowing effect, which occurs when signal paths to branches are obstructed by an object. Outage probability is used as measure of link performance for different receiver parameters.

This chapter is organized as follows: In section 2, the maximum number of achievable angle diversity channels is calculated at the receiver. Section 3 introduces a model of the IR link with diversity, under the assumption that diversity channels can be made ideal, using more complex receivers. In section 4, the ideal model is revised to

[1] The terms ‘degree of diversity’, ’order of diversity’, and ‘the number of branches’ are used interchangeably in this thesis to refer to the same quantity.

account for the inability of angle diversity to remove all multipath dispersion, using simpler receivers. Section 5 provides expressions for the performance measures used in the computer simulations. Simulation results are presented in section 6. Concluding remarks are presented in section 7.

4.2 Available Diversity Channels

Multibranch receiver is composed of several branches (photodiodes). In this section, we describe a packing method that maximizes non-overlapping branches that can encompass an entire (total) receiver field-of-view FOV_{total}. This number represents the maximum degree of diversity L_{max} that can be achieved. To help visualize the branches arrangement, a hypothetical sphere of unit radius is assumed to surround a receiver placed at its center. Each branch has a circular footprint on the sphere surface; the footprint represents the area on sphere surface that falls within the branch FOV (FOV_{branch}). New branches are added such that the centers of these circles are situated on a ring with increasing radius around the central branch. The number of branches in a given ring is evaluated with the aid of Figure 4-1, and is given by $\left\lfloor \frac{\pi \sin(2 \times n \times FOV_{branch}(rad))}{FOV_{branch}(rad)} \right\rfloor$. In this expression, n is the ring index with a central branch having index = 0, $\lfloor x \rfloor$ denotes the maximum integer smaller or equal to x. Given FOV_{total} and FOV_{branch}, the total number of achievable branches is:

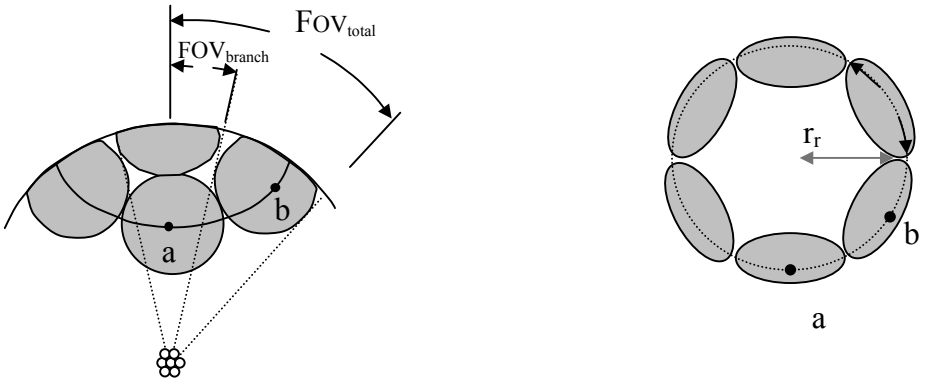

$2r_f = FOV_{branch}(rad)$

$r_r = \sin(FOV_{total} - FOV_{branch})$

(a) (b)

Figure 4-1: (a) Footprints of multibranch receiver on a hypothetical sphere of unit radius. The receiver is placed at the sphere center. (b) A top view of the footprint at ring index = 1.

$$L_{\max} = 1 + \sum_{n=1}^{V} \left\lfloor \frac{\pi \times \sin(2 \times n \times FOV_{branch})}{FOV_{branch}(rad)} \right\rfloor, \qquad (4.1)$$

where $V = \left\lfloor \frac{FOV_{total} - FOV_{branch}}{2 \times FOV_{branch}} \right\rfloor$ is the total number of rings surrounding the central branch.

For example, if $FOV_{total} = 34.5^o$ and $FOV_{branch} = 11.5^o$, the maximum diversity order is 7. The number of branches does not linearly depend on FOV_{total}, nor there is there a FOV_{total} for every number of branches. This is further demonstrated in Table 4-1, where available FOV_{total} for two different FOV_{branch} values and different number of branches are provided. Using a number of branches that fills the entire ring provides rotational symmetry at the receiver. If a different number of branches is used, the behavior of the

receiver will depend on the arrangement of branches; thus rotating the receiver changes its behavior.

Table 4-1: Available FOV_{total} for different number of branches.

Number of Branches	**FOV_{total}**	
	$FOV_{branch}=7^o$	**$FOV_{branch}=11.5^o$**
1	7^o	11.5^o
7	21^o	34.5^o
18		57.5^o
19	35^o	
32		82.5^o
36	49^o	

4.3 Channel and Noise Models

This section describes the environment and introduces an equivalent mathematical model for the infrared communication system with a diversity receiver. An empty room with the dimensions of (6m,6m,3m) is considered. The multi-beam transmitter is placed in the center of the room to produce 10 x 10 equal-intensity diffusing spots on the ceiling [46]. The ceiling and walls are modeled as Lambertian reflectors of the first order [2]. More about the environment parameters is presented in the computer simulation results of section 6.

4.3.1 Noise Model

The main degradation of a wireless optical link is caused by ambient light. Unlike in fiber communications, a wireless link has to contend with ambient light coming from the

sun through windows, light from lighting fixtures, as well as other sources of artificial light. The photocurrent generated in response to ambient light results in current fluctuations and the latter are attributed to shot noise. As discussed in chapter 3, current fluctuations are characterized by a stationary random process with Poisson statistics, which in practice, can be approximated by Gaussian statistics [35]. The two-sided spectral density of shot noise, at the output of the photodiode, is a constant given by:

$$S(f) = q\, I_{bg} = qRP_{bg}\,. \tag{4.2}$$

In Eq. (4.2), R is the detector responsivity (A/W), q is an electron charge (C), I_{bg} is photocurrent (A), and P_{bg} is the incident optical power (W). The ambient light herein results from a window in the room and 9 Tungsten Lamps on the ceiling. To calculate the incident optical power, the window surface is divided into small elements of area equal to $0.04m^2$. Each element is modeled as a first order Lambertian source. The Lamps are also modeled as Lambertian sources of second order.

Noise spectral density depends on the receiver location and branch orientation relative to the light sources. A higher current is generated when a receiver branch falls within the line-of-sight of a light source. Figure 4-2 shows the variation of incident optical power for a typical 32-branch receiver.

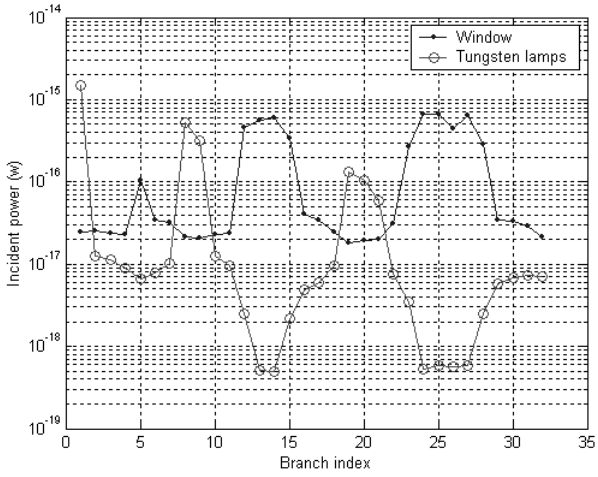

Figure 4-2: Incident optical power distribution of a receiver composed of 32 branches, FOV_{branch} =11.5°. Branches facing a window or lamps experience a higher incident power.

The variance of noise at the output of a receiver that incorporates a receive filter G(f) is given by:

$$\sigma^2 = 2qI_{bg}\int_0^{\infty}|G(f)|^2 df \ . \tag{4.3}$$

4.3.2 Channel Model

The transmission link in this chapter uses intensity modulation and direct detection (IM/DD), with on-off keying modulation. In deriving the channel model, it is first assumed that the channel to each branch can be modeled as an ideal channel, with no temporal dispersion. This assumption is not necessarily true in general, as will be explained in the next section, where the channel model is modified to account for a

residual temporal dispersion. Each channel is modeled as an additive Gaussian one, using a constant gain and a constant delay. Gain of the *j*th branch is equal to $H_j(0)$ and the delay is equal to t_j . Channel gain can be zero indicating that no signal is received through the branch. The noise terms in the L channels are assumed to be mutually statistically independent. The transmitter and receiver filters are identical, each accomplishing half the signal shaping. The *j*th channel is shown in Figure 4-3.

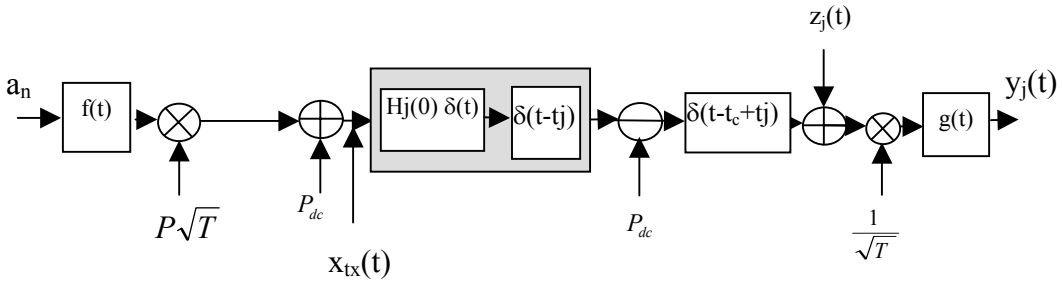

Figure 4-3: The *j*th channel with an angle diversity receiver

The receiver compensates for the delay that a signal experiences while passing through the channel. It also adds delay t_c to the signal in order to ensure causality of the receiver filter, i.e., $t_c \geq \max[t_i],\ i \in \{1, L\}$. A factor R at the receiver is added due to the photo-detector responsivity. Since noise spectral density is flat and the transmission channel is real, the transmitter and receiver filters that eliminate intersymbol interference and maximize the SNR at sampling time, for a given input power, follow from [55]:

$$F(f)G(f) = X_{rc}(f) \tag{4.4}$$

where X_{rc} is a raised cosine frequency response, F(f) and G(f) are transmitter and receiver filters, respectively. The filters magnitude is given by:

$$|F(f)| = |G(f)| = \sqrt{|X_{rc}(f)|}\,. \tag{4.5}$$

Therefore, both f(t) and g(t) have root raised cosine with a time domain representation from [54] as:

$$f(t) = g(t) = \frac{4\alpha}{\pi\sqrt{T}} \frac{\cos[(1+\alpha)\pi t/T] + \sin[(1-\alpha)(\frac{\pi t}{T})]/[4\alpha t/T]}{1-(4\alpha t/T)^2}, \tag{4.6}$$

where α is the roll-off factor, and T is the time separation between successive pulses. Two observations needed, when deriving the channel constraints, are made with regards to the root raised cosine waveform. First, the maximum value of f(t) is:

$$\max(f(t)) = f(0) = \frac{1}{\sqrt{T}}(1-\alpha+\frac{4\alpha}{\pi})\,. \tag{4.7}$$

Second, the average value of a sequence of pulses that are shaped by f(t), i.e., $\sum_{n=-N}^{N} f(t-nT)$, is:

$$\lim_{NT\to\infty} \frac{1}{2NT} \int_{-NT}^{NT} \sum_{n=-N}^{N} f(t-nT)dt = \frac{1}{T}\int_{-\infty}^{\infty} f(t)dt = \frac{F(0)}{T} = \frac{\sqrt{X_{rc}(0)}}{T} = \frac{1}{\sqrt{T}} \tag{4.8}$$

Substituting for G(f) in Eq. (4.3), the noise variance at the output of g(t) becomes:

$$\begin{aligned} \sigma^2 &= 2qI_{bg} \times (\frac{1}{\sqrt{T}})^2 \int_0^{\infty} |G(f)|^2 df = 2qI_{bg} \times \frac{1}{T} \times \frac{1}{2} \times \int_{-\infty}^{\infty} X_{rc}(f)df \\ &= qI_{bg}B = qRP_{bg}B. \end{aligned} \tag{4.9}$$

Where B is the bit rate and is equal to 1/T.

4.3.3 Channel Constraints

In IM/DD, the transmitted signal $x_{tx}(t)$ represents optical intensity. This leads to two constraints on $x_{tx}(t)$ [2]. First, the value of $x_{tx}(t)$ must be non-negative. Second, the average amplitude of $x_{tx}(t)$ must be kept below a specified value P_m, determined by the power consumption and eye safety limits. These constraints can be expressed as:

$$x_{tx}(t) \geq 0, \tag{4.10}$$

$$\text{and } \lim_{T\to\infty} \frac{1}{2\tau} \int_{-\tau}^{\tau} x_{tx}(t)dt \leq P_m . \tag{4.11}$$

To determine the parameters of $x_{tx}(t)$ that satisfy these constraints, $x_{tx}(t)$ is expressed as [54]:

$$x_{tx}(t) = P_{dc} + P\sqrt{T} \sum_{n=-N}^{N} a_n f(t-nT), \tag{4.12}$$

where 2N+1 is transmitted sequence length, and P_{dc} term is added to ensure that $x_{tx}(t)$ is positive. The value of P_{dc} is equal in magnitude to the minimum of $P\sqrt{T} \sum_{n=-N}^{N} a_n f(t-nT)$.

If $\lambda(\alpha) = \text{abs}(\min(\sum_{n=-N}^{N} a_n f(t-nT))/\max(f(t)))$ is defined, P_{dc} can be expressed as:

$$\begin{aligned} P_{dc} &= P\sqrt{T} \times \lambda(\alpha) \times \max(f(t)) \\ &= P \times \lambda(\alpha) \times (1 - \alpha + \frac{4\alpha}{\pi}). \end{aligned} \tag{4.13}$$

The value of λ is found by considering different sequences of transmitted symbols a_n, and finding the minimum of $x_{tx}(t)$. Since f(t) is a decaying function of time, a sequence of 12

symbols is used to generate the plot in Figure 4-4(a). The figure shows that for small values of α, as α increases, P_{dc} decreases.

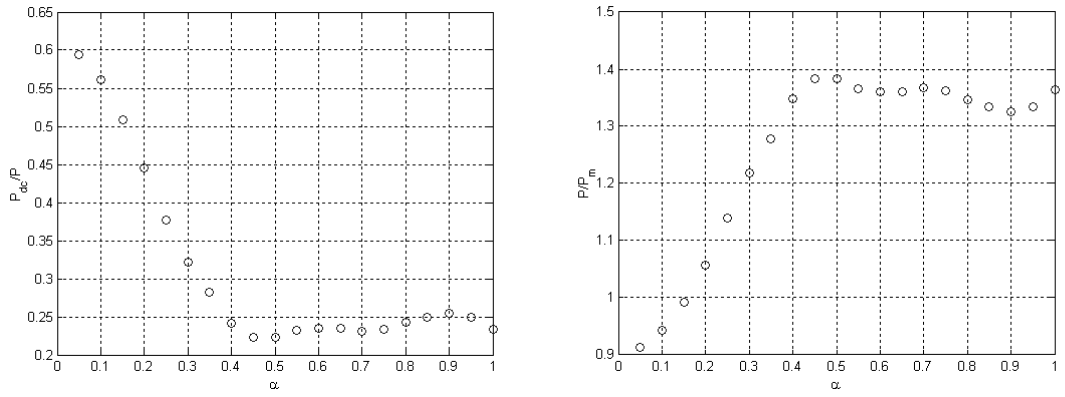

(a) (b)

Figure 4-4: (a) P_{dc}/P as a function of α , (b) Maximum normalized power P/P_m vs. α .

The second constraint is used to determine the scaling factor P. Assuming that input symbols are equally likely to be 0 and +1, the average value of $x_{tx}(t)$, for very large value of N, is given by:

$$\lim_{\tau\to\infty}\frac{1}{2\tau}\int_{-\tau}^{\tau}x_{tx}(t)dt = P_{dc} + P\sqrt{T}\times E[a_n]\times\frac{1}{\sqrt{T}} = P_{dc}+\frac{P}{2}. \tag{4.14}$$

Substituting for P_{dc}, we obtain,

$$\lambda\times(1-\alpha+\frac{4\alpha}{\pi})\times P+\frac{P}{2}\le P_m. \tag{4.15}$$

Expressing P in terms of P_m

$$P\le\frac{P_m}{[0.5+\lambda(\alpha)\times(1-\alpha+\frac{4\alpha}{\pi})]}. \tag{4.16}$$

Eq. (4.16) provides the maximum amplitude the signal can take on when its average is constrained to be less than P_m. The relationship between P and P_m as a function of α is depicted in Figure 4-4(b). The figure shows that for small values of α, any increase in α will cause an increase in P. Value of P reaches a maximum when α is close to 0.5. Increasing α beyond 0.5 has a very little effect on P.

It is worth mentioning that P_{dc} carries no information and it is subtracted from the signal at the receiver. This explains why it is desirable to have a pulse shape that has a small P_{dc} value.

4.3.4 Receiver Output

The receiver, in an angle diversity system, is composed of L branches, each of which contains a filter matching the received waveform and a delay that depends on the channel. To calculate the receiver output, an equivalent channel impulse response $h_{eq}(t)$ is defined as:

$$h_{eq}(t) = \sum_{i=1}^{L} H_i(0)\delta(t). \tag{4.17}$$

In terms of h_{eq}, the output is expressed as:

$$y(t) = RP \sum_{n=-N}^{N} a_n f(t-nT) \otimes h_{eq}(t) \otimes g(t-t_c), \tag{4.18}$$

where 2N+1 is transmitted sequence length. Substituting for $h_{eq}(t)$ and using Eq. (4.4), the expression for y(t) becomes:

$$y(t) = RP \sum_{n=-N}^{N} a_n \sum_{i=1}^{L} H_i(0) x_{rc}(t-nT-t_c). \tag{4.19}$$

The noise at the output of the receiver is equal to the summation of noise at the output of each channel. At the output of the *i*th receiver, the noise $z_i(t)$ is a zero-mean Gaussian term. The expression for the output y(t), including the noise, becomes:

$$y(t) = RP \sum_{n=-N}^{N} \sum_{i=1}^{L} a_n H_i(0) x_{rc}(t - nT - t_c) + \sum_{i=1}^{L} z_i(t). \tag{4.20}$$

The output y(t) is sampled at time $t_{sampling} = t_c+\delta+kT$, where δ is a time delay chosen to minimize intersymbol interference when the channel is not ideal (dispersion-free), as discussed in the next section. Thus, y[k] is:

$$\begin{aligned} y[k] = y[t_s + \delta + kT] = RP \sum_{n=-N}^{N} \sum_{i=1}^{L} a_n H_i(0) x_{rc}(kT - nT + \delta) \\ + \sum_{i=1}^{L} z_i(kT + t_c + \delta) \end{aligned} . \tag{4.21}$$

In this subsection, channels are assumed dispersion-less (ideal), therefore, $\delta=0$. Since $x_{rc}(nT) = 0, \forall\ n \neq 0$, Eq. (4.21) simplifies to:

$$y[k] = RP \sum_{i=1}^{L} a_k H_i(0) + \eta\,, \tag{4.22}$$

where variance of noise η is found by summing noise variance over all channels, i.e.,

$$\sigma_\eta^{\,2} = \sum_{i=1}^{L} \sigma_i^2\ . \tag{4.23}$$

A maximum likelihood receiver uses the sampled output y[k] to decide which symbol is transmitted. Assuming the 0 and 1 are equally likely to occur, the detected symbol $\hat{a}_k$ is determined according to:

$$\hat{a}_k = \begin{Bmatrix} 1 \text{ if } P(y[k] \mid a_k = 1) > P(y[k] \mid a_k = 0) \\ 0 \text{ if } P(y[k] \mid a_k = 0) < P(y[k] \mid a_k = 1) \end{Bmatrix}. \tag{4.24}$$

The multibranch equal gain receiver is illustrated in Figure 4-5.

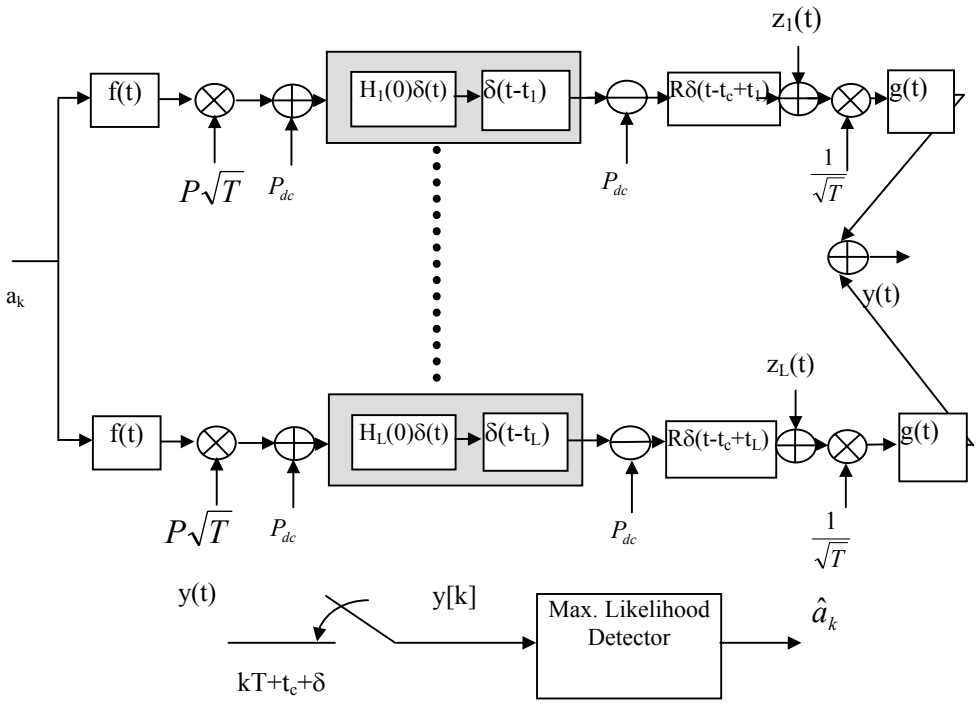

Figure 4-5: Multibranch angle diversity receiver, using equal-gain combining.

4.3.5 Link Performance

Two measures are used to evaluate the outage performance of the receiver and to determine the optimal number of branches: the probability of error and SNR that are not independent of one another. For a maximum likelihood detector, assuming symbols are equally likely to be 0 or 1, the probability of error is:

$$P_e = Q\left(\frac{P\sum_{i=1}^{L}\frac{RH_i(0)}{2}}{\sqrt{\sum_{i=1}^{L}\sigma_i^2}}\right). \qquad (4.25)$$

where $Q(.)$ is a Q-function defined as $\frac{1}{\sqrt{2\pi}}\int_x^\infty \exp(-\frac{1}{2}u^2)du, u \geq 0$. The signal-to-noise ratio, SNR, is defined as the ratio of the output signal power when $a_n = 1$ is transmitted to the noise power, and is equal to:

$$SNR = \frac{\left(P\sum_{i=1}^{L}RH_i(0)\right)^2}{\sum_{i=1}^{L}\sigma_i^2}. \qquad (4.26)$$

Expressed in terms of SNR, the probability of error is:

$$P_e = Q(\frac{\sqrt{SNR}}{2}). \qquad (4.27)$$

Equations (4.26) and (4.27) highlight the dependence of error probability on the number of channels. Increasing the number of channels increases the noise, but does not necessarily increase the SNR value. This is because some of the newly added branches might have $H_i(0)$ equal to zero or a very small value compared to added noise.

4.4 A More Accurate Channel Model

The assumption made in the previous section about the ability of diversity receiver to eliminate temporal dispersion may not apply to all indoor IR transceivers. For example, with equal-gain combining considered herein, there are two circumstances

under which temporal dispersion may not be eliminated completely. The first situation occurs when the FOV_{branch} is larger than a critical angle $FOV_{critical}$. In this case, the branch spans more than a single diffusing spot. This results in an impulse response that is made of at least two impulses. Added delay at a simple combining receiver can only align one of these impulses.

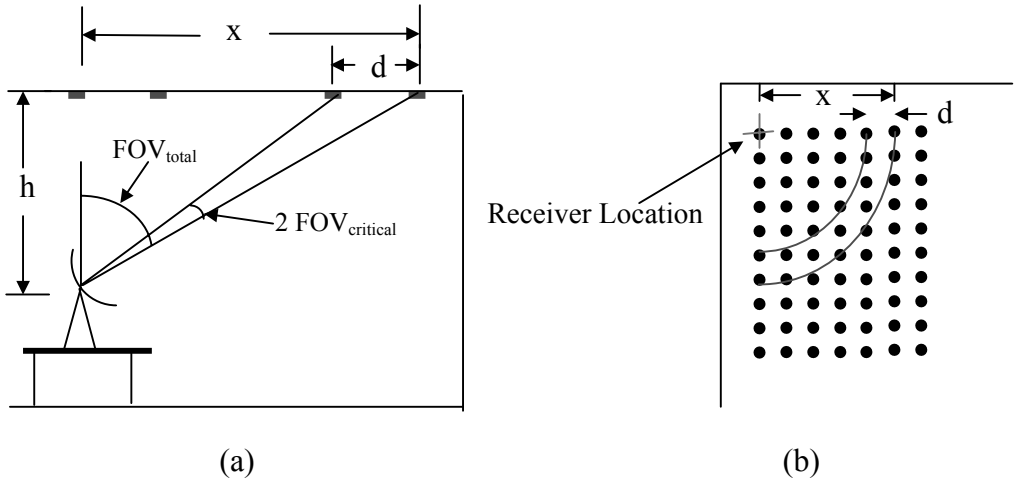

Figure 4-6: (a) Illustration of $FOV_{critical}$ calculations. (b) Top view showing diffusing spots, receiver location and distance to the farthest spot within the FOV_{total}.

The value of $FOV_{critical}$ depends on the receiver location relative to the diffusing spots. To guarantee the elimination of temporal dispersion throughout the room, the worst receiver location is considered. This location is close to the corner of the room, as illustrated in Figure 4-6. From the figure,

$$\begin{aligned} x &= h \times \tan(FOV_{total}) \\ \tan(FOV_{total} - 2 \times FOV_{branch}) &= \frac{x-d}{h} \\ FOV_{critical} &= \frac{1}{2} \times [FOV_{total} - \arctan(\frac{h \times \tan(FOV_{total}) - d}{h})], \end{aligned} \tag{4.28}$$

where x is the distance to the farthest spot that lies within FOV_{total}, h is the distance from the receiver to the surface containing spots, and d is the spacing between spots. As an example, for $FOV_{total} = 34.5^{o}$, h = 2.1 m, and $d = 0.6\,m$, the $FOV_{critical} = 6.3^{o}$.

The second case that lends itself to a dispersive channel mode, considering signals received after reflection off of walls and ceiling, as illustrated in Figure 4-7. Since the signal strength at the receiver is inversely proportional to the square of traveled distance by light, and walls do not offer perfect reflection, dispersion caused by reflections contributes smaller components to channel impulse response. This dispersion is reduced by reducing the FOV_{branch}, but may not be completely eliminated.

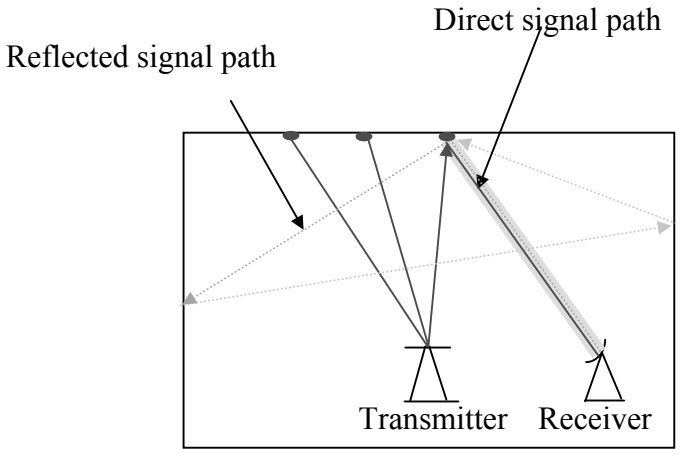

Figure 4-7: Illustration of multipath phenomenon caused by multiple reflections.

Thus, in this case, the channel can no longer be modeled as an ideal (dispersion-free) one. Instead, the channel impulse response is composed of a strong component resulting from the direct path and weaker reflected components. The diversity receiver task is to add a delay to each channel in order to align their strong components, such that the resulting

equivalent impulse response $h_{eq}(t)$ has a strong component at time t_S. The $h_{eq}(t)$, as shown in Figure 4-8, can be expressed as:

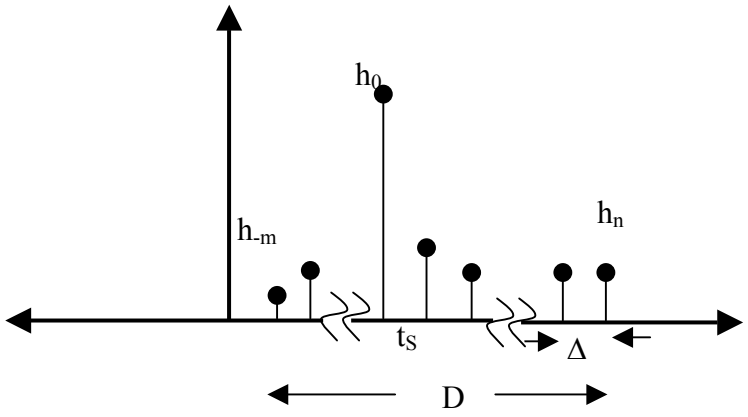

Figure 4-8: Equivalent impulse response ($h_{eq}(t)$) of L combined channels.

$$h_{eq}(t) = \sum_{l=1}^{L} h_l(t) = \sum_{i=-m}^{n} h_i \delta(t - i\Delta - t_S) \tag{4.29}$$

where $\Delta = \frac{D}{n+m}$ is the sampling time, D is the delay spread, h_l is the shifted impulse response of l-th channel, and $h_0 > h_i, \forall i \neq 0$. The h_{eq} is composed of n+m+1 impulses. Since some signals will travel shorter and others longer distances than direct path, m impulses precede h_0 and n will succeed it. For example, when three diffusing spots, of different distances from the receiver, are within a FOV_{branch}, there will be 3 components in the channels impulse response. If the middle component is the strongest, the receiver will align this component with the strong components from other branches. The impulse

response will contain a component preceding and another succeeding the strong component. The signal at the receiver output, for a single transmitted symbol a_k, is

$$\begin{aligned} y(t) &= RPa_k f(t) \otimes h_{eq}(t) \otimes g(t) \\ &= RPa_k x_{rc}(t) \otimes h_{eq}(t) \end{aligned} \tag{4.30}$$

Using Eq. (4.29) to substitute for h_{eq} (t), we obtain

$$y(t) = RP \sum_{i=-m}^{n} a_k h_i x_{rc}(t - i\Delta - t_S - kT). \tag{4.31}$$

When an infinitely long sequence of symbols is transmitted, the resultant y(t) becomes:

$$y(t) = RP \sum_{k=-\infty}^{\infty} \sum_{i=-m}^{n} a_k h_i x_{rc}(t - kT - i\Delta - t_S). \tag{4.32}$$

It can be seen from Eq. (4.32) that the receiver output suffers from intersymbol interference (ISI) caused by the residual temporal dispersion. This ISI degrades receiver performance and results in a higher probability of bit error.

4.5 Performance Measures

In deriving performance measures, two receiver circuits are considered. In the first circuit, the receiver does not account for residual temporal dispersion and samples k-th symbol at $t_{sampling} = kT + t_S$. In the second circuit, the receiver is aware of residual temporal dispersion, and therefore tries to optimize sampling time to minimize the resulting ISI. The receiver in this case samples y(t) at $t_{sampling} = kT + t_S + \delta$, where δ is chosen to minimize ISI. We will refer to these receivers as “Sub Optimal Timing Circuit” and “Optimal Timing Circuit Receivers”, respectively.

4.5.1 Receiver with Sub Optimal Timing Circuit

In a sub optimal timing circuit receiver, output is sampled without regard to the residual dispersion, i.e., δ is set to zero. Since $x_{rc}(nT) = 0, \forall n \neq 0,$ and $x_{rc}(0) = 1$, at sampling time $t_{sampling} = kT + t_S$, the receiver output y[k] is:

$$y[k] = y[kT] = RPa_k h_0 + RP \sum_{j=-\infty}^{\infty} \sum_{\substack{i=-m \\ i\neq 0}}^{n} a_j h_i x_{rc}(kT - jT - i\Delta) . \tag{4.33}$$

The second term in Eq. (4.33) can be decomposed into two components as:

$$\begin{aligned} RP \sum_{j=-\infty}^{\infty} \sum_{\substack{i=-m \\ i\neq 0}}^{n} a_j h_i x_{rc}((k-j)T - i\Delta) = RPa_k \sum_{\substack{i=-m \\ i\neq 0}}^{n} h_i x_{rc}(-i\Delta) \\ + RP \sum_{\substack{j=-\infty \\ j\neq k}}^{\infty} \sum_{\substack{i=-m \\ i\neq 0}}^{n} a_j h_j x_{rc}((k-j)T - i\Delta) \end{aligned} \tag{4.34}$$

The first term shows the effect of channel dispersion on the detected symbol. In other words, if a single symbol is transmitted, this term represents the contribution by channel dispersion to the sampled value y[k]. Surprisingly, this effect reduces the error probability, as long as max ($i\Delta$) is less than T. The second term in Eq. (4.34) is the ISI caused by other transmitted symbols. The evaluation of Eq. (4.34) can be simplified by defining an end-to-end impulse response x(t) as:

$$x(t) = R\, x_{rc}(t) * h_{eq}(t) = RP \sum_{i=-m}^{n} h_i x_{rc}(t - i\Delta) , \tag{4.35}$$

where x(t) represents the response of the equivalent channel to the input $x_{rc}(t)$ scaled by the RP. Expressing y[k] in terms of x(t), we obtain:

$$y[k] = a_k x(0) + \sum_{\substack{j=-\infty \\ j\neq k}}^{\infty} a_j x((k-j)T) . \tag{4.36}$$

When calculating the effect of ISI on the detected symbol, x(t) is recognized as a decaying function. Therefore, the detected symbol is only affected by its neighboring symbols. In this study, the effect of symbols farther than $\pm 6T$ is negligible. Mathematically, this is expressed as:

$$x(iT) \approx 0,\ i = \pm 7, 8, \cdots \infty . \tag{4.37}$$

The expression for y[k] simplifies to:

$$y[k] = a_k x(0) + \sum_{\substack{i=-6 \\ i \neq 0}}^{6} a_{k-i} x\ (iT) . \tag{4.38}$$

The effect of ISI depends on the value of the neighboring symbols. Since these symbols are equally likely to be 0 or 1, there are 2^{12} possible neighboring sequences. The *i*th sequence, $seq_i = [a_{-6},...a_{-1}, a_1,\ldots, a_6]$, has a decimal equivalent equal to i. The ISI contribution of a sequence $d_{ISI}(i)$ is given by:

$$d_{ISI}(i) = d_{ISI}(seq_i) = \frac{1}{x(0)} \sum_{\substack{j=-6 \\ j \neq 0}}^{6} a_j x(jT) , \tag{4.39}$$

where a_j is chosen from the entries of *i*th sequence. Figure 4-9 shows d_{ISI} as a function of i, for a receiver located in the middle of the room. Two observations are made with regard the figure. First, the repetition in the pattern every i equal to 512, i.e., d_{ISI} of seq_i and seq_{i+512} are approximately equal. This indicates that x(4T), x(5T) and x(6T) plays an insignificant role in determining d_{ISI}. Second, neighboring sequences have approximately equal d_{ISI}, i.e., a_{-6} and a_{-5} values have negligible effect on d_{ISI}. These observations confirm that sufficient sequence length is considered in evaluating d_{ISI}.

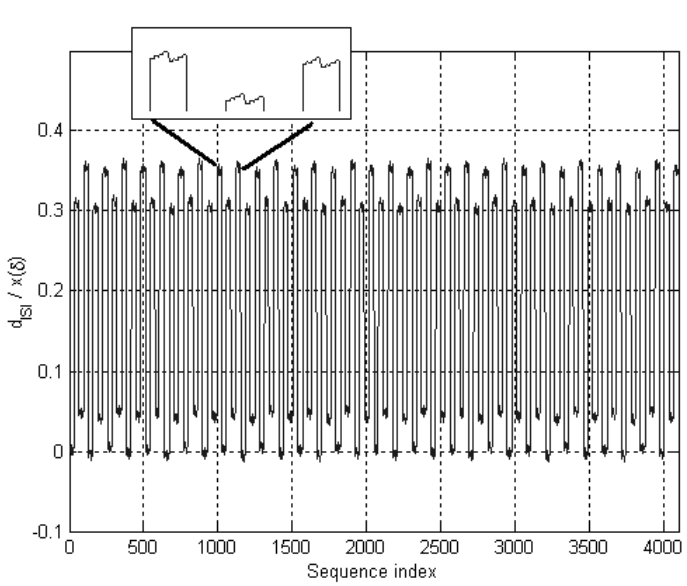

Figure 4-9: ISI contribution versus sequence index; the repetition of the pattern indicates sufficient sequence length is considered in ISI computations.

The average probability of error is calculated by averaging the conditional probability of error on each sequence. For the *i*th sequence, an error occurs if $x(0)d_{ISI}(i)$ and noise exceed a threshold value V_T , i.e.,

$$P(e \mid seq_i) = P(x(0)d_{ISI}(i) + \eta > V_T) = Q(\frac{V_T - x(0)d_{ISI}(i)}{\sigma}), \tag{4.40}$$

where $V_T = \frac{x(0)}{2}$. The probability of error is given by:

$$P_e = \sum_{i=1}^{2^{2\times 6}} P(e|seq_i)P(seq_i) \tag{4.41}$$

Since the noise is a zero-mean Gaussian process and all sequences are equally likely, the average P_e can be expressed as:

$$P_e = \frac{1}{2^{2\times 6}} \sum_{i=1}^{2^{2\times 6}} Q\left(\frac{\frac{x(0)}{2} - x(0) d_{ISI}(i)}{\sigma}\right). \tag{4.42}$$

The SNR is defined as:

$$SNR = \frac{x(0)^2}{\sigma^2}. \tag{4.43}$$

Expressing the average probability of error in terms of SNR, we obtain:

$$P_e = \frac{1}{2^{2\times 6}} \sum_{i=1}^{2^{2\times 6}} Q[\sqrt{SNR}(1/2 - d_{ISI}(i)]. \tag{4.44}$$

4.5.2 Receiver with Optimal Timing Circuit

The receiver with optimal timing circuit chooses a sampling time to reduce the effect of ISI resulting from residual temporal dispersion. To find optimal sampling time, $t_{sampling} = t_S + \delta + kT$, receiver selects a δ that maximizes the cost function C_{ISI}, defined as:

$$C_{ISI}(\delta) = \frac{x(\delta)}{\sum_{\substack{j=-6 \\ j\neq 0}}^{6} a_j x(\delta + jT)}. \tag{4.45}$$

Maximizing C_{ISI} is equivalent to reducing ISI effect on the detected symbol. The value of δ depends on the number of branches and the receiver location. Figure 4-10 shows δ as a function of the total number of branches, for a given location.

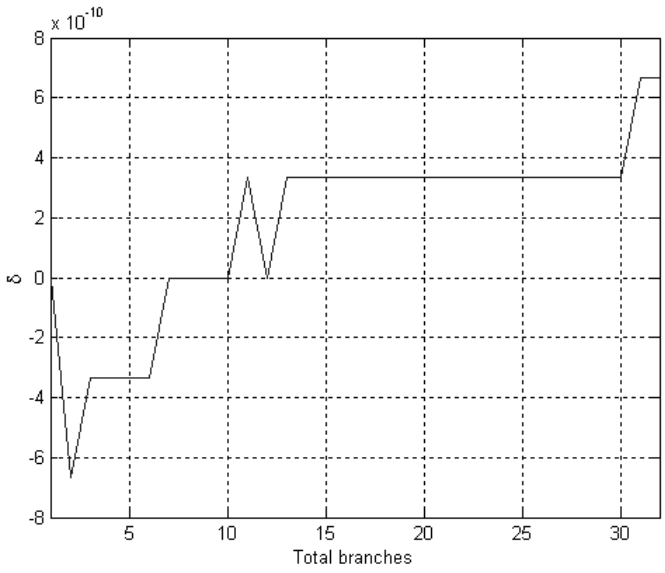

Figure 4-10: Timing offset factor δ versus the total number of branches.

The expression for P_e is similar to that in Eq. (4.44), with x(0) replaced by x(δ) and $V_T = \frac{x(\delta)}{2}$. Thus, the average probability of error is:

$$P_e = \frac{1}{2^{2\times 6}} \sum_{i=1}^{L^{2\times 6}} [Q(\frac{x(\delta)/2 - d_{ISI}(i)}{\sigma}), \tag{4.46}$$

where the $d_{ISI}(i)$ is given by:

$$d_{ISI}(i) = d_{ISI}(seq_i) = \frac{1}{x(\delta)} \sum_{\substack{j=-6 \\ j\neq 0}}^{6} a_j x(\delta + jT). \tag{4.47}$$

The SNR for the receiver with optimum timing is defined as:

$$SNR = \frac{x(\delta)^2}{\sigma^2}, \tag{4.48}$$

and the probability of error, in terms of SNR, is given by

$$P_e = \frac{1}{2^{2\times 6}} \sum_{i=1}^{2^{2\times 6}} Q[\sqrt{SNR}(1/2 - d_{ISI}(i)] \tag{4.49}$$

4.6 Simulation Results

In the computer simulations, we considered a room that resembles a typical computer laboratory. The room has dimensions of 6mx6mx3m, with one of the walls covered by a window as illustrated in Figure 4-11. The transmitter is placed in the center of the room at a height equal to 0.9m to produce 10x10 equally spaced diffusing spots of equal intensity on the ceiling. The technique in chapter 2 is adopted for the efficient calculation of channel impulse responses. Three reflections are considered in all impulse responses calculations.

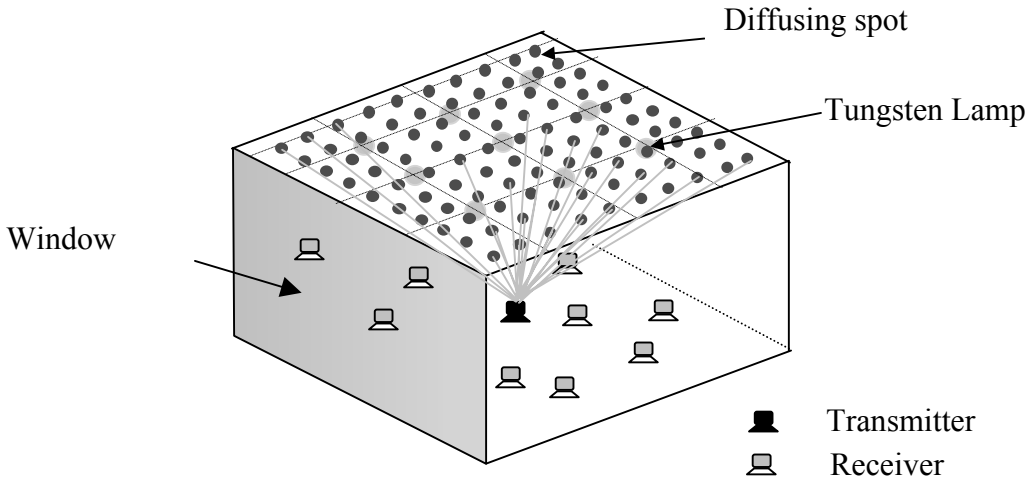

Figure 4-11: View of the room used in the computer simulations. Diffusing spots and the tungsten lamps are shown on the ceiling. The window covers one side of the room.

The receiver has a $FOV_{branch} = 11.5^{o}$, which guarantees that at least one diffusing spot is within the FOV_{branch} [52]. The total number of branches is chosen such that FOV_{total} is less than 90^{o}. A list of parameters used in this simulation is provided in Table 4-2. Error probability, SNR, and outage probability are calculated as a function of total number of receiver diversity branches. The central branch is labeled as number 1. Subsequent branches are numbered in an increasing order as they move away from the central branch, as illustrated in the Figure 4-12. The impulse responses of the channel with a single-branch and angle diversity receiver are shown in Figure 4-13 parts (a) and (b), respectively. This figure demonstrates the multibranch receiver ability to reduce temporal dispersion.

Table 4-2: Parameter values used in the computer simulations.

Parameter	**Value**
Room dimensions	(6m, 6m, 3m)
Reflection coefficients of: Walls Ceiling Window Floor	 0.7 0.7 0.04 0.2
Tungsten lamps Lamps spectral density	9 lamps located at distances equal to 1.5m apart. The corner lamp is located at (1.5,1.5) 0.037 W/nm
Window Diffused solar radiation	As shown in Figure 4-11 8.316 W/m^2
Spectral range	750 - 950 nm
Receiver locations	400 locations, 0.3m apart, at a fixed height equal to 0.9 m
Receiver FOV_{branch}	11.5^o
Photo-detector responsivity Area	0.6 A/W 1 cm^2
Average transmitted power per spot	0.02W
Bit rate	200 Mbps
Target Average BER	10^{-9}
Impulse Response	3 reflections are considered, Δ=0.33ns, and D=0.1 μs

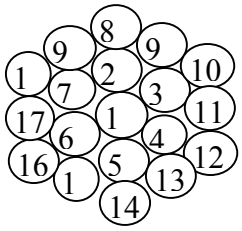

Figure 4-12: Branch numbering: branches are added in rings around a central branch and are numbered sequentially.

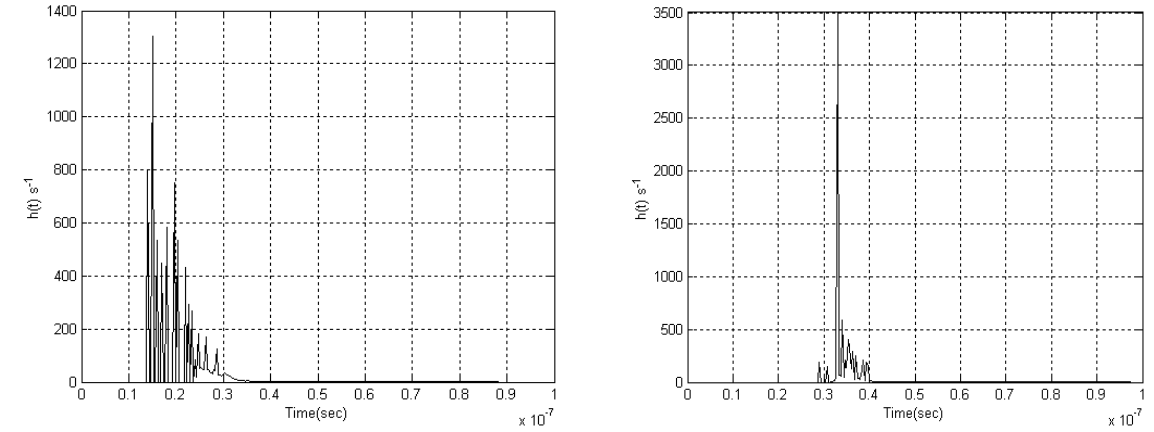

(a) (b)

Figure 4-13: (a) A typical impulse response for a single-branch receiver, (b) impulse response of a multibranch angle diversity receiver, with 32 branches. Both receivers have the same FOV_{total} equal to 82.5^{o}.

The receiver performance is evaluated at 400 different locations. The distance between two locations is 0.3m; this ensures that performance can be attained throughout the room by moving a receiver a maximum distance less than or equal to 0.3m. Figure 4-14 shows the average probability of error for 400 locations, as a function of the total number of branches. From the figure, an average probability of error equal to 10^{-9} (shown as a horizontal line) is achieved by 8 and 9 branches for a receiver using optimal and sub optimal timing circuit, respectively. Increasing the number of branches beyond 11

increases P_e for a sub optimal timing receiver. The optimal timing receiver achieves a minimum average P_e with 18 branches.

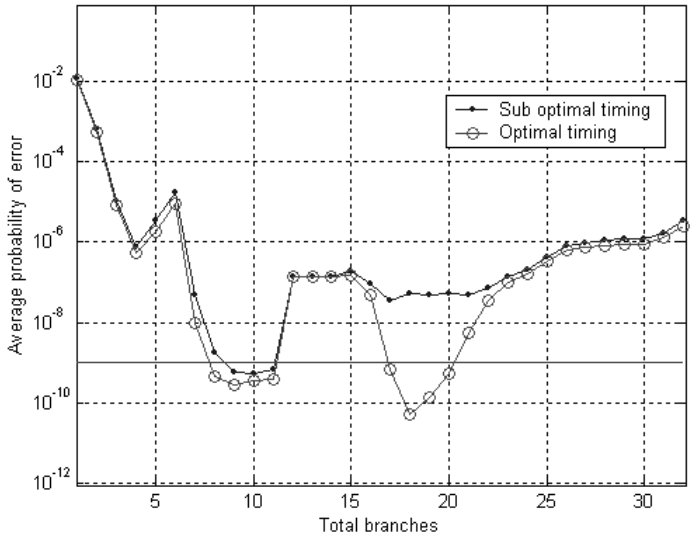

Figure 4-14: Average probability of error for 400 receiver locations.

Although the average error probability provides an insight into the link performance, a more meaningful measure is achieved using outage probability. This is true since with a large number of receiver locations considered, few locations that fall within a high exposure of ambient light might result in a small average error probability. Outage probability is defined as the percentage of locations that fails to meet P_e requirement (10^{-9}) for a given number of branches. The plot of outage probability in Figure 4-15 shows that the minimum outage probabilities of 0.5% and 1.5% are achieved using 9 and 10 branches for receivers employing optimal and sub optimal timing circuit, respectively.

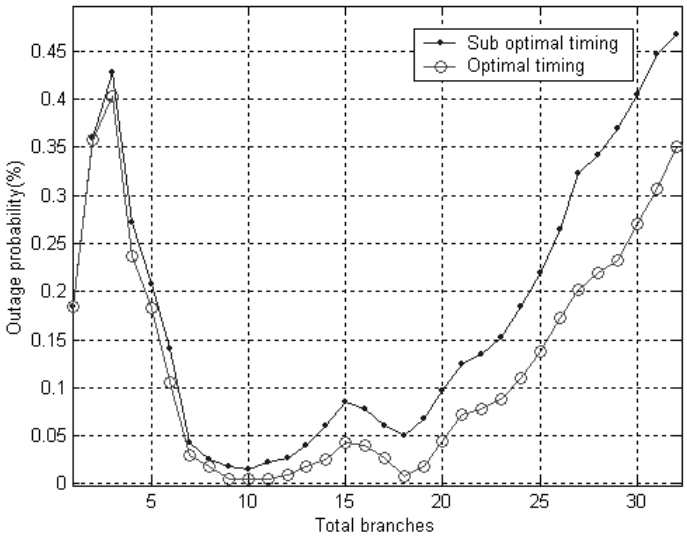

Figure 4-15: Outage probability defined by percentage of locations which has an error probability greater than 10^{-9}.

The average SNR is plotted in Figure 4-16. The figure shows the variation in average SNR as new branches are added. The maximum average SNR achieved has 23 branches. It interesting to note this number of branches does not correspond to a minimum average probability of error. This is the case since the SNR calculation does not account for ISI effect.

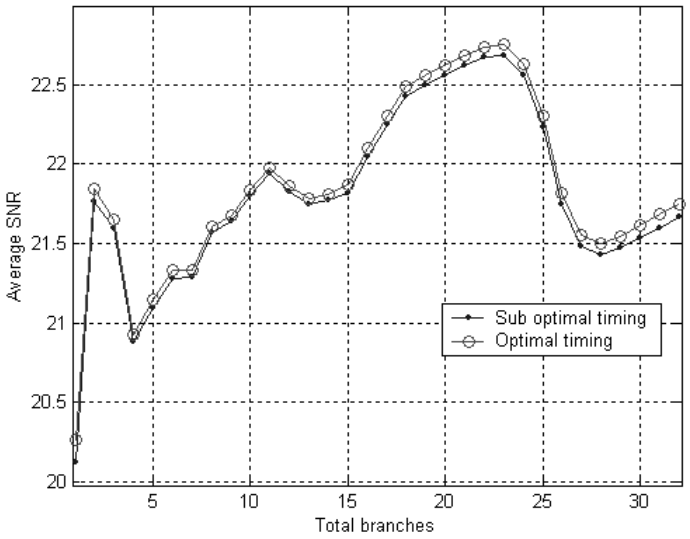

Figure 4-16: Average SNR vs. total number of branches.

4.7 Conclusions

Indoor wireless infrared link suffers from multipath temporal dispersion caused by the different path lengths traveled by a transmitted signal. This chapter demonstrates that angle diversity at the receiver is an effective technique to reduce the channel dispersion effect, in turn, reducing the ISI and the probability of error. In designing an angle diversity receiver, three parameters must be specified: FOV_{total}, FOV_{branch}, and the total number of branches. The choice of FOV_{branch} depends on the pattern of diffusing spots, their separation distances, and the distance between the receiver and the spots region. A trade-off is needed in choosing the FOV_{branch}. Reducing the FOV_{branch} enhances the receiver's ability to combat temporal dispersion, but it also reduces the branch's ability to capture diffusing spots. The number of branches depends on the noise level and the

relative contribution of the newly added branches. It has been demonstrated through evaluation of outage probability that there exists an optimal number of branches that achieves the desired performance requirements. The number is optimal in the sense that it is the smallest number of branches that achieves a desired set of performance requirements. This, in turn, reduces receiver cost, complexity and the susceptibility to shadowing that occurs when an obstacle blocks the signals paths. The impact of using the optimal timing circuit at receivers is insignificant when the FOV_{branch} is small. This is because the impulse response to the branches contains, at most, one strong component, which can be aligned by the receiver. As FOV_{branch} increases, the channel impulse response for some branches contain two or more strong components and the receiver is only able to align one. Thus, the timing circuit plays a more significant role in reducing the ISI in this case. The improvement using timing circuit becomes less significant as the number of branches increases, because the newly added branches contribute a weaker signal as the spot becomes at larger angles and distances.

Chapter 5

ON OPTIMUM ORDER OF ANGLE DIVERSITY WITH MAXIMAL RATIO COMBINING RECEIVERS

5.1 Introduction

Angle diversity is an effective technique to compensate for multipath temporal dispersion in an optical wireless environment. Diversity is accomplished by using a multibranch receiver capable of resolving multipath. In designing an angle diversity receiver, three parameters must be specified: FOV_{total}, FOV_{branch}, and the total number of branches. The choice of FOV_{branch} depends on the pattern of diffusing spots, their separation, and the distance between the receiver and spots region. A trade-off is needed in choosing the FOV_{branch}. Reducing the latter enhances the receiver ability to combat temporal dispersion and reduces ambient noise, but it can result also in branch inability to capture any diffusing spots and thus contribute only noise power to the receiver. The number of branches choice depends on performance requirement, noise power and the relative contribution of the newly added branches.

This chapter investigates the impact of choosing FOV_{branch} on optimal number of branches for a link that employs maximal ratio combining MSD configuration. The receiver front-end and the environment parameters are similar to those developed in chapter 4. Therefore, similar development is avoided whenever possible to reduce

redundancy. The chapter is organized as follows: section 2 introduces maximal ratio combining and models the IR link with diversity, under the assumption that diversity channels can be made ideal, using more complex receivers. In section 3, the ideal model is revised to account for the inability of the angle diversity to remove all multipath dispersion, using simpler receivers. Section 4 provides computer simulation for different receiver parameters. Concluding remarks are presented in section 5.

5.2 Maximal Ratio Combining

The signals received through the wireless IR communication link suffer two impairments. First, as signals take on different paths to a receiver, they arrive at different times, giving rise to temporal dispersion. Second, at a receiver, the transmitted signal cannot be separated from the noise caused by ambient light. This noise is not constant; instead it varies depending on the location and orientation of receiver branch relative to a light source. In order to alleviate these impairments, the receiver has to be capable of performing two tasks. First, it has to compensate for the variable delay of received signals. Second, since the noise power on different branches is not uniform, it has to weigh less noisy branches heavier than the noisy ones. A receiver that is able to perform both these tasks is the one that employs Maximal Ratio Combining (MRC) [55]. An MRC receiver performs these tasks by multiplying the received signal through a channel with a gain proportional to its SNR. Since the same amount of power is transmitted through every diffusing spot, the gain at *j*th channel is:

$$G_j = \frac{H_{j0}}{\sigma_j^2}, \tag{5.1}$$

where H_{j0} is the channel gain and σ_j^2 is the noise variance. The receiver first estimates the arrival time of each delayed path. Then, it introduces a variable delay to align the strongest component from each channel. A delay t_c is added to ensure causality of the receiver filter, i.e., $t_c \geq \max[t_j],\ j \in \{1, L\}$. The *j*th channel is shown in Figure 5-1. Factor R at the receiver is added in because of the photo-detector responsivity. The transmitter F(f) and receiver G(f) filters are identical, each accomplishing half of the signal shaping. Since the noise spectral density is flat and the transmission channel is real, the transmitter and receiver filters that maximize SNR at sampling time, for a given input power, follow from [55]:

$$F(f)G(f) = X_{rc}(f), \tag{5.2}$$

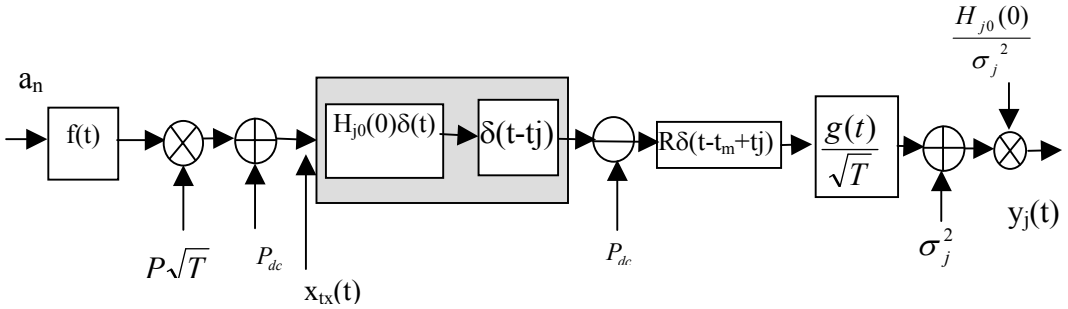

Figure 5-1: The *j*th channel with an angle diversity receiver.

where X_{rc} is a raised cosine frequency response. The receiver filter magnitude is given by:

$$|F(f)| = |G(f)| = \sqrt{|X_{rc}(f)|}. \tag{5.3}$$

Therefore, both f(t) and g(t) have root raised cosine with a time domain representation given by Eq.(4.6). Substituting for G(f) in Eq. (4.5), the noise variance becomes:

$$\begin{aligned}\sigma_j^2 &= 2qI_{bg} \times (\frac{1}{\sqrt{T}})^2 \times \int_0^\infty |G(f)|^2 df = 2qI_{bg} \times \frac{1}{T} \times \int_0^\infty |X_{src}(f)|^2 df, \\ &= qI_{bg}B,\end{aligned} \tag{5.4}$$

where *B* is the bit rate and is equal to 1/T. The noise variance at the output of the receiver is

$$\sigma_{jout}^2 = \sigma_j^2 \times (\frac{H_{j0}}{\sigma_j^2})^2 = \frac{H_{j0}^2}{\sigma_j^2}. \tag{5.5}$$

5.2.1 Receiver Output

The receiver, in an angle diversity system, is composed of multiple branches, each of which contains a filter matched to the received waveform and a delay that depends on the channel. To calculate the receiver output, an equivalent channel impulse response $h_{eq}(t)$ is defined:

$$h_{eq}(t) = \sum_{i=1}^{L} H_{i0}(0)\delta(t) \times \frac{H_{i0}}{\sigma_i^2} = \sum_{i=1}^{L} \frac{H_{i0}^2}{\sigma_i^2}\delta(t). \tag{5.6}$$

In terms of h_{eq}, the output is expressed as:

$$y(t) = RP \sum_{n=-N}^{N} a_n \times f(t-nT) \otimes h_{eq}(t) \otimes g(t-t_c). \tag{5.7}$$

Substituting for $h_{eq}(t)$, the expression for y(t) becomes:

$$y(t) = RP \sum_{n=-N}^{N} a_n \sum_{i=1}^{L} \frac{{H_{i0}}^2(0)}{\sigma_i^2} x_{rc}(t - nT - t_c). \tag{5.8}$$

The noise at the output of the receiver is equal to the summation of noise at the output of each channel. At the output of the *i*th receiver, the noise $z_i(t)$ is a zero-mean Gaussian term. The expression for the output y(t), including the noise term, becomes:

$$y(t) = RP \sum_{n=-N}^{N} \sum_{i=1}^{L} a_n H_{i0}(0) x_{rc}(t - nT - t_c) + \sum_{i=1}^{L} z_i(t). \tag{5.9}$$

The output y(t) is sampled at time $t_s = t_c + kT$. Thus, y [k] is:

$$y[k] = y[t_c + kT] = RP \sum_{n=-N}^{N} \sum_{i=1}^{L} a_n H_{i0}(0) x_{rc}(kT - nT) + \sum_{i=1}^{L} z_i(kT + t_m). \tag{5.10}$$

Since $x_{rc}(nT) = 0, \forall\ n \neq 0$, Eq. (5.10) simplifies to:

$$y[k] = RP \sum_{i=1}^{L} a_k H_{i0}(0) + \eta, \tag{5.11}$$

where variance of noise η is found by summing the noise variance over all channels, i.e., ${\sigma_\eta}^2 = \sum_{i=1}^{L} \sigma_{iout}^2$. A maximum likelihood receiver uses the sampled output y[k] to decide which symbol is transmitted. Assuming that 0 and 1 are equally likely to occur, the detected symbol $\hat{a}_k$ is determined according to:

$$\hat{a}_k = \begin{Bmatrix} 1 \text{ if } P(y[k] \mid a_k = 1) > P(y[k] \mid a_k = 0) \\ 0 \text{ if } P(y[k] \mid a_k = 0) < P(y[k] \mid a_k = 1) \end{Bmatrix}. \tag{5.12}$$

5.2.2 Performance Measures

Two measures, that are not independent of one another, are used to evaluate the performance of the receiver and to determine the optimal number of branches: the probability of error and SNR. For maximum likelihood detector, assuming symbols are equally likely to be 0 or 1, the probability of error is:

$$P_e = Q\left(\frac{RP\sum_{i=1}^{L}\frac{{H_{i0}}^2(0)}{2\sigma_i^2}}{\sqrt{\sum_{i=1}^{L}\sigma_{iout}^2}}\right) = Q\left(RP\sqrt{\sum_{i=1}^{L}\frac{H_{i0}^2(0)}{2\sigma_i^2}}\right). \tag{5.13}$$

The signal-to-noise ratio SNR is defined as the ratio of the output signal power when $a_n = 1$ is transmitted and the noise power, and is equal to:

$$SNR = \frac{\left(RP\sum_{i=1}^{L}\frac{{H_{i0}}^2(0)}{\sigma_i^2}\right)^2}{\sum_{i=1}^{L}\frac{H_{i0}^2(0)}{\sigma_i^2}} = R^2P^2\sum_{i=1}^{L}\frac{H_{i0}^2(0)}{\sigma_i^2} \tag{5.14}$$

Expressed in terms of SNR, the probability of error is:

$$P_e = Q\left(\sqrt{\frac{SNR}{2}}\right) \tag{5.15}$$

Equations (14) and (15) highlight the dependence of error probability on the number of channels. Increasing the number of channels increases the total received power, but does not necessarily increase the SNR value. This is because some of the newly added branches might have $H_{i0}(0)$ equal to zero or a very small value compared to added noise.

5.3 A More Accurate Channel Model

For the reasons discussed in section 4.4, the channel impulse response is more accurately modeled as a strong component resulting from the direct path and weaker components that suffer reflections. The diversity receiver task is to add a delay to each channel in order to align their strong components, such that the resultant equivalent impulse response $h_{eq}(t)$ has a strong component at time t_m. The receiver also multiplies each channel by a factor proportional to its SNR. The $h_{eq}(t)$, shown in the Figure 4-8, can be expressed as:

$$h_{eq}(t) = \sum_{l=1}^{L} h_l(t) = \sum_{i=-m}^{n} H_i \delta(t - i\Delta - t_S), \tag{5.16}$$

where $\Delta = \frac{D}{n+m}$ is the sampling time, D is the delay spread, h_l is the shifted impulse response of the *l*th channel, and H_is are given by:

$$H_i = \sum_{k=1}^{L} \frac{H_{k0}}{\sigma_i^2} \times H_{ki}, \tag{5.17}$$

where H_{k0} is the maximum component in the *k*th channel impulse response, and H_{ki} is the component occurring at time equals $i\Delta$ away from H_{k0}. The equivalent channel response is composed of n+m+1 impulses. Since some signals will travel shorter distances, and others longer distances than the direct path, m impulses precede h_0 and n will succeed it. For example, when three diffusing spots, of different distances from the receiver, are within a FOV_{branch}, there will be three components in the channel impulse response. If the middle component is the strongest, the receiver will align this component with the strongest components from other branches. The impulse response will contain a

component preceding and another succeeding the strong component. The signal at the receiver output, for a single transmitted symbol a_k, is:

$$y(t) = RPa_k x_{rc}(t) \otimes h_{eq}(t). \tag{5.18}$$

When an infinitely long sequence of symbols is transmitted, and using (21) to substitute for $h_{eq}(t)$, the resultant y(t) becomes:

$$y(t) = RP \sum_{k=-\infty}^{\infty} \sum_{i=-m}^{n} a_k H_i x_{rc}(t - nT - i\Delta - t_m). \tag{5.19}$$

It can be seen from Eq. (5.19) that the receiver output suffers from ISI caused by the residual temporal dispersion. This ISI degrades the receiver performance and results in a higher probability of bit error.

5.3.1 Performance Measures

The performance measures derived under dispersion-free equivalent channel have to be modified to account for the residual temporal dispersion. At sampling time $t_{sampling}$ = kT+ t_S, the receiver output y[k] is:

$$y[k] = y[kT] = R\,Pa_k H_0 + RP \sum_{j=-\infty}^{\infty} \sum_{\substack{i=-m \\ i\neq 0}}^{n} a_n H_i x_{rc}(kT - jT - i\Delta). \tag{5.20}$$

This happens, because $x_{rc}(nT) = 0, \forall n \neq 0,$ and $x_{rc}(0) = 1$. The evaluation of Eq. (5.20) can be simplified by defining an end-to-end impulse response x(t) that represents the response of the equivalent channel to the input $x_{rc}(t)$ scaled by the RP i.e. $x(t) = R\,x_{rc}(t) * h_{eq}(t)$. Expressing y[k] in terms of x(t), we obtain:

$$y[k] = a_k x(0) + \sum_{\substack{n=-\infty \\ n \neq k}}^{\infty} a_n x((k-n)T) . \tag{5.21}$$

When calculating the effect of ISI on the detected symbol, x(t) is recognized as a decaying function. Therefore, the detected symbol is only affected by its neighboring symbols. In this study, the effect of symbols farther than $\pm 6T$ is found negligible. The expression for y[k] simplifies to:

$$y[k] = a_k x(0) + \sum_{\substack{i=-6 \\ i \neq 0}}^{6} a_{k-i} x\ (iT) . \tag{5.22}$$

The effect of ISI depends on the value of the neighboring symbols. Since symbols are equally likely to be 0 or 1, there are 2^{12} possible neighboring sequences. The *i*th sequence, $seq_i = [a_{-6},...a_{-1},a_1 \ldots a_6]$, has a decimal equivalent equal to i. The ISI contribution of a sequence $d_{ISI}(i)$ is given by:

$$d_{ISI}(i) = d_{ISI}(seq_i) = \frac{1}{x(0)} \sum_{\substack{j=-6 \\ j \neq 0}}^{6} a_j x(jT) , \tag{5.23}$$

where a_j is chosen from the entries of the *i*th sequence. The average error probability is calculated by averaging the conditional probability of error on each sequence. For the *i*th sequence, an error occurs if $x(0)d_{ISI}(i)$ and noise exceed a threshold value V_T , i.e.,

$$P(e \mid seq_i) = P(x(0)d_{ISI}(i) + \eta > V_T) = Q(\frac{V_T - x(0)d_{ISI}(i)}{\sigma}) , \tag{5.24}$$

where $V_T = \frac{x(0)}{2}$. Since the noise is a zero-mean Gaussian process, and all sequences are equally likely, the average P_e can be expressed as:

$$P_e = \sum_{i=1}^{2^{12}} P(e|seq_i)P(seq_i) = \frac{1}{2^{12}} \sum_{i=1}^{2^{12}} Q(\frac{x(0)/2 - x(0)d_{ISI}(i)}{\sigma_\eta}) . \quad (5.25)$$

Expressing the average probability of error in terms of SNR, defined as $SNR = \frac{x(0)^2}{\sigma_\eta^{\ 2}}$, we obtain:

$$P_e = \frac{1}{2^{2\times 6}} \sum_{i=1}^{2^{2\times 6}} Q[\sqrt{SNR}(1/2 - d_{ISI}(i)] . \quad (5.26)$$

5.4 Simulation Results

In our computer simulations, we considered a room and link set up similar to the one in chapter 4 (Table 4-2). The room has the dimensions of 6mx6mx3m, with one of the walls covered by a window. The ceiling contains 9 equally spaced Tungsten lamps. The receiver's parameters, transmitted power, bit rate, and P_e used in simulation are summarized in Table 5-1.

Table 5-1: Parameters used in computer simulation.

Parameter	**Value**
Receiver FOV_{branch}	5.75^o, 11.5^o,
Average transmitted power per spot	0.01W
Bit rate	100 Mbps
Targeted P_e	10^{-9}

The transmitter (access point) is placed at the center of the room to produce 10x10 equally spaced diffusing spots of equal intensity on the ceiling. Receivers (terminals) assume random locations within the room at a constant height equal to 0.9m. To account for random receiver locations, the performance is evaluated at 1156 different locations generated according to:

$$\begin{aligned} x_{rcvr} &= \frac{i + v_i}{6}, \quad i \in [1,34] \\ y_{rcvr} &= \frac{j + v_j}{6}, \quad j \in [1,34] \end{aligned}, \tag{5.27}$$

where v_i and v_j are uniformly distributed random variables, that take on values between 0 and 1. Meeting performance requirements at these location guarantees the performance at any location within the room by moving a receiver a maximum of 0.5m along x or y direction. Three values for FOV_{branch} are used 5.75^o, 11.5^o, and 23^o. FOV_{branch} equal to 11.5^o guarantees at least one diffusing spot is within the FOV_{branch} [52]. Since diffusing spots are placed above receivers, branches are added as long as the performance is not met and the FOV_{total} is less than 90^o.

Error probability, SNR and outage probability are calculated as a function of the total number of branches. The central branch is labeled as branch number 1. Subsequent branches are numbered in increasing order as they move away from the central branch.

The average error probability for the 1156 locations, as a function of the total number of branches, is shown in Figure **5-2**. From the figure, an average probability of error equal to 10^{-9}(shown as horizontal line), is achieved by 5 branches with $FOV_{branch}=11.5^o$, and 11 branches with $FOV_{branch} = 5.75^o$. When FOV_{branch} is equal to 23^o, the receiver

reaches the maximum number of branches allowed without successfully achieving targeted P_e.

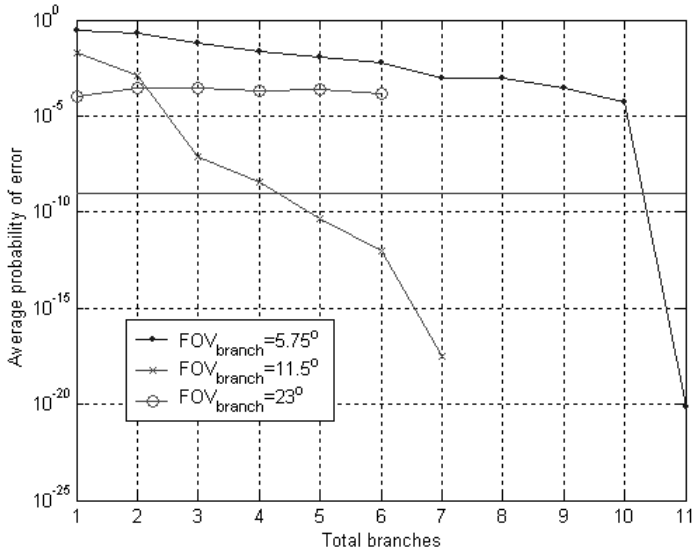

Figure 5-2: Average probability of error for 1156 receiver locations.

Although the average probability of error gives information about link behavior, it cannot solely be used for determining link performance. This is true since receivers are subjected to a highly varying environment. A few receivers that fall under light sources or window, can compromise the average probability values. More insight is achieved by utilizing outage probability defined as the percentage of locations that fail to meet the P_e requirement for a given number of branches. The exact figure to use for outage probability depends on cost and link usage. In this study, we require the link to meet 0% outage i.e. 100% availability.

The outage probability vs. number of branches is plotted in Figure **5-3**. The figure shows 0% outage is achieved by 7 branches for a receiver using FOV_{branch} equal to 11.5^o,

reducing FOV_{branch} to 5.75° increases the required branches to 11. The minimum outage possible with FOV_{branch} equal to 23° is 27.7%.

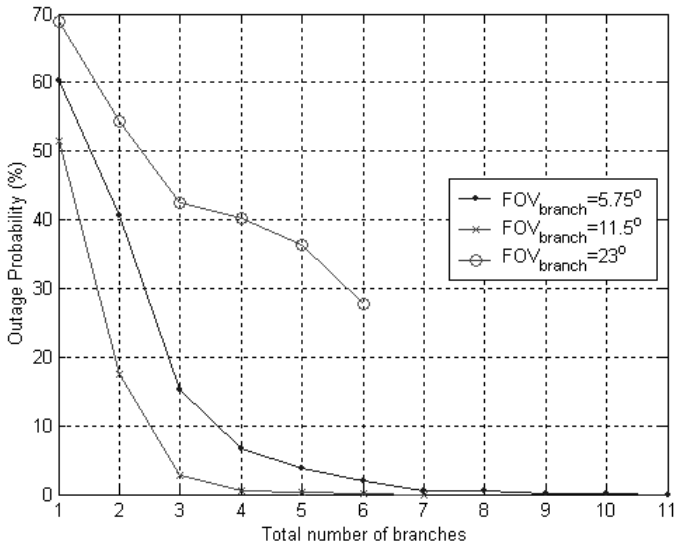

Figure 5-3: Outage probability versus number of branches for different FOV_{branch} used.

The results of outage probability should come as no surprise in lieu of the discussion in the previous section. When FOV_{branch} is small, noise power and ISI are minimal. Since at the most a single spot falls within the branch FOV, the receiver is able to align strong impulse together, thus minimizing ISI. At the same time, a small branch FOV, means less likelihood to intercept a diffusing spot. Increasing FOV_{branch} to 11.5° guarantees that each branch will intercept at least a diffusing spot. More than a single spot might fall within FOV_{branch}, but these spots are located very close to each other, thus resulting in a negligible ISI. Increasing FOV_{branch} increases noise power as well. Further increase in FOV_{branch} causes a branch to intercept a number of diffusing spots. Since these spots are at larger distances, the impulse response contains several strong impulses resulting from the direct path reception. As these impulses occur at farther times, ISI is more severe

hindering the link ability to achieve targeted P_e. Degrading the performance further is the large noise power caused by large FOV_{branch}. This can be seen by examining Figure **5-4**, which depicts the average SNR for the three structures.

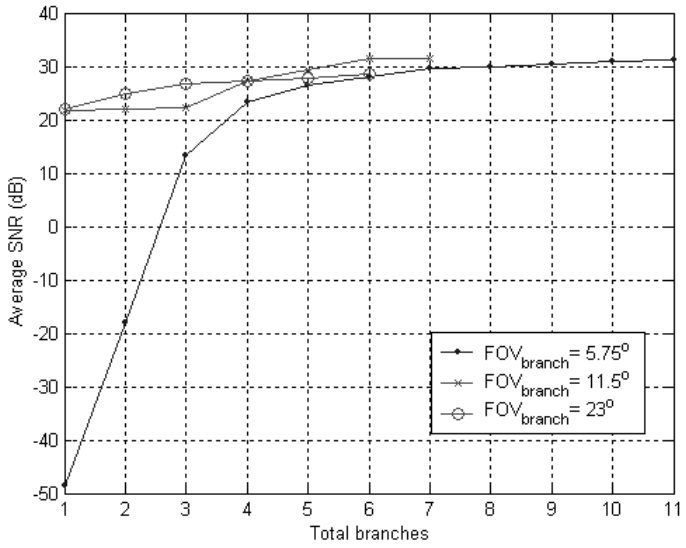

Figure 5-4: Average SNR versus the total number of branches (for all 1156 locations).

The inability of a large number of receiver locations with small FOV_{branch} (5.75^o) to capture diffusing spots, using small number of branches, results in a very small average SNR. The SNR of FOV_{branch} equals to 11.5^o and 23^o are comparable in spite of outage performance variations. This is a direct result of ISI term in Eq. (5.26), which becomes more significant as FOV_{branch} increases.

5.5 Conclusions

The indoor wireless infrared link suffers from multipath temporal dispersion caused by different path lengths traveled by a transmitted signal. This chapter demonstrates that

angle diversity at the receiver is an effective technique to reduce the channel dispersion effect, in turn, reducing the ISI and the probability of error.

In designing an angle diversity receiver, three parameters must be specified: FOV_{total}, FOV_{branch}, and the total number of branches. The choice of FOV_{branch} depends on the pattern of diffusing spots, their separation, and the distance between the receiver and the spots region. A trade-off is needed in choosing the FOV_{branch}. Reducing the latter, enhances the receiver ability to combat temporal dispersion and reduces ambient noise, but it can result also in the branch's inability to capture any diffusing spots, and thus contribute only noise power to receiver. The number of branches depends on performance requirement, noise power and the relative contribution of the newly added branches.

The optimal number of branches, i.e., the minimum number of branches that minimizes outage, depends on the choice of FOV_{branch}. Choosing a FOV_{branch} value such that at least a single diffusing spot is within the FOV results in the optimal number of branches. Decreasing FOV_{branch} results in a higher number of branches to meet the outage requirement. Increasing FOV_{branch} results in the inability of a receiver to meet performance requirements.

The noise power at the receiver branches depends on the orientation of a branch relative to ambient light sources. The varying nature of noise at branches prompted the use of maximal ratio combining at the receiver. Thus, less noisy channels are weighted more heavily than noisy ones.

Chapter 6

SPATIAL CODING IN INDOOR OPTICAL WIRELESS LINK
Reducing Power and Bandwidth Requirements

6.1 Introduction

Although the uniform distribution of optical power is one of the main requirements for multi-access support in a wireless optical link, Multi Spot Diffusing Configuration (MSDC) provides uniformity, along with spatial independence that allows spatial diversity techniques over the link. Independent spatial channels are generated by a multibeam transmitter producing spatially confined diffusing spots, and a multibranch receiver with narrow field-of-view branches. In this chapter, we propose an orthogonal spatial coding technique that utilizes the independence of channels to reduce power and bandwidth requirements. The technique is based on treating the m channels between transceivers as an m-dimensional space. This enables data transmission through varying signal levels and its location in space.

In MSDC, a transmitter (access point) projects optical power through multiple narrow beams to form diffusing spots on a ceiling or walls as illustrated in Figure 6-1. A multibranch receiver (terminals) is used with each branch having access to a single diffusing spot. Thus, diffusing spots can be considered as line-of-sight sources. The multibranch receiver, in effect, creates multi-input multi-output (MIMO) channels with

the number of input channels being equal to the number of diffusing spots and output channels equal to the number receiver branches capturing diffusing spots.

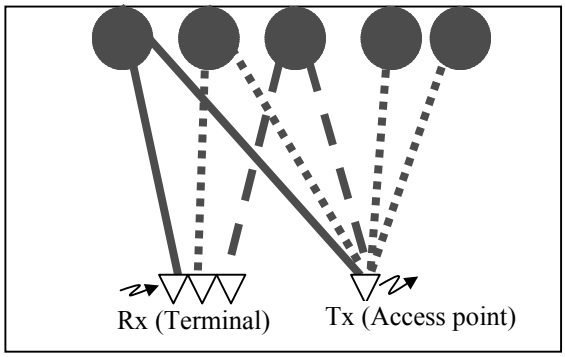

Figure 6-1: Cross section of MSDC indoor link. By properly selecting receiver parameters, uncorrelated spatial channels are created.

Several factors limit the achievable bit rate in an OW link under normal operation, i.e., no shadowing and typical ambient light condition. First, due to eye safety and other practical considerations, the average transmitted power must be kept below a specified value, limiting signal-to-noise ratio at the receiver output. Second, temporal dispersion caused by multipath results in ISI that increases the probability of error. Finally, achievable bit rate is limited by the electrical bandwidth of transmitter and receiver circuits and their processing speed.

In this chapter, orthogonal spatial coding technique (OSC) is proposed based on the availability of independent channels between the transmitter and the receiver. In section 2, we model the MSDC link to obtain the channel impulse response and show that under stated conditions, channels can be modeled as ideal ones. Section 3 looks at spot

configuration to determine the availability of the spatial channels and the spacing required of spots. The design of an optical link is presented in section 4 along with the special requirements that limit transmitted power. Orthogonal spatial diversity coding technique is introduced in section 5. The simulation results are presented in section 6. Finally, the findings are summarized in the Conclusions.

6.2 Channel Response

The link in MSDC is composed of many channels; the number of which depends on the number of diffusing spots and receiver parameters. In this section, we model the channel and show that for a small branch FOV, it can be approximated by an ideal one. To do that, we present the mathematical model to obtain channel impulse response. When calculating channel impulse response, direct path, as well as reflections off walls and ceiling must be taken into account. Using the development in chapter 2, the channel impulse response is obtained by dividing the room's internal surface into *N* equally sized reflective elements. Each element is identified by its index. Thus, ρ_i and A_i refer to the reflection coefficient and the area of the *i*th element. The radiation pattern of diffusing spots as well as reflecting elements is assumed first order Lambertian. The impulse response between the diffusing spots and a receiver made of a single branch can be expressed as:

$$H = D \cdot G_r + F_s \cdot \Phi_n \cdot G_r, \tag{6.1}$$

where H is a polynomial with coefficients equal to the amplitude and powers proportional to delay, i.e., $H = a_0 x^0 + a_1 x^{t_1}$ is equivalent to $h(t) = a_0 + a_1 \delta(t - t_1)$. The vector D is the direct response vector, F_s is transmitter vector, Φ_n is geometry matrix, and G_r is receiver's branch vector.

In this chapter, we consider a room with dimensions equal to (6m, 6m, 3m). The receiver is located in a plane of height equals to 0.9m, and is composed of branches each with a FOV = 7^o. The transmitter generates 10x10-diffusing spots equally spaced on the ceiling of the room. Figure 6-2 shows a typical impulse response for a receiver located at (0.9m, 0.9m, 0.9m) when 3 reflections are considered. The graph shows that impulse response components that suffered reflections are at least 28 dB weaker in amplitude than direct response. This location represents a worst-case receiver location, since the receiver is located very close to two walls. For other locations, the difference between the direct component and the reflected component is even larger; the difference for a receiver located at (1.5m,1.5m,0.9m) exceeds 70 dB. Thus, signals received through reflections are largely attenuated, and their impact can be ignored.

By properly distributing diffusing spots on the ceiling and using a FOV_{branch} value that captures a single diffusing spot, the contribution of reflected signals (the second term in Eq.(6.1) becomes insignificant compared to direct signal. This implies a negligible correlation between the channels, and channel impulse responses are ideal. Therefore, in this chapter, the channels to branches are safely assumed ideal and uncorrelated. To further simplify the analysis, the channel attenuation factor H is assumed equal on all

channels, otherwise, the transmitter varies the signal amplitude on each channel to ensure same signal levels are received at all receiver branches.

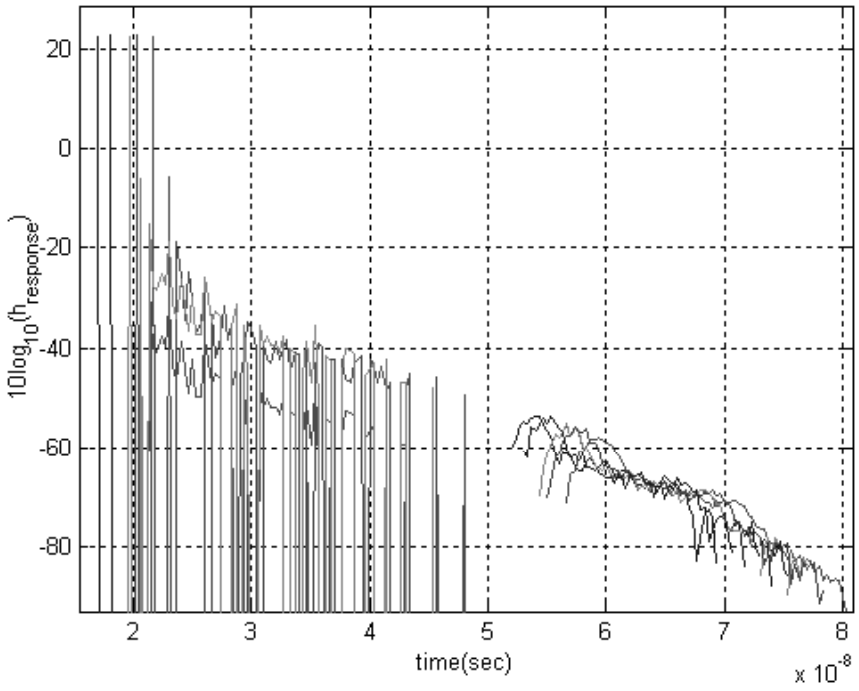

Figure 6-2: The channel impulse responses as seen by 8-branch receiver.

6.3 Receiver Front-End Design

The improvement achieved by spatial techniques is directly proportional to the number of available channels. In order to use spatial diversity, channels have to be available for the majority of receiver locations to provide a guaranteed service throughout the room. In this chapter, we assume a receiver that is composed of 8 branches each with

a field-of-view small enough to prevent the reception of more than a single spot. This can be achieved by ensuring the minimum spacing between spots is larger than $2\times \mathrm{h} \times \tan(\mathrm{FOV}_{\mathrm{branch}})$, where h is the height of the ceiling plane relative to receiver plane. The branches are arranged to form a coverage area illustrated in Figure 6-3.

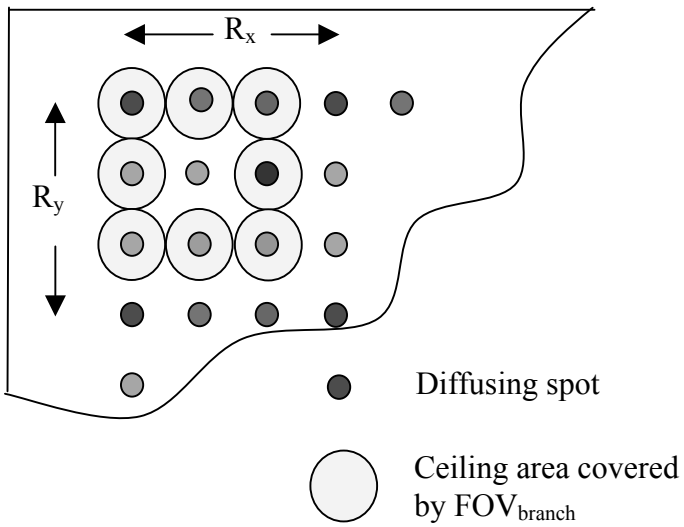

Figure 6-3: Ceiling view showing diffusing spots and receiver coverage area.

The 8 spots carry independent data. This does not require that all the diffusing spots to be generated by independent sources; it suffices to have each group of neighboring spots generated by independent sources.

6.4 Link Design

Although the exact link design varies between combining and spatial coding receivers, they have common components, as shown in Figure 6-4. Both links use intensity modulation/direct detection IM/DD with on-off keying. This results in two

constraints on transmitted signal shape. First, the signal has to be non-negative, and second, the average transmitted power has to be constrained by a value P_m determined by the eye safety and other practical considerations.

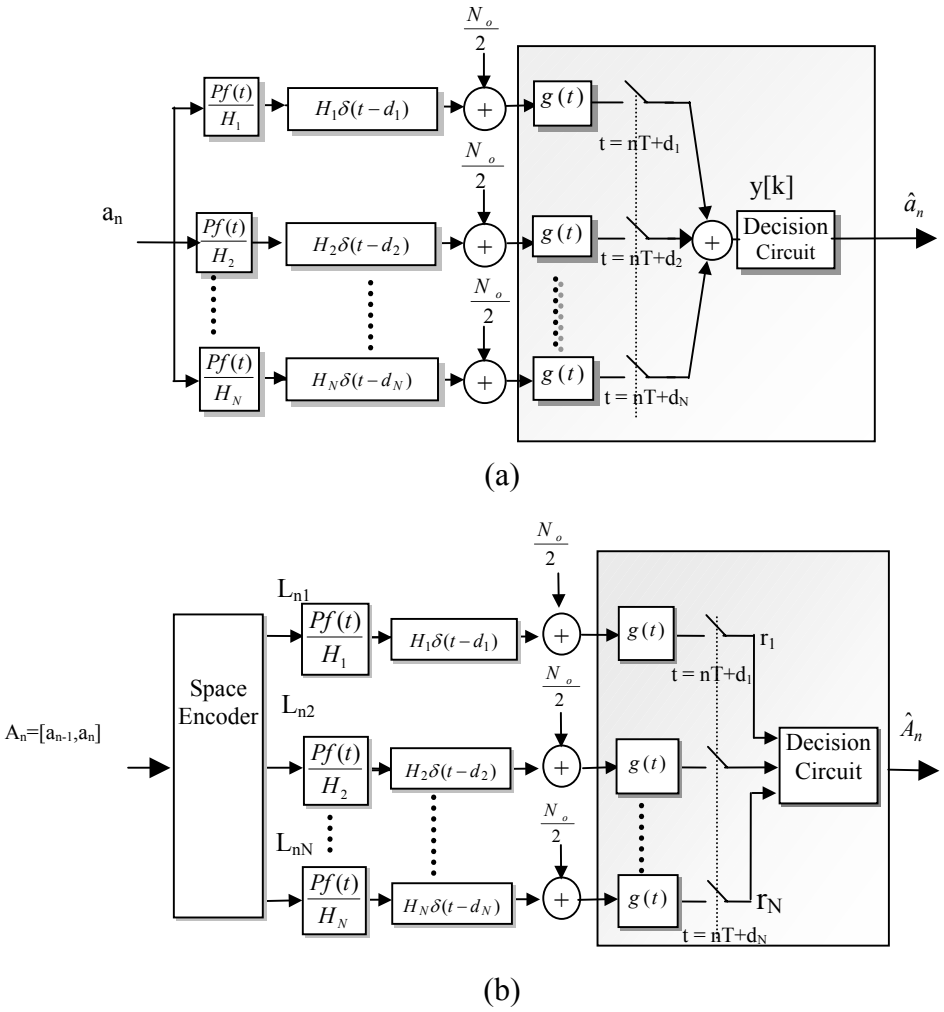

Figure 6-4: (a) Equivalent link model using combining. (b) Link model using spatial coding.

The transmitter employs a rectangular pulse shaping filter f(t). Assuming 0 and 1 are equally likely, the average transmitted power is equal to P/2. Where P is the amplitude of transmitted signal when 1 is sent, 0 is transmitted by the absence of a pulse. The pulse duration is equal to T. The *i*th channel has a constant gain H_i and introduces a delay d_i. The receiver compensates for different path delays by sampling the received signal at time $nT+d_i$. Pulse shaping filter g(t) at the receiver produces a raised cosine pulse shape for a rectangular input, i.e., $x_{rc}(t)=f(t)*g(t)$. The channel noise is assumed to be a zero-mean Gaussian process. Noise at sampler output has a variance equal to [49][36]:

$$\sigma^2 = 2 \times 0.56 qRBP_{bg}, \tag{6.2}$$

where R is the photodetector responsitivity, B is pulse rate and is equal to 1/T, q is electron charge, and P_{bg} is incident background optical power. The multiplicative factor 0.56 results from receiver filter and is equal to $\int_0^\infty |G(f)|^2 df$. Equation ((6.2) shows that noise power is directly proportional to the data rate through its dependence on B. Nonbinary signaling improves bandwidth efficiency by transmitting more bits per symbol. It also reduces noise power by a factor proportional to the number of bits carried per symbol. This is important, since noise and transceivers bandwidth play a significant rule in determining achievable bit rates in OW links.

In evaluating link performance in section 6, two cases are considered in determining the value of P_m. The first case, referred to as fixed power per user, the power constraint is specified in terms of the total power allocated per user P_M, P_m is calculated by dividing P_M by the number of channels to a user N, i.e., $P_m = P_M/N$. In the second case, referred to as fixed power per channel, the power constraint is specified in terms of the maximum

power allowed per channel. Therefore, $P_m = P_M$. The total power per user is equal to the sum of power to all channels. Specifying the constraint in terms of the channel or the user depends on transmitter design and method used in generating diffusing spots. It also provides a means for comparing schemes that use different number of channels.

6.5 Space Diversity Coding Techniques

As mentioned in earlier, space diversity techniques are accomplished by considering the m channels between transceivers as an m-dimensional space. A transmitted signal is represented by a single point in this space; this enables information transmission through varying any of the signal coordinates. When received signals are combined as in equal gain combining, the space reduces to a single dimension, i.e., a line, thus limiting the coordinates to a single parameter.

The performance of combining is used as a benchmark for comparing the performance of OSC. For each technique, the average transmitted power per channel, as well as the total average transmitted power per user is calculated.

6.5.1 Equal Gain Combining

In equal gain combining, the same signal is transmitted over all channels. The receiver adds signals on branches before a decision is made (Figure 6- 4(a)). A binary 1 is sent by transmitting a pulse (a_n=1), while 0 is sent by its absence. When a_n=1, the combined received signal y(t) can be expressed as:

$$y(t) = P\sum_{i=1}^{N} f(t) * g(t) = NPx_{rc}(t) + n(t). \tag{6.3}$$

At sampling time t =nT, y[n] becomes:

$$y[n] = NP + n, \tag{6.4}$$

where n is a zero mean Gaussian process with variance equal to:

$$\sigma_T{}^2 = N\sigma^2 = N \times 2 \times 0.56qRBP_{bg}. \tag{6.5}$$

The probability of bit error using an ML detector is:

$$BER = Q(\frac{NP/2}{\sqrt{N}\sigma}) = Q(\frac{\sqrt{N}P}{2\sigma}). \tag{6.6}$$

The average transmitted power on each channel $P_{avg} = P/2$, and the average total transmitted power $P_{Total} = NP/2$.

6.5.2 Orthogonal Spatial Signaling

In orthogonal signaling, each channel is dedicated to the transmission of one of M symbols. Thus, M channels are needed to transmit M symbols. This technique resembles pulse position modulation (PPM) [58] with symbols encoded spatially rather than temporally. The gain obtained is $\log_2$M reduction in transceivers bandwidth. The receiver decision circuit decides on a transmitted symbol by comparing its M inputs, a decision $\hat{\mathrm{A}} = \mathrm{A_j}$ is made if $\mathrm{r_j} > \mathrm{r_i}\ \forall \mathrm{i} \neq \mathrm{j}$. The expression for BER is given by [55]:

$$BER = \frac{2^{m-1}}{2^m - 1} - \frac{2^{m-1}}{(2^m - 1) \times \sqrt{2\pi}} \int_{-\infty}^{\infty} \left[1 - \left(\frac{1}{\sqrt{2\pi}} \int_{-\infty}^{y} e^{-x^2/2} dx \right)^{M-1} \right] \exp\left[-\frac{1}{2} \left(y - \frac{\sqrt{m}P}{\sigma} \right)^2 \right] dy \tag{6.7}$$

The average power on each channel and average total power are P/M and P, respectively, where P is the pulse amplitude on the channel carrying a symbol.

6.6 Simulation Results

To evaluate the performance of OSC, we define three performance measures. First, coding gain is defined as the power reduction compared to a 2-channel combining to achieve the same BER. Second, the ratio of filters bandwidth relative to 2-channel combining for the same bit rate is defined as a bandwidth saving factor. Finally, since power can be traded for bandwidth, a bit rate factor is defined as the achievable bit rate compared to 2-channel combining when both links use the same amount of power and have the same BER. The bit rate factor is calculated by finding the transceiver bandwidth that results in BER equals to 2-channel combining. When a technique has a positive coding gain, transceiver bandwidth can be increased (increasing noise power) till BER is equal to that of the 2-channel combining, increasing bandwidth increases bit rate.

6.6.1 Fixed Power Per User

When the power per user is fixed, the power transmitted through all channels to a user must add to the total allocated power per user P_M. Figure 6-5 shows the probability of bit error for different number of channels as a function of P_M/σ. The figure reveals the possibility of achieving a coding gain of 2.2 dB and bandwidth saving equal to 3, when OSC is used over 8 channels. Compared to combining with the same number of channels,

spatial coding results in 5.2 dB coding gain. When both links use the same average power, it is possible to transmit with orthogonal signaling over 8 channels at approximately 12 times higher than combining. As the number of channels increases, the coding gain and BW saving increase. The resultant coding gain, BW saving, and data rate factor are summarized in Table 6-1.

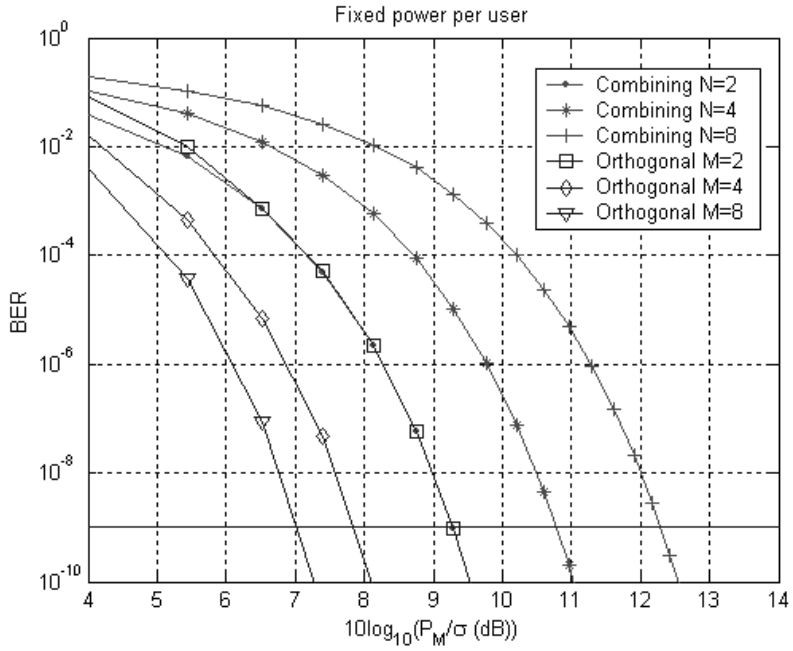

Figure 6-5: Probability of bit error when power allocated per user is fixed

6.6.2 Fixed Power Per Channel

When the average power allocated per channel is defined in terms of P_M, each channel can have an average power P_m equal to P_M. The resulting probability of bit error versus P_M/σ is shown in Figure 6-6. The improvement achieved by spatial coding is

larger than that achieved in the fixed power per user with over 8 dB coding gain and 3 times saving in BW when 8 channels are used. For a given power per channel, it is possible using 8-channels spatial coding to transmit at a rate 10 times higher than 8-channels using combining. The resultant coding gain, BW saving, and data rate factor are summarized in Table 6-1.

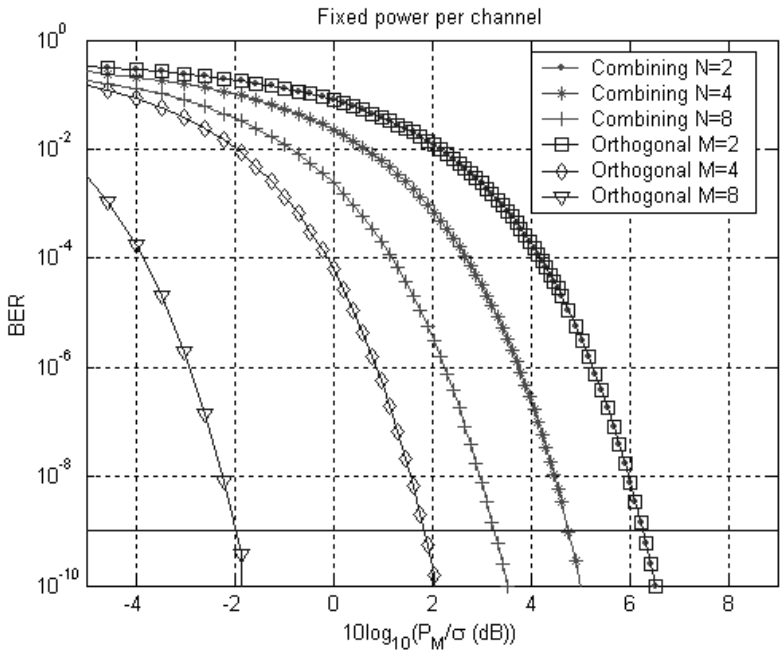

Figure 6-6: Comparing coding gain and bandwidth saving for different coding techniques.

Table **6-1**: Comparing coding gain and bandwidth saving for different coding techniques.

Technique	Fixed power per user			Fixed power per channel		
	Coding gain	BW saving	Bit rate factor	Coding gain	BW saving	Bit rate factor
Combining	-	-	-	-	-	-
N=4	-1.5	1	½	1.5	1	2
N=8	-3.0	1	1/4	3.0	1	4
Orthogonal						
M=2	0	0	1	0	0	1
M=4	1.4	2	2	4.4	2	7
M=8	2.2	3	3	8.2	3	40

6.7 Conclusions

Optical wireless links operate under stringent power budget. This motivates searching for ways to use available power efficiently. In this paper, we introduced orthogonal spatial coding technique that utilizes channels independence to provide an added degree of diversity. This enables data transmission through varying the signal level as well as the channel.

When the power allocated per user is fixed, and power has to be divided among channels, spatial coding with 8 channels achieves 12 higher bit rate compared to combining for same amount of power and BER. When power per channel is fixed, 8 channels spatial coding achieves 10 times higher bit rate compared to combining using same number of channels.

The improvement in data rate is directly proportional to the number of available independent channels. However, increasing the number of channels beyond 8, increases the gain at the cost of added complexity and equipment cost and most importantly, susceptibility to shadowing.

Chapter 7

ON MERITS OF SPATIAL CODING IN MULTILEVEL OPTICAL WIRELESS LINKS

7.1 Introduction

Spatial confinement of paths traveled by infrared signals enables bandwidth and resources reuse in adjacent indoor environments. This property can also result in the undesired effect of shadowing, which occurs whenever an obstacle blocks signal path between transceivers. This can be caused by moving objects or receiver misalignment. Shadowing compromises link reliability by increasing error rate, and can result in service interruption. The number of blocked signal paths determines the severity of shadowing. In well-designed links, the shadowing effect can be minimized, but not eliminated. Several researchers have considered the impact of shadowing on link characteristics. In [21], shadowing caused by a person (shadower) on a diffused link was studied through measurements. The work shows that shadowing increases delay spread and path loss. An analytical calculation of throughput in a shadowed optical wireless link was provided in [57]. Through Markovian channel model, throughput variation caused by shadowing was analyzed.

In this chapter, two spatial coding techniques are proposed. The first alleviate the number of channels requirement constraint of orthogonal spatial coding presented in the

previous chapter. The new technique does not require 2^m channels for a symbol to carry m bits. The second coding technique is presented as a means of maintaining a reliable link in the presence of shadowing. Data is transmitted not only through changing signal levels, but also through the channels carrying them. Section 2 looks at indoor environment to determine availability of spatial channels at different receiver locations. Combining and spatial coding techniques are compared in section 3 under normal operating conditions. The impact of shadowing is studied in section 4. Finally, the findings are summarized in the Conclusions.

7.2 Available Spatial Channels

In order to use spatial diversity, independent channels must be available throughout the service area. This section looks at the available spatial channels in the MSDC environment and determines the number of these channels. The receiver is composed of a central branch pointing towards the ceiling and two tiers of branches. The first is tilted from the ceiling by 14^o and contains 6 branches placed 60^o apart. The second tier is tilted 28^o and contains 4 branches placed 90^o apart. As a result, the ceiling area that falls within receiver FOV can be approximated by 11 adjacent circles.

The number of available channels is illustrated in Figure 7-1. The service area covers a plane of height equal 0.9m and excludes 0.7m strips adjacent to walls. Approximately 8600 locations spaced 0.05m apart are considered. The percentage of locations versus the number of channels is plotted in Figure 7-2. The figure shows that at least 4, 5 and 6 channels are available at 100%, 99% and 96% of locations, respectively.

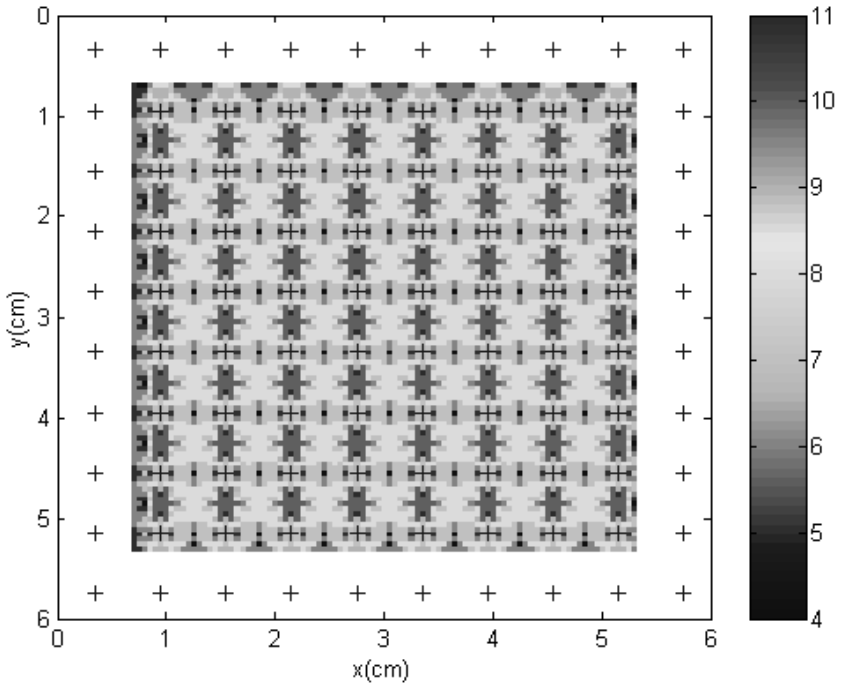

Figure 7-1: Available spatial channels for different receiver locations. A '+' symbol represents a diffusing spot.

In this chapter, no special layout is assumed for the receiver locations, i.e., receivers are assumed equally likely to exist anywhere in service area. When receivers assume a subspace due to room layout and usage, diffusing spots location can be optimized to allow for fewer branches at the receiver.

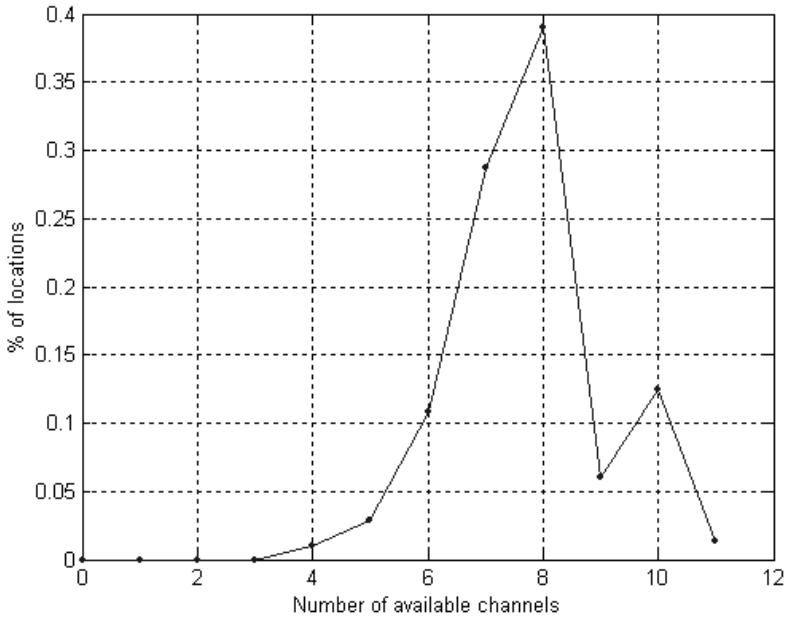

Figure 7-2: Percentage of locations vs. the number of available channels for an 11-branch receiver.

7.3 Spatial Coding Technique

As mentioned in the previous chapter, space diversity techniques are accomplished by regarding the m channels between the transmitter and the receiver as an m-dimensional space. A transmitted signal is considered as a single point in this space, this enables information transmission through varying any of the signal coordinates. When received signals are combined as in equal gain combining, the space reduces to a single dimension i.e. a line, thus limiting the coordinates to a single parameter. The link equivalent model

is similar to the one presented in chapter 6 (Figure 6-4). The only difference is in the algorithm used by the decision circuit at the receiver to decide on a transmitted symbol.

7.3.1 Multi-Level Signaling with Equal Gain Combining

In multi-level signaling with equal gain combining, one of $M=2^m$ signals levels are transmitted over all the channels to carry m bits. The receiver adds signals on all branches before a decision is made. Thus, when signal level L is transmitted, the input of the decision circuit y(t) can be expressed as :

$$y(t) = \frac{L}{H_0} H_0 \sum_{i=1}^{N} f(t) * g(t) = NLx_{rc}(t) + n(t). \tag{7.1}$$

At sampling time t =nT, y[n] is

$$y[n] = NL + n, \tag{7.2}$$

where n is a zero mean Gaussian process with variance equal:

$$\sigma_T^{\,2} = N\sigma^2 = N \times 2 \times 0.56 qRBP_{bg}. \tag{7.3}$$

The probability of bit error using a ML detector is

$$BER = \frac{2(M-1)}{m \times M} Q\left(\frac{NL}{2(2^m - 1)\sigma}\right), \tag{7.4}$$

where L is the maximum transmitted pulse amplitude. The average transmitted power on each channel $P_{avg} = L/2$, and the average total transmitted power $P_{Total} = NL/2$.

7.3.2 Spatial Coding

In spatial coding, we seek to alter the signal level transmitted over each channel to achieve a maximum separation between symbols. In general, the coding of M symbols over N channels can be expressed in matrix form G_{MN} as:

$$G_{MN} = \begin{bmatrix} L_{11} & \cdots & L_{1N} \\ \vdots & \ddots & \vdots \\ L_{M1} & \cdots & L_{MN} \end{bmatrix}, \tag{7.5}$$

where L_{ij} is the level representing symbol i on *j*th channel. The decision circuit decides on the symbol that maximizes the correlation between the received vector and the codes representing the symbols (the rows of G_{MN}), this is equivalent to minimizing the Euclidean distance to the received symbol [55]. An approximate upper bound on BER can be expressed as:

$$BER = \frac{1}{M \log_2 M} \sum_{i=1}^{M} \sum_{\substack{j=1 \\ j \neq i}}^{M} h_{ij} Q\left(\frac{d_{ij}}{2\sigma}\right), \tag{7.6}$$

where h_{ij} is the hamming distance between the symbols represented by *i*th and *j*th rows and d_{ij} is the Euclidean distance between row i and j, respectively. With a power limited budget d_{ij} is determined by both M and N. Increasing M decreases the value L representing a symbol. In obtaining the elements in G_{MN} matrix, the BER is treated as a cost function and L_{ij}'s that minimize are sought. Considering the cases of M= 4 and 8 and iterating over all possible values of G_{MN}, the matrices that minimize BER are:

$$G_{42}=\begin{bmatrix}0&0\\0&L\\L&0\\L&L\end{bmatrix},\ G_{43}=\begin{bmatrix}0&0&0\\L&0&0\\0&L&0\\0&0&L\end{bmatrix},\ G_{44}=\begin{bmatrix}L&0&0&0\\0&L&0&0\\0&0&L&0\\0&0&0&L\end{bmatrix},\ G_{45}=\begin{bmatrix}L&0&0&0&0\\0&L&0&0&0\\0&0&L&0&L\\0&0&0&L&0\end{bmatrix}$$

$$G_{83}=\begin{bmatrix}0&0&0\\0&0&L\\0&L&0\\0&L&L\\L&0&0\\L&0&L\\L&L&0\\L&L&L\end{bmatrix},\quad G_{84}=\begin{bmatrix}0&0&L&0\\0&0&L&L\\0&L&0&0\\0&L&0&L\\L&0&0&0\\L&0&0&L\\L&L&L&0\\L&L&L&L\end{bmatrix},\ G_{85}=\begin{bmatrix}0&0&0&0&0\\0&0&L&L&0\\0&L&0&L&L\\0&L&L&0&L\\L&0&0&0&L\\L&0&L&L&L\\L&L&0&L&0\\L&L&L&0&0\end{bmatrix} \tag{7.7}$$

To obtain G_{46}, G_{42} is concatenated 3 times and G_{86} is obtained by using G_{85} and selecting the 6^{th} column that minimizes BER. The values of L are determined by the power constraint placed on the link.

7.3.3 Simulation Results

To compare the performance of different coding techniques, we define the coding gain of a scheme as the power reduction to achieve same BER for same number of channels. The fixed power per user and fixed power per channel are considered separately.

7.3.3.1 Fixed Power Per Channel

When the average power allocated per channel is constrained to P_M, each channel can have an average power P_m equals P_M. The value of L, representing a symbol in G, is determined by the number of levels M. For the same number of channels, L is reduced by half when the number of levels is doubled. The BERs are shown in Figure 7-3 for different coding schemes and the power requirements to achieve targeted BER are

summarized in Table 7-1. From the table, a coding gain of 3.3, 5.4, 6.1, 5.7, and 6.4 dB is achieved using spatial coding with 4 levels compared to combining over 2, 3, 4, 5, and 6 channels, respectively. Using 8 levels results in 6.2, 5.7, 6.7, and 6.2 dB coding gain over 3, 4, 5 and 6 channels, respectively.

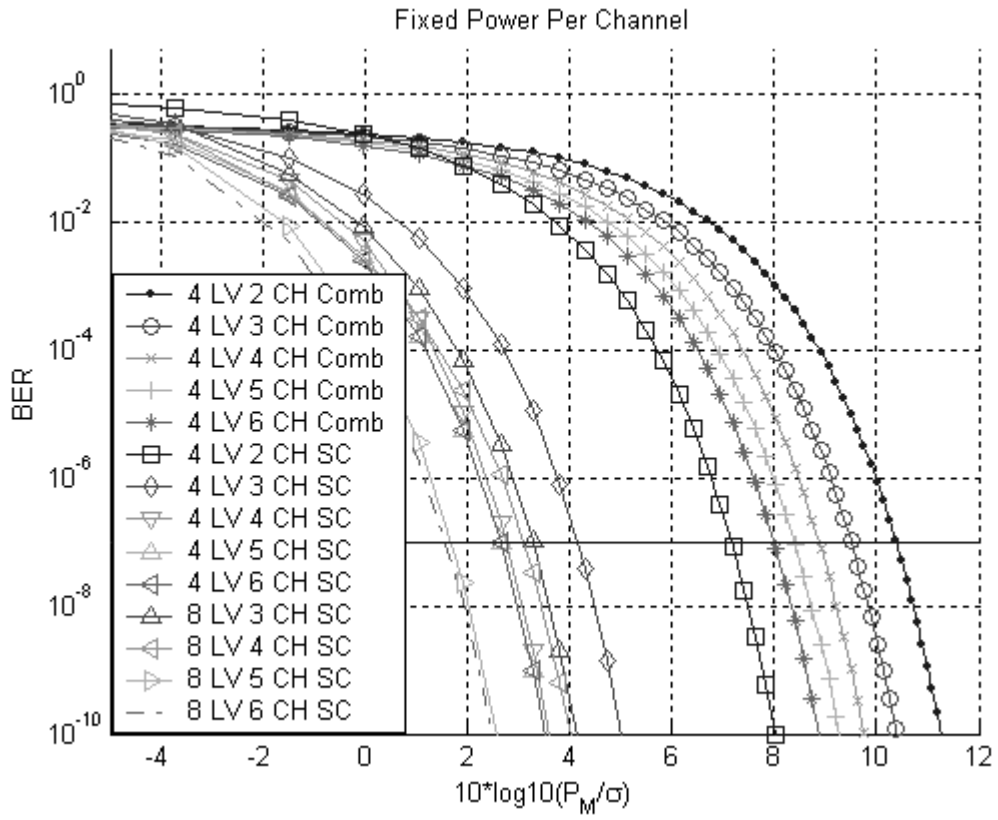

Figure 7-3: Probability of bit error when power allocated per channel is fixed.

7.3.3.2 Fixed Power Per User

When the power per user is fixed, the average power transmitted through all the channels to a user must add up to the average power allocated per user P_M. Power allocated per channel P_m is equal to P_M divided by the total number of channels. Figure 7-4 compares the performance of different transmission techniques, and the power required to meet target BER are summarized in Table 7-1. From the table, a coding gain of 3.3, 5.3, 6.2, 5.7, and 5.3 dB is achieved using spatial coding with 4 levels compared to combining over 2, 3, 4, 5, and 6 channels, respectively. Using 8 levels results in 6.2, 5.9, 6.7, and 6.4 dB coding gain over 3, 4, 5, and 6 channels, respectively.

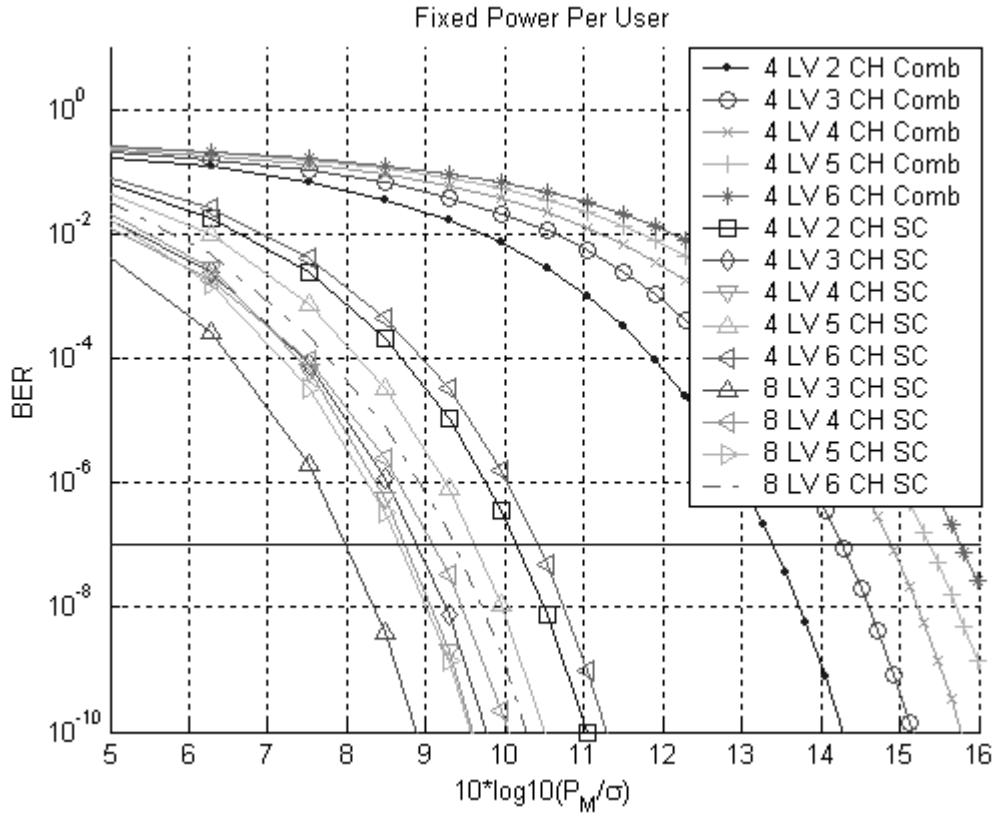

Figure 7-4: Probability of bit error when power allocated per user is fixed.

Table 7-1: Power requirements for different coding schemes.

	Fixed power per channel			Fixed power per user		
	4 Levels Combining	4 Levels SC	8 Levels SC	4 Levels Combining	4 Levels SC	8 Levels SC
2 channels	10.4	7.1	-	13.4	10.1	-
3 channels	9.5	4.1	3.3	14.2	8.9	8.0
4 channels	8.8	2.7	3.1	14.9	8.7	9.0
5 channels	8.3	2.6	1.6	15.3	9.6	8.6
6 channels	7.9	2.6	1.5	15.7	10.4	9.3

7.4 Impact of Shadowing

In this section, we propose a new coding scheme and compare its performance to combining in presence of shadowing. A single shadowed channel is assumed, since this has the most likely occurrence. Moreover, even with a single shadowed channel, performance might be compromised to the extent it is not possible to maintain a reliable link.

7.4.1 Multi-Amplitude Signaling with Combining

In a multi-amplitude signaling with combining, one of $M=2^m$ signals levels is transmitted over all channels to carry m bits. The receiver adds signals on all branches before a decision is made. Increasing the number of levels reduces the bandwidth requirement of transceiver filters, which in turns reduces noise power. It also decreases the separation between symbols. It can be shown that m=2 has the best error performance among multilevel signaling techniques. Therefore, m=2 is selected in this section. Using

Gray coding, the binary bits 00, 01, 11, and 10 are transmitted by L equal 0, 2P/3N, 4P/3N and 2P/N over each channel. When S channels are shadowed, the expression for received signal r[k] becomes:

$$r[k] = (N - S)L + n \tag{7.8}$$

Shadowing impact can be understood by considering the decision making at the receiver. Receiver unaware of shadowing decides on a transmitted symbol based on signal amplitude according to normal conditions. Shadowing has no effect when a symbol carrying 00 is transmitted since signal levels are already zero. All other symbols are affected. When 10 is transmitted, the detector makes a correct decision if r[k] is larger than 5P/3, shadowing reduces r[k] by S×2P/N, resulting in a smaller noise margin and higher probability of wrong decision. For large SNR, dominant errors occur when 11 and 10 are transmitted, in this case, BER can be approximated by:

$$BER = \frac{1}{2 \times 4}\left(Q(\frac{P/3 - 4SP/3N}{\sigma_T}) + Q(\frac{P/3 - 2SP/N}{\sigma_T}) \right). \tag{7.9}$$

With combining, shadowing is independent of channel location, since all channels carry the same signal.

7.4.2 Spatial Coding

For spatial coding to alleviate the impact of shadowing, the codes representing symobl must have a large hamming distance. Therefore, we construct our codes by searching for matrices with maximum minimum hamming distance. Iterating over all possible values, the matrices that provide maximum minimum hamming distance are:

$$G_{44}=\begin{bmatrix}0&0&0&0\\L&0&L&0\\0&L&0&L\\L&L&L&L\end{bmatrix},\ G_{45}=\begin{bmatrix}0&0&0&0&0\\0&L&0&L&L\\L&0&L&0&L\\L&L&L&L&0\end{bmatrix},\ G_{46}=\begin{bmatrix}0&0&0&0&0&0\\0&L&0&L&L&L\\L&0&L&0&L&L\\L&L&L&L&0&0\end{bmatrix}. \tag{7.10}$$

The hamming distance is equal to 2,3 and 4 for G_{44}, G_{45} and G_{46}, respectively. The bits 00,01,10, and 11 are represented by 1st,2nd,3rd and 4th row. When a channel is shadowed, the symbols affected are those that have a nonzero signal over the channel. For a large SNR, these symbols set the limit on achievable error rate. The method used to obtain BER is described below for shadowed symbols, for unshadowed symbols Eq. (7.6) applies. For a 4-channel link, shadowing does not affect the symbol carrying the 00 bits, since these bit are represented by the absence of signals over all channels. Shadowing of the second channel does not affect the symbol carrying 01, similarly, shadowing of the first channel does not affect the symbol carrying 10. When the a symbol is transmitted and a channel carrying a nonzero signal is shadowed, an error occurs if the received vector **r** is at a larger Euclidean distance from the transmitted symbol than any other symbols. To further illustrate this, let us consider the transmission of the symbol 01 represented by the [L 0 L 0] over a 4 channels link. When 01 is transmitted and the first channel is shadowed, the received vector **r** is equal to $[n_1\ n_2\ L+n_3\ n_4]$. The probability that **r** is decoded as 10 is equal to the probability that the Euclidean distance from **r** to the code representing 10 is smaller than that representing 01 i.e.

$$\begin{aligned}P(d(r,c_{10})<d(r,c_{01})) &= P(\left[(n_1-L)^2+n_2^2+n_3^2+n_4^2\right]< \\ &\qquad \left[n_1^2+(n_2-L)^2+(n_3+L)^2+(n_4-L)^2\right]), \\ &= Q(\frac{L}{\sqrt{4\sigma}})\end{aligned} \tag{7.11}$$

where d(x,y) is the Euclidean distance between x and y, and c_{ij} is the code representing the bits ij. The BER is calculated by considering the impact of each channel on all the symbols. Assuming all channels are equally likely to experience shadowing, the probability of the *i*th channel being shadowed $P(ch_i)$ is equal to 1/N, and BER can be expressed as:

$$BER = \sum_{i=1}^{N} (BER \mid ch_i) \times P(ch_i) . \tag{7.12}$$

7.4.3 Computer Simulation

The computer simulation is carried out for 4, 5 and 6 channels link. A link is classified as reliable if it maintains BER that is equal to or less than 10^{-7}. The link performance under normal operation is compared in Figure 7-5 and Figure 7-6 when the power per channel and user is constrained, respectively. Figure 7-5 shows that under normal operation, spatial coding achieves a power per channel saving of approximately 3.8 dB. When a channel is shadowed, links with 5 and 6 spatial channel are able to maintain a reliable link. The links suffers power penalty approximately equal to 3 dB with 6 channels and 4.5 dB with 5 channel i.e. the power per channel has to be increased approximately 2 and 3 folds to maintain the link with 5 and 6 channels, respectively. When the power per user is constrained, spatial coding achieves approximately 3.8 dB coding gain under normal operation. In this case, however, decreasing the number of channels improves link performance. Under shadowing, the configurations that maintain a reliable link use spatial coding with 5 and 6 channels. Shadowing results in 4.6 dB

coding loss compared to normal operating conditions with 5 channels and 2.9 dB coding loss with 6 channels. All other configurations fail to meet the targeted BER, irrespective of transmitted power.

Spatial coding complicates link design, since it requires the ability to switch spots independently. For delay insensitive traffic, the choice between different coding methods depends on the average duration of shadowing. If shadowing is infrequent and lasts for a small duration, it might be more efficient to tolerate traffic loss during shadowing for an increase in data rate under normal conditions. However, when the traffic is delay-sensitive such as video or other multimedia, the added cost and complexity of a 6 channel spatial coding is justified, since it can guarantee link reliability.

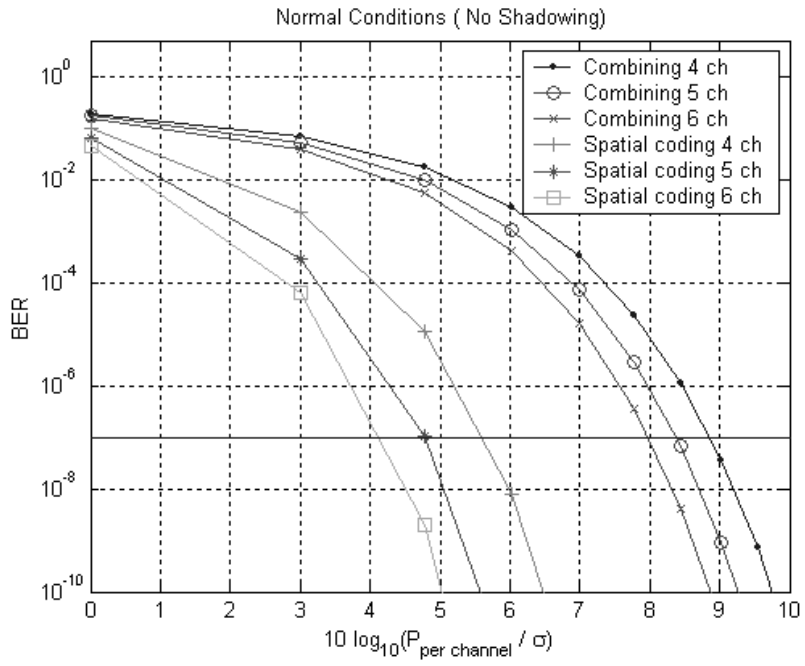

(a)

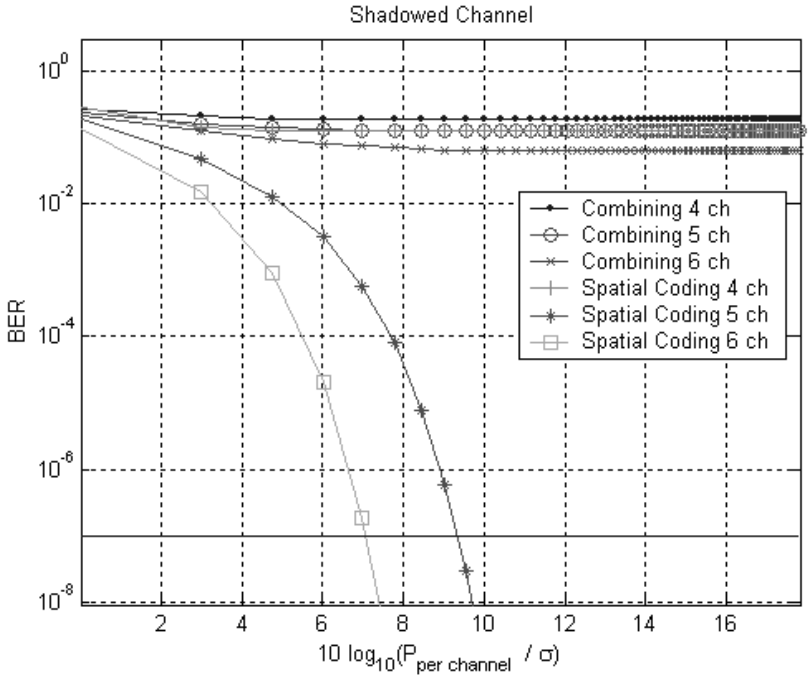

(b)

Figure 7-5: Comparing BER for combining and spatial coding links under normal operation (a) and shadowing (b) when the power per channel is fixed.

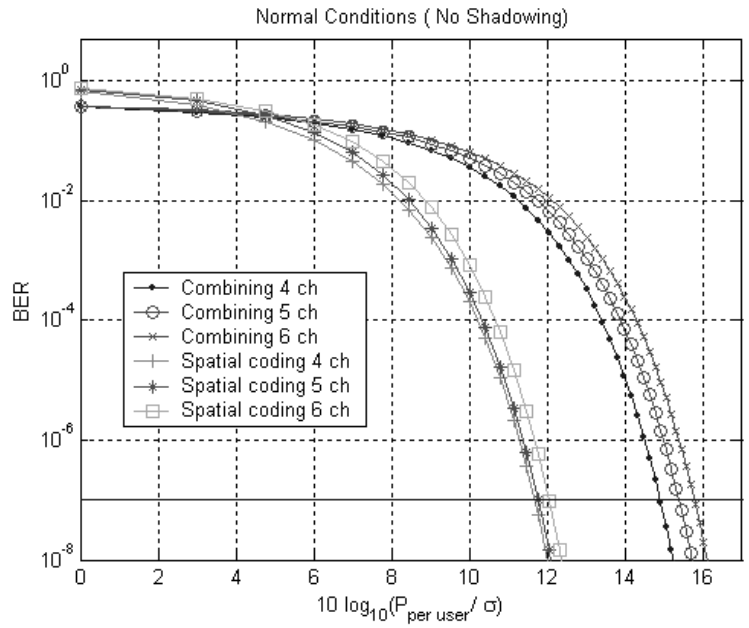

(a)

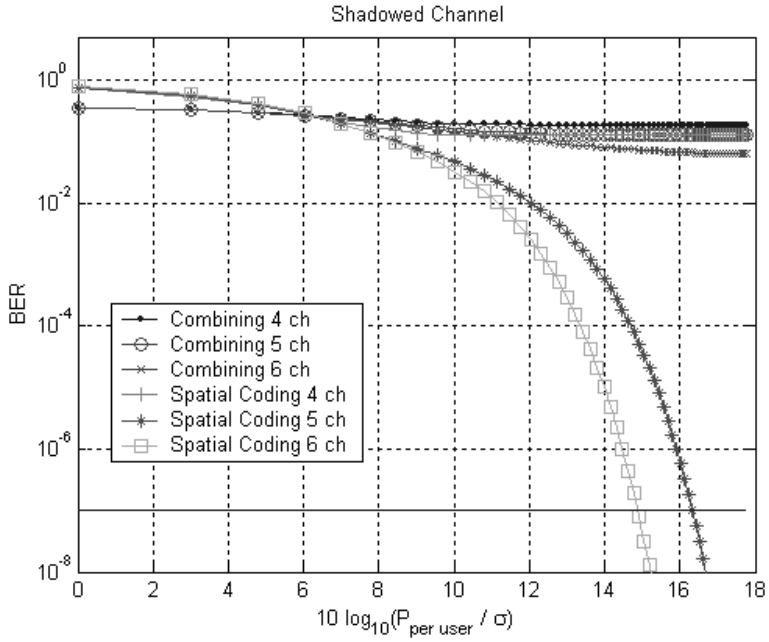

(b)

Figure 7-6: Comparing BER for combining and spatial coding links under normal operation and the power per user is fixed.

7.5 Conclusions

This chapter introduces a spatial coding technique that utilizes channels independence to provide an added degree of diversity. This enables data transmission through varying signal levels as well as the channel. When the power per channel is fixed, the improvement brought upon using spatial coding increases with the number of channels the link holds. Up to 6.1 dB coding gain is achieved using 4 channels link. Increasing the number of levels results in insignificant coding gain. When the power allocated per user is fixed, and thus power has to be divided among channels, spatial coding can achieve 6.2 dB coding gain over in a 4-channel link.

A new paradigm in link design is proposed. Here, the performance requirements have to be met, not only under normal operating conditions, but also for most likely impairment. Spatial coding is presented as a solution that can meet both performance requirements. Under normal operation, spatial coding can result in as much as 3.8 dB coding gain. With a shadowed channel, a reliable link is achieved by using 5 or 6 channels and 3 or 4.5 dB increase in optical power, respectively. Combining meets performance requirement under normal operation, but fails with a shadowed channel irrespective of transmitted power.

Although spatial coding comes with added cost and link complexity, its usage can be justified when the link carries delay-sensitive traffic and it is subject to frequent periods of shadowing.

Chapter 8

ASSESSING THE FEASIBILITY OF NEW DIFFUSED CONFIGURATION FOR OPTICAL WIRELESS LINK DESIGN

8.1 Introduction

Traditionally, diffused infrared configuration has been studied with the assumption that the illuminated region is placed at room ceiling as shown in Figure 8-1(a) [2]. This is done to ensure minimum path loss to a maximum number of receiver locations. This is because, this region is accessible to the largest number of receiver locations. In many practical situations, this arrangement might be difficult to implement, either due to the ceiling structure, or the difficulty in illuminating the entire ceiling uniformly without introducing an intrusive transmitter. A transmitter placed at the ceiling center is used to illuminate the walls as illustrated in Figure 8-1 (b). In this chapter, we propose a new configuration, in which the upper regions of the walls are illuminated. Path loss and delay spread are used as performance measures to assess the feasibility of the proposed configuration.

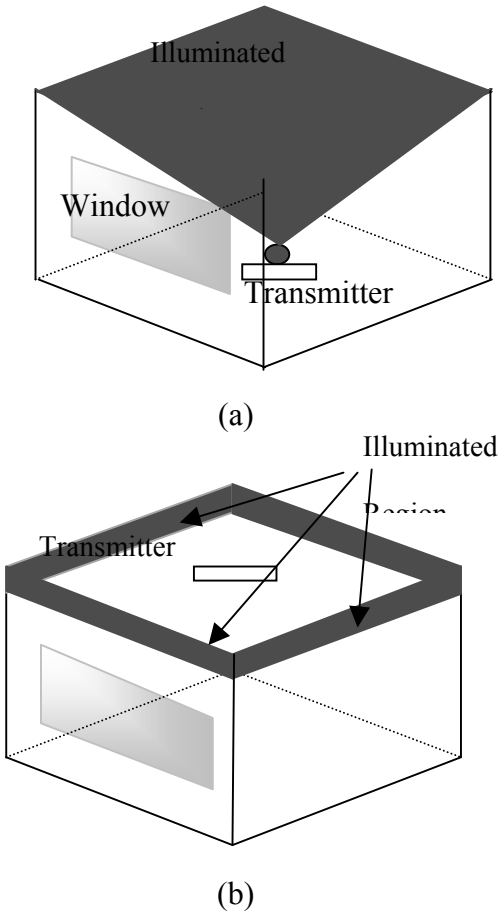

Figure 8-1: (a) Traditional diffused configuration. A transmitter placed at the room center is used to illuminate the ceiling. (b) Proposed configuration. A transmitter placed at the ceiling is used to illuminate the upper regions of the walls

8.2 Channel Model

Multipaths, the signals take in traveling between a transmitter and a receiver, complicate the calculations of channel impulse response in an indoor environment. These multipaths result from reflections off of room surfaces, furniture, etc. As the signal

undergoes a reflection, its amplitude is reduced, and its arrival time is increased. To obtain an accurate model of the channel, several reflections must be considered. Due to attenuation that high order reflections suffer, most of the signal energy is confined in the first three reflections.

As explained in chapter 2, the impulse response of an indoor environment is obtained by dividing the room surface into N adjacent elements of equal size. Each element is identified by an index, (x, y, z) coordinates, an orientation, and a reflection coefficient ρ. The number of elements determines time resolution of an impulse response, increasing the elements improves resolution at the cost of increasing calculation time. The elements illuminated directly by a transmitter act like sources, and thus are referred to as such. The impulse response can be expressed as:

$$\begin{aligned} H &= \sum_{i=0}^{n} H^{(i)} \\ &= F_{eq} \cdot \Phi_{n} \cdot G_{r} + D \cdot G_{r}, \end{aligned} \tag{8.1}$$

where $H^{(i)}$ is the impulse response resulting from *i*th reflection, F_{eq} is the source vector, Φ_n is the environment matrix, G_r is the receiver vector, and D is the direct response vector. To account for the multiple sources in a diffused configuration, an equivalent source vector F_{eq} is calculated according to:

$$F_{eq} = \sum_{i=1}^{S} F_i = [f_{eq1} \quad \cdots \quad f_{eqN}], \tag{8.2}$$

where S is the total number of sources and $f_{eqj} = \sum_{i=1}^{S} f_{ij}$. In a ceiling diffused case, these elements belong to the ceiling, while for a wall diffused; the elements belong to the upper

region of walls. In carrying out this simulation on a personal computer, entries in F, Φ, G, and D are represented as complex numbers with phase equal to time delay. Since the delay takes on very small values, it is expressed as an integer multiple of sampling time T_s, where T_s is equal to the time it takes light to travel between neighboring elements, i.e. $T_s = d/c$, where d is the distance between neighboring elements. When performing addition, only terms that have equal delay are added together. The impulse response is defined as the received optical power when transmitted optical power is equal to a delta function with unit-area, i.e., 1W. The room parameters used in this simulation are summarized in Table 8-1.

Table 8-1: Room parameters used in study.

Parameter	Ceiling Diffused	Wall Diffused
Width	6m	6m
Length	6m	6m
Height	3m	3m
$\rho_{walls} = \rho_{ceiling}$	0.7	0.7
ρ_{Window}	0.04	0.04
ρ_{floor}	0.2	0.2
Window height	1.2m	1.2m
Window width	4.6m	4.6m
Window elevation	1.0m	1.0m
Transmitter Location	(3,3,0.9)	(3,3,3)
Receiver FOV	90^o	90^o
d	0.2m	0.2m
N	3600	3600
Diffused region	Ceiling, 900 elements	Upper 0.4m of walls, 240 elements

The impulse responses for a receiver located at (1,2,0.9) are shown in. Figure 8-2. The figure shows several peaks in the ceiling diffused impulse response since the diffusing elements are adjacent to each other, in the wall diffused, four peaks are shown corresponding to the four walls.

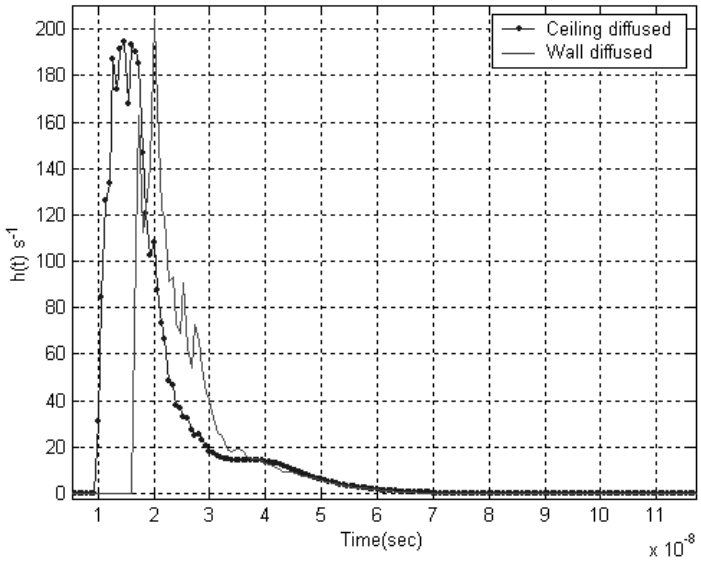

Figure 8-2: Comparing the impulse response of a receiver located at (1,2,0.9).

8.3 Link Profile

Two parameters are used to examine the link performance. These are path loss and RMS delay spread.

8.3.1 Path Loss

The signal-to-noise ratio (SNR) at the receiver is one of the determining factors of the achievable bit rate. In any communication system, it is desirable to have as large of a SNR as possible. In an infrared link, the amount of optical power transmitted is limited by eye safety considerations. Since the receiver in both configurations is exposed to the

same ambient light, the noise value is the same for fixed receiver parameters in either configuration. Therefore, a comparison of SNR is possible through comparing received power. A measure of received power is provided by path loss defined as the dc value of channel frequency response [21]:

$$\begin{aligned} PL &= -10 * \log_{10}(\mathbf{H}(0)) \\ &= -10 * \log_{10}(\sum_{i=0}^{K-1} T_s H_i)\,(\text{dBo}). \end{aligned} \tag{8.3}$$

Figure 8-3 compares a path loss histogram for the two configurations. The average path loss of the ceiling diffused configuration is equal to 58.33 (dBo) compared to 59.26 (dBo) of the wall diffused configuration. Another consideration is the uniformity of the received power loss throughout the room; this is illustrated in Fig. 4. The figure shows that the constant path loss region in the ceiling diffused belongs to rings surrounding the room center. The wall diffused case is depicted in Figure 8-4 (b).

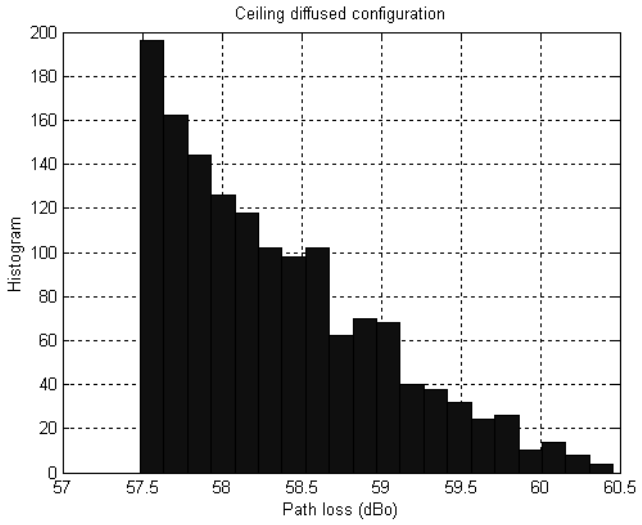

(a)

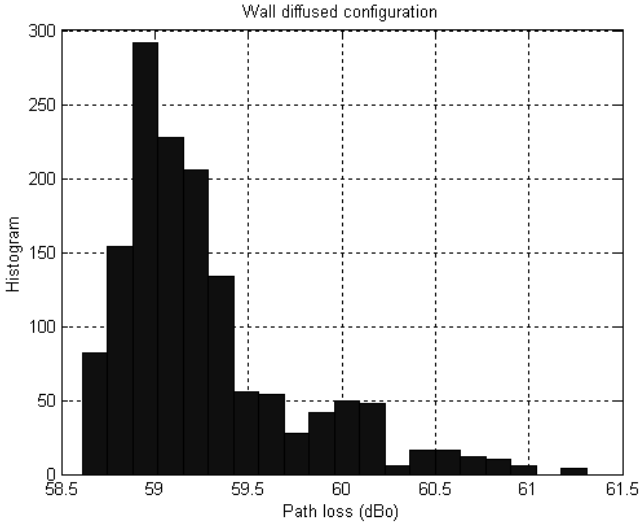

(b)

Figure 8-3: (a) Histogram plot of path loss for a ceiling diffused configuration. (b) Histogram of path loss for wall diffused configuration.

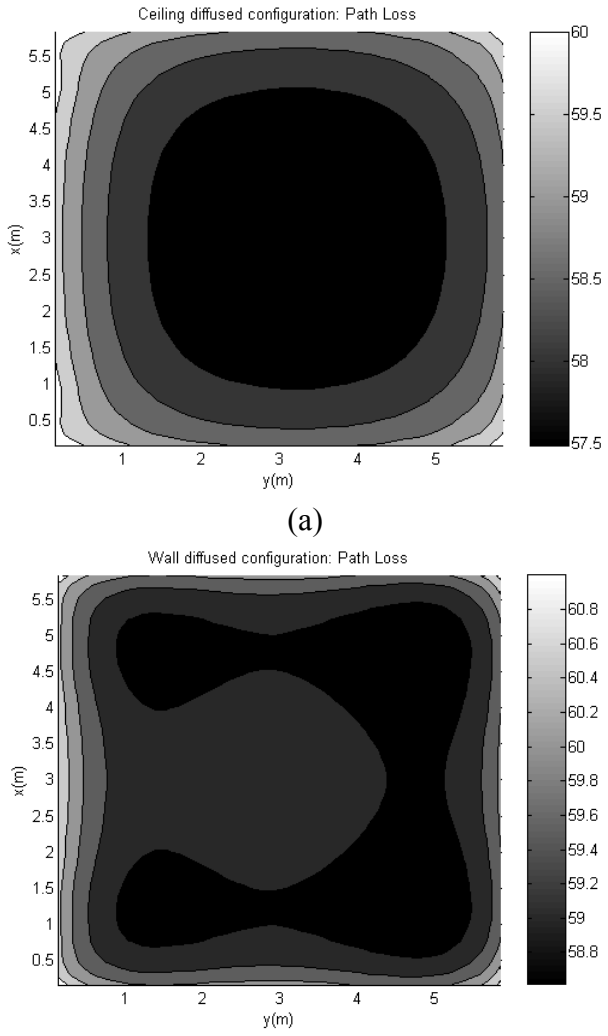

Figure 8-4: (a) Contour plot of path loss (dBo) for a ceiling diffused configuration. (b) Contour plot of path loss (dBo) for a wall diffused configuration.

8.3.2 Delay Spread

Intersymbol interference (ISI) resulting from propagation in a dispersive channel is a major problem in the design of a broadband wireless link. Dispersion sets the limit on the

symbol length that can be used. As dispersion increases, symbols have to be placed at farther time intervals in order to reduce the adverse effect of ISI. This, in turn, reduces the achievable bit rate. A measure of dispersion is provided by the mean square delay spread ($T_{delayspread}$), defined as the second moment of the impulse response [25]:

$$T_{delayspread} = \sqrt{E(\tau^2) - (E(\tau))^2} \ . \tag{8.4}$$

Profiles of the ceiling diffused and wall diffused are shown in Figure 8-5. The average delay spread is 4.46 (ns) in the ceiling diffused compared to 3.93 (ns) in the wall diffused configuration. The constant delay spread locations form a ring around the room center in the ceiling diffused configuration, with the highest spread being at the room center. In the wall diffused, the highest delay spread is located midway adjacent to walls, with room center experiencing lowest delay spread. This is illustrated in Figure 8-6.

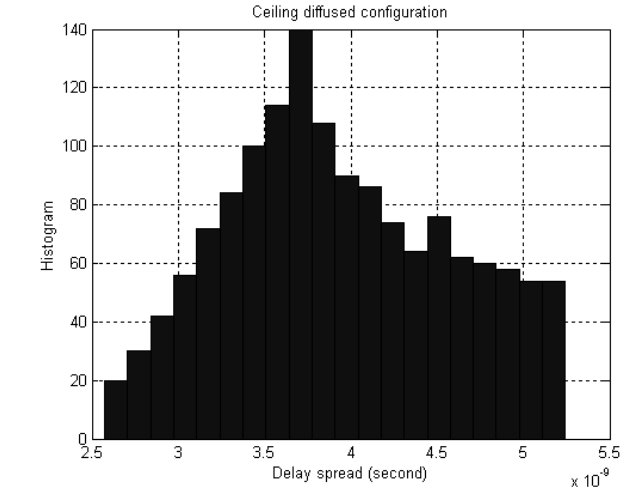

(a)

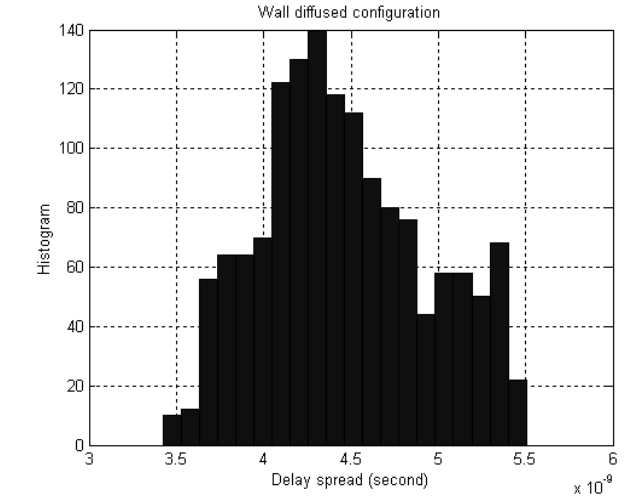

(b)

Figure 8-5: (a) Histogram plot of delay spread for a ceiling diffused configuration. (b) Histogram of delay spread for wall diffused configuration.

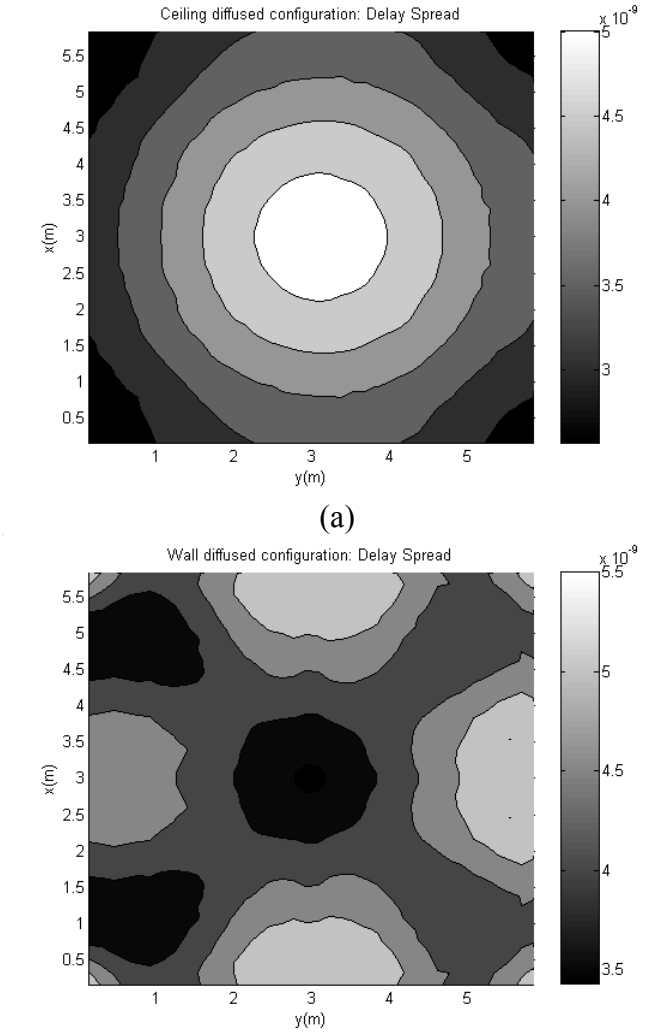

Figure 8-6: (a) Contour plot of delay spread (sec) for a ceiling diffused configuration. (b) Contour plot of delay spread (sec) for wall diffused configuration.

8.4 Conclusions

In this chapter, we proposed a new diffused configuration. The upper regions on the walls are illuminated instead of the ceiling. The preliminary evaluation is encouraging. The average path loss is less than 1.0 (dBo) higher than that of the ceiling diffused, and the average delay spread is approximately 13% higher.

Although not considered in this study, it is obvious that when the ceiling is used to hold light fixtures, the wall diffused receiver can be designed to block the signals coming directly from the ceiling to reduce the noise caused by ambient light. This can be accomplished by utilizing a multibranch receiver with branches tilted at an angle surrounding a ring.

Practical considerations, such as the unavailability of room center, or when the room center is constantly blocked by moving objects, makes the wall diffused configuration a promising alternative.

Chapter 9

CONCLUSIONS AND FUTURE WORK

9.1 Summary of Results

Optical wireless provides a viable alternative to radio frequency for carrying broadband data for indoor connectivity. This dissertation has focused on analytical methods and design issues of indoor links. Emphasis has been placed on different spatial diversity techniques that are made possible by the narrow paths traveled by optical signals. Diversity techniques that use combining at the receiver were studied through an accurate model of the link to determine their performance and parameters that optimize it. The available independent channels between transceivers are used to propose novel spatial coding code techniques. In these techniques, multibranch receivers decide on transmitted data based on received signals and channels carrying them. We conclude this dissertation by summarizing its major contributions as follows:

1. A novel approach for modeling indoor environment. The model divides the physical path between a transmitter and a receiver into stages. Each stage consolidates a set of parameters upon which an impulse response depends. This results in a tremendous savings in calculation time, especially when only one of the parameters is changed, such as location of a transmitter or a receiver. The new model also enables us to calculate received power per reflection for a very high order of reflections and to generate profiles based on delay spread and path loss

for any indoor environment efficiently. This approach enables the characterization of different environments to estimate expected data rates.

2. Design and analysis of a link that employs diversity transmission with equal gain combining. The work demonstrates the ability of angle diversity at the receiver is to effectively reduce channel dispersion, in turn, reducing ISI and the probability of error. In designing an angle diversity receiver, three parameters must be specified: FOV_{total}, FOV_{branch}, and the total number of branches. The choice of FOV_{branch} depends on the pattern of diffusing spots, their separation distances, and the distance between the receiver and spots region. A trade-off is needed in choosing the FOV_{branch}. Reducing the FOV_{branch} enhances the receiver ability to combat temporal dispersion; it also reduces the branch's ability to capture diffusing spots. The choice of number of branches depends on noise level and the relative contribution of the newly added branches. It has been demonstrated through evaluation of the outage probability that there exists an optimal number of branches that achieves the desired performance requirements. The number is optimal in the sense that it is the smallest number of branches that enables achieving a desired set of performance requirements. This, in turn, reduces receiver cost, complexity, and susceptibility to shadowing that occurs when an obstacle blocks signals path. The impact of using optimal timing circuit at receivers is insignificant when the FOV_{branch} is small. This is because the impulse response to the branches contains, at most, one strong component, which can be aligned by the receiver. As FOV_{branch} increases, the channel impulse response for some branches contain two or more strong components and the receiver is only

able to align one. Thus, the timing circuit plays a more significant role in reducing the ISI in this case. The improvement using timing circuit becomes less significant as the number of branches increases, because the newly added branches contribute a weaker signal as the spots become at larger angles and distances.

3. Design and analysis of a link that employs diversity transmission with maximal ratio combining. This work looks at the impact the choice of FOV_{branch} has on link performance. Choosing FOV_{branch} value such that at least a single diffusing spot is within FOV results in the optimal number of branches. Decreasing FOV_{branch} results in a higher number of branches to meet outage requirement. Increasing FOV_{branch} results in the inability of a receiver to meet performance requirements.
4. Orthogonal spatial coding to use available power and transceivers bandwidth more efficiently. This technique utilizes channels independence to provide an added degree of diversity. Thus enabling data transmission through varying signal level as well as the channel. M channels between transceivers are used to carry M symbols. The channel carries a non-zero signal only if it is carrying a symbol. The receiver decides on a transmitted symbol based on the branch that has a maximum signal. When the power allocated per user is fixed, and thus power has to be divided among channels, spatial coding with 8 channels achieves 12 times higher bit rate compared to combining for same amount of power and BER. When power per channel is fixed, 8 channels spatial coding achieves 10 times higher bit rate compared to combining using same number of channels.

5. A new paradigm in link design is introduced, in which, the performance requirements have to be met, not only under normal operating conditions, but also for most likely impairment. Spatial coding based on transmitting code words through available channels is presented as a solution that can meet both performance requirements. Under normal operation, spatial coding can result in as much as a 6 dB coding gain. With a shadowed channel, a reliable link is achieved by using 6 channels and a 4.5 dB increase in optical power. Combining meets performance requirement under normal operation, but fails with a shadowed channel irrespective of transmitted power.
6. A novel diffuse configuration in which upper regions on the walls are illuminated instead of the ceiling. The preliminary evaluation is encouraging. The average path loss is less than 1.0 (dBo) higher than that of the ceiling diffuse and the average delay spread is approximately 13% higher.

9.2 Recommendations for Future Work

Based on the contributions and tools developed in the thesis, future research in the development of broadband optical wireless technologies for indoor access will focus on three lines of research. Each line of research yields specific research tasks:

- Environment profile generation through the characterization of channels in different indoor environments
- Design and analysis of spatial coding technique in the MIMO configuration.

- Multi user access through spatial channel hopping

The future research is briefly overviewed below.

9.2.1 Environment Characterization

Indoor environments requiring wireless connectivity vary according to their structure, size, shape, and usage. A conference room in an educational setting for instance might have to provide service for a large number of users, while a residential room provides connectivity to few devices or users. The variation in the environments necessitates different designs to meet required capacity.

Traditionally, the ceiling is thought of as crossover between the wireless access point and receivers in non line-of-sight environments. Thus, light is projected on the ceiling and receivers are oriented towards the ceiling to capture as much of the transmitted power as possible. In many environments, however, the ceiling is not available either due to the environment structure such as the ceiling's height, or the low reflectivity of the material covering the ceiling.

Through an efficient technique developed in chapter 2, the calculation of the channel impulse response is divided in stages following the path an optical signal takes. Using this technique facilitates optimizing the location of illuminated region according to availability and expected terminals locations. Thus, further research tasks in environment characterization include:

- Generating profiles for different indoor environments. Profiles are generated through the form of maps of delay spread and optical received

power. These values will be used to determine approximate achievable bit rates.

- Determining optimal location of illuminated regions for environments, where ceiling is not available or room configuration prohibits the use of the ceiling. This region is optimal in minimizing path loss and delay spread to largest number of receiver locations.
- Validating impulse response calculation through measurements.

9.2.2 Spatial Coding

The multispot diffusing configuration overcomes many of IR's challenges. The narrow FOV of the receiver branches allows utilization of very efficient optical filters having narrow bandwidth, thus reducing the optical noise coming from ambient light sources to an acceptable level. Also, with proper joint optimization of the receiver and the transmitter, MSD links can be made multipath distortion-free. Then, several virtually ideal communication channels are established between the access point and each portable and the transmission speed is determined only by the speed of the electronics.

In future research, channels between transceivers are used to carry different signals according to transmitted symbols. Thus with M channels, a symbol is represented by M signals. The receiver, rather than combining signals at its branches, correlate signal with codes representing different symbols. This technique increases transceivers efficiency, reduces power, and most importantly provides an added degree of protection against shadowing. Future work will consider:

- Novel transmitter optics designs that will provide the following advantages: improved power budget and independent communications channels (different information streams are launched through different diffusing spots), thus providing a means for spatial diversity.
- Searching for different coding techniques that can be used to transmit data. Both binary and multilevel signal will be considered. Techniques are compared based on their power requirement, transceivers bandwidth, and most importantly, their ability to survive in presence of shadowing.
- Investigating the implementation of multibranch receiver optical front-end as well as receiver decision-making circuit.

9.2.3 Spatial Channel Hopping (SCH) Multiple Access

Through the channels made available by MSD configuration, it is possible to provide simultaneous access for multiple users. This is essential for real time and delay-sensitive traffic. To achieve multiple access, users are required to interpret the same data according to codes assigned to their receiver branches. Each user decodes the received signal over branches according to their unique codes. The research in multiple access focuses on:

- Investigating different layouts of diffusing spots to maximize the coverage area of transmitters. Configurations with continuous illumination will be investigated.

- The efficiency of proposed technique will be studied and compared to techniques that utilize TDM. Performance is evaluated based on average power requirement and transceivers bandwidth.
- The parameters of receiver optics design that enables independent reception from diffusing spot will be determined.
- The reliability of the link when a receiver is unable to intercepts all diffusing spot will be evaluated.
- Different traffic patterns will be used to evaluate the throughput of SCH and TDA to identify traffic that necessitates the use of SCH.

9.3 Publications

The following is a list of publications.

Journal Publications

- Y. A. Alqudah, M. Kavehrad, "MIMO Characterization of Indoor Wireless Optical Link using Diffused Configuration," *accepted for publication in the IEEE Transactions on Communications*.
- Y. A. Alqudah, M. Kavehrad, "On Optimum Order of Angle Diversity with Equal-Gain Combining Receivers for Broadband Indoor Optical Wireless Communications," *accepted for publication in the IEEE Transactions on Vehicular Technology.*

- Y. A. Alqudah, M. Kavehrad, "On Optimum Order of Angle Diversity with Maximal Ratio Combining Receivers for Broadband Indoor Optical Wireless Communications," *submitted for publication in the IEEE Transactions on Transactions on Communications.*

Conference Proceedings

- Y. A. Alqudah, M. Kavehrad, "Assessing Feasibility of a New Diffused Configuration for Broadband Wireless Infrared Links," WCNC 2003, New Orleans, LA, 2003.
- Y. A. Alqudah, M. Kavehrad, "On Merits of Spatial Coding in Multilevel Wireless Infrared Links," submitted, Globecom 2003 -Wireless Communications.
- S. Jivkova, Y. A. Alqudah, M. Kavehrad, "Optical Wireless Multi-Spot Diffusing Configuration: Link Quality," submitted, MILCOM 2003.
- Y. A. Alqudah, M. Kavehrad, "Orthogonal Spatial Coding in Indoor Wireless Optical Link," submitted, OptiComm 2003.
- Y. A. Alqudah, M. Kavehrad, "Multilevel Spatial Coding in Indoor Wireless Optical Link Reducing Power and Bandwidth Requirements," to be submitted.

Poster Session

- Y. A. Alqudah, M. Kavehrad, "Indoor Broadband Optical Wireless Communications," Graduate Research Exhibition, University Park, PA, 2003.

Bibliography

1. F. R. Gfeller and U. H. Bapst, "Wireless in-house data communication via diffuse infrared radiation," Proc. IEEE, vol. 67, pp. 1474-1486, 1979.

2 J. R. Barry, Wireless Infrared Communications, Kluwer Academic Publishers, 1994.

3 J. Kahn and A. Khwaja, Building Secure Wireless Networks with 802.11, Wiley Publishing, Inc, 2003.

4 J. M. Kahn and J. R. Barry, "Wireless infrared communications," *Proc. IEEE*, vol. 85, no. 2, pp. 265-298, Feb. 1997.

5 D.J.T Heatley, D. R. Wisely and I. Neild, P. Cochrane, "Optical wireless: the story so far," *IEEE Communications Magazine*, vol. 36, issue 12, Dec. 1998.

6 J. M. Kahn, J. R. Barry, M. D. Audeh, J. B. Carruthers, W. J. Krause and G. W. Marsh, "Non-directed infrared links for high-capacity wireless LANs," *IEEE Personal Communications*, vol.1, issue: 2, 2nd Qtr., 1994.

7 J. Bellon, M. J. N. Sibley, D. R. Wisely, and S. D. Greaves, "Hub architecture for infra-red wireless networks in office environments," *IEE Proc. of Optoelectronics*, vol. 146, no. 2, pp. 78-82, April 1999.

8 D. R. Wisely, "A 1 Gbit/s optical wireless tracked architecture for ATM delivery," *IEE* Colloquium on Optical Free Space Communication Links, pp. 14/1-14/7, Feb. 1996.

9 G. W. Marsh and J. M Kahn, "50-Mb/s diffuse infrared free-space link using on-off keying with decision-feedback equalization," *5th IEEE International Symposium on Personal, Indoor and Mobile Radio Communications*, vol. 4, pp. 1086 -1089, Sep. 1994.

10 J. R. V. Alvarez, F. J. L. Hernandez, A. S. Galdón, R. P. Jimenez, and J. A. R. Borges, "Infrared wireless DSSS system for indoor data communication links," *Proc. of SPIE*, vol. 3850, pp. 92-99, Sep. 1999.

11 G. Yun and M. Kavehrad, "Spot diffusing and fly-eye receivers for indoor infrared wireless communications," *Proc. IEEE Int. Conf. on Sel. Topics in Wireless Communications*, Vancouver, BC, Canada, pp. 262-265, June 1992.

12 Eric J. Lerner, "Free-space communications struggles to find its niche," Laser Focus World, June 2002.

13 J. R. Barry, J. M. Kahn, W. J. Krause, E. A. Lee and D. G. Messerschmitt, "Simulation of multipath impulse response for indoor wireless optical channels," *IEEE J. on Selected Areas in Comm*., vol. 11, no. 3, pp. 367-379, April 1993.

14 F. J. Lòpez-Hernàndez, R. Pèrez-Jimènez and A. Santamaria, "Modified Monte Carlo scheme for high-efficiency simulation of the impulse response on diffuse IR wireless indoor channels," *Electronics Letters*, vol. 34, no. 19, pp. 1819-1820, Sep. 1998.

15 R. Pérez Jiménez, J. Berges and M.J. Betancor, "Statistical model for the impulse response on infrared indoor diffuse channels," *Electronics Letters*, vol. 33, no. 15, pp.1298-1301, 1997.

16 F. J. Lòpez-Hernàndez and M. J. Betancor, "DUSTIN: Algorithm for calculation of impulse response on IR wireless indoor channels," *Electronics Letters*, vol. 33, no. 21, pp.1804-1806, Oct. 1997.

17 J. B. Carruthers and J. M. Kahn, "Modeling of nondirected wireless infrared channels," *IEEE Transactions on Communications*, vol. 45, no. 10, pp. 1260-1267, Oct. 1997.

18 M. R. Pakravan, "Estimation of indoor infrared channel parameters using neural networks," *IEEE International Symposium on Personal, Indoor and Mobile Communications*, vol. 6.1, pp. 311-315, 1998.

19 V. Pohl, V. Jungnickel and C. von Helmont, "A channel model for wireless infrared communication," *11th IEEE International Symposium on Personal, Indoor and Radio Communications,* vol. 1, pp. 297-303, 2000.

20 M. R. Pakravan and M. Kavehrad, "Distribution of infrared light power for indoor broadband wireless communications," *6th IEEE International Symposium on Indoor and Mobile Radio Communications*, vol. 1, 27-29, pp. 316 -320, Sep. 1995.

21 M. R. Pakravan, M. Kavehrad and H. Hashemi, "Indoor wireless infrared channel characterization by measurements," *IEEE Trans. on Vehicular Technology*, vol. 50, no.4, July 2001.

22 M. R. Pakravan, M. Kavehrad and H. Hashemi, "Measurement of rotation effects in an indoor infrared channel," *48th IEEE Vehicular Technology Conference*, vol. 3, pp. 2100–2103, May 1998.

23 Q. Jiang, M. Kavehrad, M. R. Pakravan and M. Tai, "Wideband optical propagation measurement system for characterization of indoor wireless infrared channels," *IEEE ICC*, vol. 2, pp. 1173–1176, June 1995.

24 H. Hashemi, G. Yun, M. Kavehrad, F. Behbahani and P. Galko, "Indoor propagation measurements at infrared frequencies for wireless local area networks Applications," *IEEE Trans. on Vehicular Technology*, vol. 43, no. 3, pp. 562-576, August 1994.

25 J. M. Kahn, W.J. Krause, and J. B. Carruthers, "Experimental characterization of nondirected indoor infrared channels," *IEEE Transactions on Communications*, Vol. 43, pp. 1613-1623, Feb./Mar./Apr. 1995.

26 L. B. Wolff, "Diffuse reflection," *IEEE Computer Vision and Pattern Recognition*, pp. 472-478, 1992.

27 X. D. He, K. E. Torrance, F. X. Sillion and D. P. Greenberg, "A comprehensive physical model for light reflection," *ACM Computer Graphics*, vol. 25, no. 4, pp. 175-186, July 1991.

28 M. Oren and S. K. Nayar, "Generalization of Lambert's reflectance model," *ACM Computer Graphics Proceedings*, 1994.

29 A. C. Boucouvalas, "Indoor ambient light noise and its effect on wireless optical links," *IEE Proc. of Optoelectronics*, vol. 334-338, no. 143, p. 6, Dec. 1996.

30 A.J.C. Moreira, R. T. Valadas and A. M. de Oliveira Duarte, "Reducing the effects of artificial light interference in wireless infrared transmission systems optical free space communication links," *IEE Colloquium on Optical Free Space Communication Links*, pp. 5/1 –510, Feb. 1996.

31 A.J.C. Moreira, R. T. Valadas and A. M de Oliveira Duarte, "Performance of infrared transmission systems under ambient light interference," *IEE Proc. of Optoelectronics*, vol. 143, issue: 6, pp. 339 –346, Dec. 1996.

32 A.J.C. Moreira, R. T. Valadas and A. M. de Oliveira Duarte, "Characterization and modeling of artificial light interference in optical wireless communication systems,", *6th IEEE International Symposium on PIMRC*, vol.1, pp. 326 –331, Sep.1995.

33 R. Narasimhan, M. D. Audeh, J. Kahn, "Effect of electronic-ballast fluorescent lighting on wireless infrared links," *IEE proceedings on Optoelectronics*, vol. 143, issue: 6, Dec. 1996.

34 C. J. Geogopulos, "Suppressing background light interference in an in-house infrared communication system by optical filtering," *International journal of Optoelectronics*, vol. 3, No. 3, 1988.

35 G. P. Agrawal, Fiber-Optic Communication Systems, John Wiley & Sons, inc, 1997.

36 S. B. Alexander, Optical Communication Receiver Design, SPIE Optical Engineering, 1997.

37 S. D. Personick, Fiber Optics Technology and Applications, Plenum Press, New York, 1985.

38 W. Marion and S. Wilcox, Solar Radiation Data Manual for Buildings, National Renewable Energy Laboratory, 1995.

39 M. Iqbal, An Introduction to solar radiation, New York, Academic Press, 1983.

40 R. T. Valadas and A. M. de Oliveira Duarte, "Sectored receivers for indoor wireless optical communication systems," *5th IEEE Int. Symp. on PIMRC*, vol. 4, pp. 1090-1095, Sept. 1994.

41. A. Tavares, R. T. Valadas and A. M. de Oliveira Duarte, "Performance of an optical sectored receiver for indoor wireless communication systems in presence of artificial and natural noise sources," SPIE, vol. 2601, pp. 264-273, 1995.

42 J. B. Carruthers and J. M. Kahn, "Angle diversity for nondirected wireless infrared communication," *IEEE Transactions on Communications*, vol. 48, no. 6, pp. 960-969, June 2000.

43 P. Dajani and J. M. Kahn, "Analysis of infrared wireless link employing multi-beam transmitters and imaging diversity receivers," *IEEE Transactions on Communications*, vol. 48, no 12, pp. 2077-2088, Dec. 2000.

44 W. -C. Jeong, M. Kavehrad and S. Jivkova, "Broadband Infrared Access with a Multi-Spot Diffusing Configuration: Performance, " *International Journal of Wireless Information Networks*, vol. 8, no. 1, Jan. 2001.

45 J. M. Kahn, P. Djahani, A. G. Weisbin, K. T. Beh, A. P. Tang, R. You, "Imaging Diversity Receivers for High-Speed Infrared Wireless Communications," IEEE Communications Magazine, vol. 36, no. 12, pp. 88-94, December 1998.

46 S. Jivkova and M. Kavehrad, "Multi-spot diffusing configuration for wireless infrared access," *IEEE Transactions on Communications*, vol. 48, no. 6, pp. 970-978, June 2000.

47 E. Simova and M. Kavehrad, “Light shaping diffusers for indoor wireless infrared communications via a holographic approach, ” *Proceedings of SPIE Photonics*, San Jose, California, Feb. 1996.

48 E. Simova, M. Tai and M. Kavehrad, “Indoor wireless infrared link with a holographic multiple-spot diffuser, ” *Proceedings of ICAPT*, Montreal, August 1996.

49 S. Jivkova and M. Kavehrad, “Indoor wireless infrared local access, multi-spot diffusing with computer generated holographic beam-splitter, ” *Proceedings of ICC*, Vancouver, Canada, June 1999.

50 S. Jivkova and M. Kavehrad “Holographic optical receiver front-end for wireless infrared indoor communications,” *OSA Applied Optics Journal*, June 2001.

51 S. Jivkova and M. Kavehrad, “Receiver designs and channel characterization for multispot high bit rate wireless infrared communications, ” *IEEE Transactions on Communications*, vol. 49, no. 12, pp. 2145-2153, Dec. 2001.

52 K. Akhavan, M. Kavehrad and S. Jivkova, “Wireless infrared in-house communications: How to achieve very high bit rates, ” *Proceedings of the IEEE WCNC 2000*, Chicago, September 2000.

53 K. Akhavan, M. Kavehrad and S. Jivkova, “High-speed power-efficient indoor wireless infrared communication using code combining, PART-- II,” *IEEE Transactions on Communications*, vol. 50, no. 9, Sep. 2002.

54 K. Akhavan, M. Kavehrad and S. Jivkova, “High-speed power-efficient indoor wireless infrared communication using code combining, PART-- I,” *IEEE Transactions on Communications*, vol. 50, no. 7, July 2002.

55 J. G. Proakis, Digital Communications, McGraw-Hill, Inc., 1995.

56 J. Anderson, Digital Transmission Engineering, Prentice Hall, 1998.

57 K. Samaras, D. C. O’Brien and D. J. Edwards, “Analytical calculation of throughput of ALOHA based protocols in optical wireless data networks,” *IEE Proceedings on Optoelectronics*, vol. 147, issue: 4, Aug. 2000.

58 M. D. Audeh, J.M. Kahn, “Performance evaluation of L-pulse-position modulation on non-directed indoor infrared channels,” *ICC 94*, pp. 660–664, vol.2, 1994.

Yazan A. Alqudah was born in 1971 in Ajloun, Jordan. He received his B.S degree in Electrical Engineering from University of Jordan in 1993. After graduation, he worked as a lab instructor at the Yarmouk University, Irbid, Jordan. Yazan began his graduate studies in 1994 in Electrical Engineering at the Pennsylvania State University. During his studies towards his M.S. degree, he worked as a teaching assistant where he assisted with the design and building of experiments for the digital control laboratory. His Master thesis work investigated using feedback control to reduce motion artifacts in Magnetic Resonance Imaging (MRI). He received his M.S. degree in 1997. In 1997, he joined Schlumberger as part of his practical training. He worked as an applications and software engineer. During his assignments, he was responsible for the personalization of Subscriber Identity Modules (SIM) and over-the-air customization services for GSM carriers in North America. In fall 2000, he started his PhD work. He received teaching and research assistantship positions at Penn State's EE department. His current research interests include communication systems, channel modeling, and broadband optical wireless communication.